

# **Thiophene Oligomers for Photovoltaic Applications: Synthesis, Self-assembly and Optoelectronic Properties**

THESIS SUBMITTED TO ACADEMY OF SCIENTIFIC AND INNOVATIVE  
RESEARCH (AcSIR) FOR THE AWARD OF THE DEGREE OF  
**DOCTOR OF PHILOSOPHY IN CHEMISTRY**  
UNDER THE FACULTY OF SCIENCE



By  
**TANWISTHA GHOSH**  
**Enrollment No: 10CC13A39005**

Under the Supervision of  
**Dr. Vijayakumar C.**



**PHOTOSCIENCES AND PHOTONICS SECTION**  
**CHEMICAL SCIENCES AND TECHNOLOGY DIVISION**  
**CSIR-NATIONAL INSTITUTE FOR INTERDISCIPLINARY**  
**SCIENCE AND TECHNOLOGY (CSIR-NIIST)**  
**THIRUVANANTHAPURAM - 695019, KERALA**

**FEBRUARY 2019**

## DECLARATION

I hereby declare that the matter embodied in the Ph.D. thesis entitled: **“Thiophene Oligomers for Photovoltaic Applications: Synthesis, Self-assembly and Optoelectronic Properties”** is the result of an independent work carried out by me at the Photosciences and Photonics Section, Chemical Sciences and Technology Division of the CSIR-National Institute for Interdisciplinary Science and Technology (CSIR-NIIST), Thiruvananthapuram, under the supervision of Dr. Vijayakumar C. and the same has not been submitted elsewhere for any other degree or diploma.

In keeping with the general practice of reporting scientific observations, research materials obtained from other investigations has been duly cited and acknowledged in the thesis.

*Tanwistha Ghosh*  
**Tanwistha Ghosh**

Thiruvananthapuram  
February 25, 2019

**National Institute for Interdisciplinary Science and Technology (NIIST)**

Council of Scientific and Industrial Research, Thiruvananthapuram - 695 019, INDIA

**Dr. Vijayakumar C., PhD**

Scientist, Photosciences and Photonics Section, CSTD

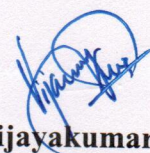
Tel: +91-471-2515-484; E-mail: [cvijayakumar@niist.res.in](mailto:cvijayakumar@niist.res.in)



February 25, 2019

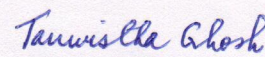
## CERTIFICATE

This is to certify that the work embodied in the thesis entitled: “**Thiophene Oligomers for Photovoltaic Applications: Synthesis, Self-assembly and Optoelectronic Properties**” has been carried out by Ms. Tanwistha Ghosh under my supervision and guidance at the Photosciences and Photonics Section, Chemical Sciences and Technology Division of the CSIR-National Institute for Interdisciplinary Science and Technology (CSIR-NIIST), Thiruvananthapuram and the same has not been submitted elsewhere for a degree.



**Dr. Vijayakumar C.**

(Thesis Supervisor)



**Tanwistha Ghosh**

## ACKNOWLEDGEMENTS

*I have great pleasure in placing on record my deep sense of gratitude to Dr. Vijayakumar C., my thesis supervisor, for suggesting the research problem and for his guidance, immense knowledge, endearing care, constant support, and motivation, leading to the successful completion of this work.*

*I would like to express my sincere thanks to Professor M. V. George for his constant help and encouragement during my stay at CSIR-NIIST.*

*I wish to thank Dr. A. Ajayaghosh, Director and Dr. Gangan Pratap and Dr. Suresh Das, former Directors of the CSIR-National Institute for Interdisciplinary Science and Technology for providing me the necessary facilities for carrying out the work.*

*I sincerely thank Prof. Akinori Saeki, Prof. Shu Seki, Dr. Anesh Gopal, Dr. Shinji Nagasawa for all the experiments conducted at Osaka University, Japan.*

*I sincerely acknowledge Dr. Mangalam S. Nair and Dr. R. Luxmi Varma, former and present AcSIR coordinators for their help in the successful completion of the course work.*

*I am thankful to Dr. Bhoje Gowd E and Dr. K. K. Maiti for the XRD and Raman studies.*

*I am very much thankful to Dr. Joshy Joseph, Dr. K. Yoosaf and Dr. Biswapriya Deb, my Doctoral Advisory Committee members for their valuable comments and suggestions to improve the quality of my work.*

*I would also like to thank Dr. K. N. Narayana Unni, Photosciences and Photonics Section head for all the help and support extended to me.*

*I would like to thank Dr. D. Ramaiah, Dr. K.R. Gopidas, Dr. C. H. Suresh, Dr. V. Karunakaran, Dr. Suraj Soman, Dr. Bijitha Balan, Dr. J. D. Sudha, Dr. Rakhi B. and all other scientists of the Photosciences and Photonics Section, Chemical Sciences and Technology Division, for all the help and support extended to me.*

*I would like to thank Mr. Robert Philip and Mr. Kiran Mohan for general help and TEM analysis and Mrs. Saumini Mathew, Mr. Saran and Mr. Shyam for NMR analysis and Mrs. Viji, and Ms. Athira for HRMS data, Mr. Aswin, Mr. Vishnu and Mr. Vibhu Darshan for AFM analysis.*

*I express my sincere thanks to my labmates Mr. Naeem K.C., Mrs. Jayanthi S Panicker, Mr. Chinnadurai M., Mr. Johnpaul K. P., Mrs. Neethi Raveendran, Ms. Susanna Poulouse, Mrs. Neethu M., Mrs. Anuja Vijayan, Mr. Arjun P., Mr. Vishnu Vijayakumar, Mrs. Reshma P., Ms. Parvathy P. R. and Ms. Devika S. for their valuable help and support. I also thank all M. Sc. project students who have worked with me.*

*Words are inadequate to express my gratitude to my dear friends at photosciences for their care, love, support, and encouragement, which made my life in NIIST memorable. I also thank all the present and former members of the Photosciences and Photonics and other Divisions of CSIR-NIIST for their help and cooperation.*

*I am deeply indebted to my parents, brother and sister, family members and friends for their support and encouragement. I would also like to extend my thanks and appreciation to all my teachers for their help and blessings.*

*Finally, I sincerely thank the University Grant Commission (UGC) JRF and SRF for financial assistance.*

**Tanwistha Ghosh**

# CONTENTS

|  | Page |
|--|------|
| <b>Declaration</b>   | i    |
| <b>Certificate</b>   | ii   |
| <b>Acknowledgements</b>  | iii  |
| <b>Contents</b>  | v    |
| <b>Preface</b>   | viii |
| <b>List of Abbreviations</b>   | xi   |
| <br>   |      |
| <b>Chapter 1    An Overview of Organic Solar Cell Materials and Devices</b>                      |      |
| <br>   |      |
| 1.1            Abstract  | 1    |
| 1.2            Introduction  | 2    |
| 1.3            Organic solar cell materials  | 5    |
| 1.4            Working principle of organic solar cell   | 10   |
| 1.4.1          Photoexcitation and exciton formation   | 10   |
| 1.4.2          Exciton diffusion   | 12   |
| 1.4.3          Exciton dissociation  | 12   |
| 1.4.4          Charge transport and collection   | 13   |
| 1.5            Photovoltaic characteristics  | 14   |
| 1.5.1          Short circuit current ( $I_{sc}$ ) and short circuit current density ( $J_{sc}$ ) | 14   |
| 1.5.2          Open circuit voltage ( $V_{oc}$ )   | 15   |
| 1.5.3          Fill factor ( $FF$ )  | 16   |
| 1.5.4          Power conversion efficiency   | 16   |
| 1.6            Device architecture   | 17   |
| 1.6.1          Planar heterojunction   | 17   |
| 1.6.2          Bulk heterojunction   | 19   |

|                  |   |    |
|------------------|---|----|
| 1.6.3            | Conventional OSCs vs inverted OSCs  | 20 |
| 1.7              | Thiophene-based conjugated materials  | 21 |
| 1.7.1            | Solution-processed thiophene-based polymers   | 23 |
| 1.7.2            | Solution-processed thiophene-based oligomers  | 28 |
| 1.8              | Objective of the present investigation  | 39 |
| 1.9              | References  | 40 |
| <b>Chapter 2</b> | <b>Molecular and Supramolecular Effects on p/n -Polarity of Thiophene Oligomers in Photovoltaic Cells</b> |    |
| 2.1              | Abstract  | 45 |
| 2.2              | Introduction  | 46 |
| 2.3              | Results and discussion  | 51 |
| 2.3.1            | Synthesis and characterization  | 52 |
| 2.3.2            | Photophysical properties in the solution state  | 54 |
| 2.3.3            | HOMO-LUMO levels and optical bandgap  | 57 |
| 2.3.4            | Photovoltaic properties   | 59 |
| 2.3.5            | Energy minimized structure  | 61 |
| 2.3.6            | Film state absorption properties  | 62 |
| 2.3.7            | Solid state packing and thermal stability   | 64 |
| 2.3.8            | Blend with P3HT and PCBM  | 66 |
| 2.3.9            | Photoconductivity analysis  | 67 |
| 2.4              | Conclusions   | 71 |
| 2.5              | Experimental section  | 72 |
| 2.6              | References  | 81 |
| <b>Chapter 3</b> | <b>Optimization of Photovoltaic Efficiency and Structure-Property Correlation of Thiophene Oligomers</b>  |    |
| 3.1              | Abstract  | 84 |

|                  |   |     |
|------------------|---|-----|
| 3.2              | Introduction  | 85  |
| 3.3              | Results and discussion  | 89  |
| 3.3.1            | Synthesis and photophysical characterization                              | 90  |
| 3.3.2            | Photoconductivity analysis  | 96  |
| 3.3.3            | Photovoltaic properties   | 98  |
| 3.3.4            | PL quenching and 2D-GIXRD analysis  | 108 |
| 3.4              | Conclusions   | 112 |
| 3.5              | Experimental section  | 113 |
| 3.6              | References  | 121 |
| <b>Chapter 4</b> | <b>Preferential Face-on or Edge-on Orientation in Thiophene Oligomers</b> |     |
| 4.1              | Abstract  | 125 |
| 4.2              | Introduction  | 126 |
| 4.3              | Results and discussion  | 133 |
| 4.3.1            | Synthesis and photophysical characterisation                              | 135 |
| 4.3.2            | Solid state packing and thermal stability                                 | 137 |
| 4.3.3            | Differential scanning calorimetry   | 139 |
| 4.3.4            | Grazing-incidence X-ray diffraction studies                               | 140 |
| 4.3.5            | Atomic force microscopy analysis  | 143 |
| 4.3.6            | Raman spectroscopy analysis of the oligomers                              | 145 |
| 4.3.7            | Conducting atomic force microscopy (c-AFM) measurement                    | 146 |
| 4.3.8            | Photovoltaic properties   | 148 |
| 4.4              | Conclusions   | 151 |
| 4.5              | Experimental section  | 151 |
| 4.6              | References  | 156 |
|                  | <b>List of Publications</b>   | 159 |



## PREFACE

Organic solar cells have recently appeared as a promising technology within the photovoltaic industry due to their low-cost fabrication and great flexibility enabling a widespread distribution. In this context, design and development of oligomers or small molecules are an active area of research due to their distinct advantages over their polymer counterparts. These advantages include the ease to synthesize in high purity, possess well-defined structures, and show no batch-to-batch variations. However, dependence on supramolecular interactions is more pronounced in oligomers when compared to that in polymers, which demands careful molecular designing and rational fabrication techniques for obtaining optimum performances. Also, significant variations are observed in optoelectronic properties of comparable oligomers even when the structural differences between them are minimal. The current thesis makes an effort to study in detail how minimal change in the molecular structure can bring about significant variation in the optoelectronic properties.

The thesis is organized into four Chapters. The first Chapter introduces the research background with a brief description of the importance of organic photovoltaic device and its future applications. Oligothiophenes provide an excellent platform to explore various synthetic modifications, morphology tuning, and electronic relationships in organic semiconductor systems. These short-chain

systems serve as models for establishing valuable structure-property relationships to their polymer analogs. This chapter highlights some of the historic and recent developments in the designing and synthesis of thiophenes, as polymers, oligomers and small molecules, and evaluation of their potential for the development of efficient organic photovoltaic devices.

In the second Chapter, we have discussed the design and synthesis of two acceptor–donor–acceptor type semiconducting thiophene oligomers end-functionalized with oxazolone/isoxazolone derivatives. Oxazolone and isoxazolone are positional isomers which differ in the respective positions of nitrogen atoms and the phenyl group on the 5-membered heterocyclic ring. The oligomers were found to exhibit unique p/n-polarity in BHJ photovoltaic cells. The suitable HOMO–LUMO energy levels of the isoxazolone derivative favored it to act as a better n-type material in the presence of P3HT. On the other hand, better supramolecular interaction in the oxazolone derivative helped it to form a stable bicontinuous network with PCBM and hence acted as a p-type material, which is consistent with the FP-TRMC evaluations.

The third Chapter describes the synthesis and characterization of oligomers having same end group (*N*-ethylrhodanine) but different central core (thiophene, bithiophene, thienothiophene) connected through thiophene  $\pi$ -linker (alkylated terthiophene) for solution processable bulk-heterojunction solar cells. The effect of the incorporation of extra thiophene to the central thiophene unit either through

C–C bond linkage to form bithiophene or by fusing two thiophenes together to form thienothiophene on the optoelectronic properties and photovoltaic performances of the oligomers were studied in this chapter. Photoconductivity analysis of thienothiophene core based derivative showed significantly higher value when compared to other derivatives. However, the initial photovoltaic devices fabricated from all three oligomers gave similar PCEs (~1%), which was counterintuitive to the observation made above. By performing adequate solution engineering, we could observe a 5-fold enhancement in the device efficiency of thienothiophene core based derivative. The structure-property correlation and the fundamental reasons for the improvement in device performance were also studied in detail.

The last chapter deals with the synthesis and characterization of two acceptor-donor-acceptor type oligothiophene derivatives. The oligomers having 2-(1,1-dicyano-methylene)rhodanine as acceptor favored a face-on packing, while that of functionalized with *N*-octyl rhodanine preferred an edge-on packing. This unique packing was analyzed by 2D-grazing incidence angle X-ray diffraction. Tapping-mode atomic force microscopy and Raman spectroscopy analyses were also carried out to further confirm their preferred orientation. As an outcome of the preferred orientation, the oligomers exhibited anisotropic conductivity in the self-assembled state, revealed by the conducting AFM experiment. The photovoltaic properties of the self-assembled oligomers were also evaluated in an inverted device architecture using PC<sub>61</sub>BM as an acceptor.

## LIST OF ABBREVIATIONS

1. AM- Air Mass
2. AuNPs – Gold nanoparticles
3. Å - Angstrom
4. AFM- Atomic force microscopy
5. Ar - Argon
6. AcOH- Acetic Acid
7. BBTz - Benzobisthiazole
8. BDT- Benzodithiophene
9. BHJ- Bulk heterojunction
10. BT- Benzothiadiazole
11. B3LYP- Becke 3-parameter, Lee-Yang-Parr
12. CN-1-Chloronaphtalene
13. CIGS- Copper Indium Gallium Selenide
14. CTE-Charge Transfer Exciton
15. CV-Cyclic Voltammetry
16. °C – Degree Celsius
17. CDCl<sub>3</sub> – Deuterated Chloroform
18. CH<sub>3</sub>CN – Acetonitrile
19. Calcd. – Calculated
20. Chl-a – Chlorophyll-a
21. DIO- 1,8-Diiodooctane
22. DPP- Diketopyrrolopyrrole

23. DFT- Density Functional Theory
24. DSC - Differential Scanning Calorimetry
25. DTS- Dithienosilole
26. DCM – Dichloromethane
27. DMSO - Dimethyl sulfoxide
28. DMF - Dimethylformamide
29. DCV- Dicyanovinyl
30. Eg- Bandgap
31. EQE- External quantum efficiency
32. *et al. – Et alii/alia*
33.  $\varepsilon$  – Molar extinction coefficient
34. eV – Electron volt
35. FET – Field-Effect Transistor
36. FTIR – Fourier-Transform Infrared Spectroscopy
37. FP-TRMC – Flash Photolysis -Time-Resolved Microwave Conductivity
38. *FF*- Fill factor
39. g - Gram
40. GIXRD - Grazing Incidence X-ray Diffraction
41. HR-MS- High Resolution Mass Spectrometry
42. h – Hour
43. HOMO – Highest Occupied Molecular Orbital
44. HCl – Hydrochloric acid
45. ICT – Intramolecular Charge Transfer
46. IR – Infrared

47.  $I_{sc}$  – Short circuit current
48. ITO– Indium Tin Oxide
49.  $J_{sc}$ – Short circuit current density
50. K – Kelvin
51. LUMO – Lowest Unoccupied Molecular Orbital
52.  $\lambda_{max}$  – Wavelength maximum
53. MW– Molecular Weight
54. MALDI-TOF- Matrix-Assisted Laser Desorption/Ionization-Time of Flight
55. M – Molar
56. mg – Milligram
57. mL – Millilitre
58.  $\mu\text{M}$  – Micromolar
59.  $\mu\text{s}$  – Microseconds
60.  $\mu\text{m}$  – Micrometer
61. mM – Millimolar
62. mmol – Millimole
63. NBS - N-Bromosuccinimide
64. NIR- Near Infrared
65. NFA- Non-Fullerene Acceptor
66. NREL - National Renewable Energy Laboratory
67. nm – Nanometer
68. NMR – Nuclear magnetic resonance
69. ns – Nanosecond
70. OSC – Organic Solar Cell

71. OTFT– Organic Thin Film Transistor
72. PS– Polystyrene
73.  $P_{\max}$  – Maximal power
74.  $P_{\text{in}}$ - Power input
75. PEDOT:PSS – Poly(3,4- ethylenedioxythiophene)polystyrenesulfonate
76. PCE – Power Conversion Efficiency
77. PC<sub>71</sub>BM – [6,6]-Phenyl-C<sub>71</sub>-Butyric acid Methyl Ester
78. PC<sub>61</sub>BM – [6,6]-Phenyl-C<sub>61</sub>-Butyric acid Methyl Ester
79. PDI- Perylene diimide
80. PV– Photovoltaic
81. PYS- Photoelectron Yield Spectroscopy
82. PHJ- Planar heterojunction
83. PL – Photoluminescence
84.  $\Phi_{\text{F}}$  – Quantum yields of fluorescence
85. rpm – Rotation per minute
86. SEM – Scanning electron microscope
87. SERS - Surface-enhanced Raman spectroscopy
88. STM- Scanning Tunneling Microscope
89. s – Seconds
90. TOPV- Ternary Organic Photovoltaics
91. TEM- Transmission Electron Microscopy
92. TLC – Thin Layer Chromatography
93. TGA – Thermogravimetric Analysis
94. THF – Tetrahydrofuran

95. TMS – Tetramethylsilane
96.  $\tau_f$ – Fluorescence lifetime
97. TEM – Transmission electron microscope
98. TCSPC- Time-Correlated Single Photon Counting
99. TT - Thiazolothiazole
100. TzTz - Thiazolothiazole
101. UV-vis – Ultraviolet- visible
102.  $V_{oc}$  –Open circuit voltage
103. WAX – Wide angle X-ray
104. XRD - X-ray diffraction



---

## An Overview of Organic Solar Cell Materials and Devices

---

### 1.1. Abstract

*Organic photovoltaic cells based on bulk-heterojunction architecture have been a topic of intense research for the past two decades. Recent reports on power conversion efficiency surpassing 10% suggest these devices are a viable low-cost choice for a range of applications where conventional silicon solar cells are not suitable. Among a large variety of organic semiconductors, thiophene based polymers and oligomers are known to be the most potential candidate for photovoltaic application. Oligothiophenes provide an excellent platform to explore various synthetic modifications, morphology tuning, and electronic relationships in organic semiconductor systems. These short-chain systems serve as models for establishing valuable structure-property relationships to their polymer analogs. In contrast to their polymer counterparts, oligothiophenes afford high-purity and well-defined structures that can be easily modified with a variety of functional groups. The current chapter highlights the recent developments in the area of oligothiophenes and the evaluation of their potential for the development of efficient organic photovoltaic devices.*

## 1.2. Introduction

Solar radiation is the prime source of energy and its abundant availability on Earth's surface makes it a perfect candidate for clean and renewable sources of electricity.<sup>1-3</sup> Development in the field of solar energy harvesting will help to reduce the world's dependence on exhaustible, expensive and polluting sources of energy, thereby help countries tackle their manifold energy challenges. Scientists are therefore putting enormous efforts in the field of photovoltaic technology as it can serve as the most high-potential prospect for harnessing solar energy. Silicon solar cells, the first generation solar technology, can convert ~25% of the energy in sunlight to electricity and the second generation cells composed of amorphous silicon, cadmium telluride (CdTe) and copper indium gallium selenide (CIGS) shows typical performance in the range of ~22%.<sup>4-6</sup> Though both these photovoltaic technologies have good performance and stability, they need highly expensive clean-room technology and require a lot of energy in production.<sup>7</sup> To address these problems, scientists have done intense research in the field of third generation photovoltaics, particularly organic solar cells (OSC) as it has the potential to serve as an alternative to silicon-based cells in terms of cost-effectiveness, light weightiness, roll-to-roll fabrication, mechanical flexibility, in addition to the use of low-cost solution processing techniques for large area fabrication.<sup>8-13</sup> Most of the current research is focusing on the development of novel materials with improved efficiencies through molecular engineering.<sup>14-18</sup> Recent reports suggest that OSCs have entered the phase of commercialization, although

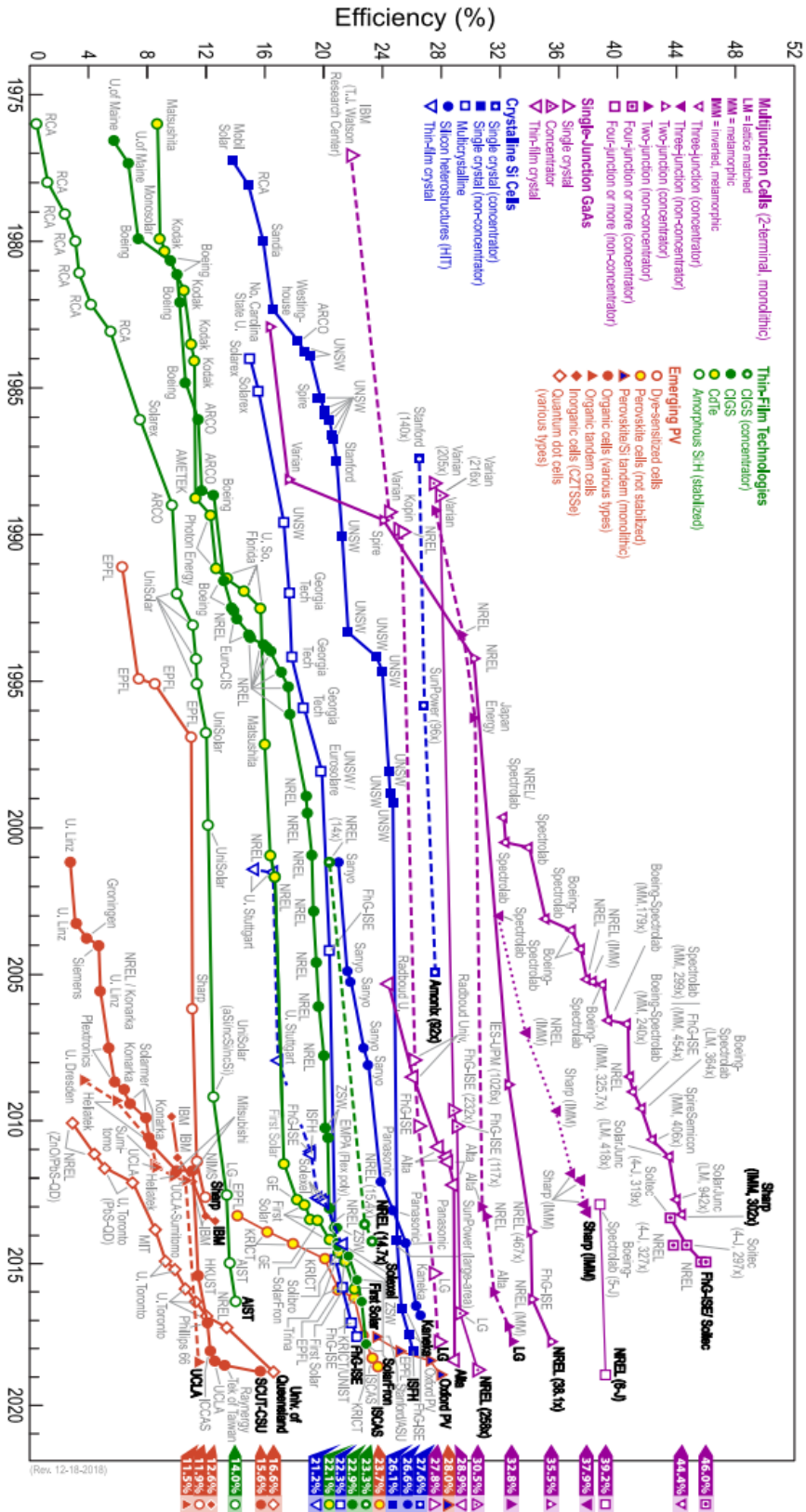
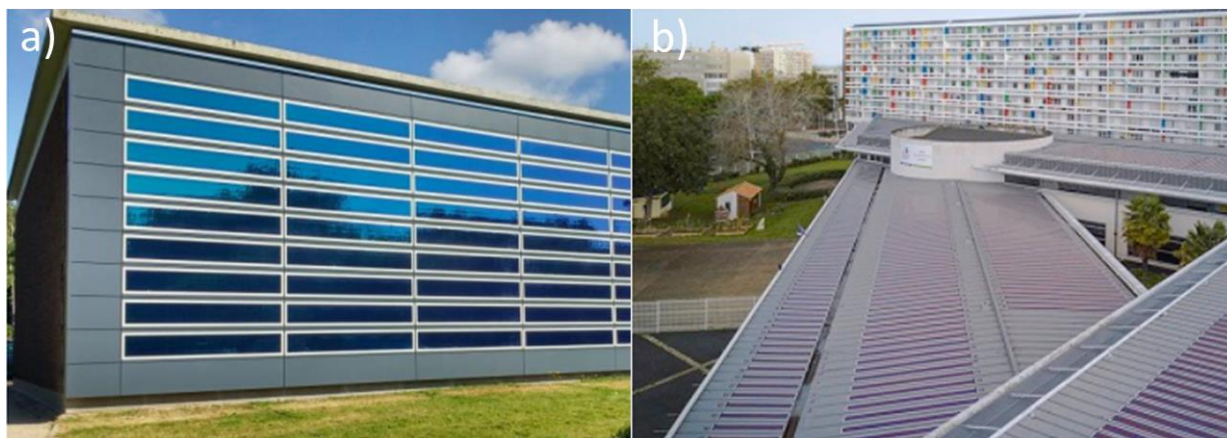


Figure 1.1 National Renewable Energy Laboratory (NREL)'s chart on the best research solar cell efficiencies reported by various groups as on December 21, 2018 (Downloaded from <https://www.nrel.gov/pv/> on 12 February 2019).

improvements in efficiency and stability are still desirable.<sup>19-21</sup> Companies like Heliatek GmbH in Germany, infinityPV in Denmark and Solarmer Energy Inc. in the United States are working rigorously to commercialize successful solar energy-related products based on organic materials.

**Figure 1.1** shows the NREL chart displaying the best research-cell efficiencies under various categories reported by groups around the world. NREL has placed OSCs in the emerging photovoltaics along with dye-sensitized solar cells, perovskite cells, tandem cells, and quantum dot cells.<sup>22</sup> Even though the fabrication costs of OSCs are effectively low, their low efficiencies and limited lifetimes present major challenges before researchers that have to be addressed to enable the large-scale, commercial production. However, innovations in the design and synthesis of materials, and engineered device architectures are pushing the efficiency and stability limits of OSCs. The recently reported efficiency of tandem organic solar cell has been as high as ~15% (for 2 mm<sup>2</sup> cells) with significant stability.<sup>23</sup> Such developments move the field of OSCs further forward to commercialization.

OSCs due to its semi-transparency, flexibility in shape and variable color, present a perfect playground for building architects. It could be perfectly integrated into roof top of buildings, windows, and no longer being forced to the rigid and square-shaped standard modules.



**Figure 1.2.** Heliatek solar films integrated a) into the Asahi Glass Company windows at the entrance of the building; b) on the roof top of the Pierre Mendes France middle school in France (*Adapted from reference 24, 25*).

**Figure 1.2a** shows solar films manufactured by Heliatek that have been incorporated into the facade windows to demonstrate the potential of colored modules as facade decoration.<sup>24</sup> Very recently, they have installed 500 m<sup>2</sup> HeliaSol solar films on the roof of the Pierre Mendes France middle school in France (**Figure 1.2b**), which is the world's largest building integrated organic photovoltaics.<sup>25</sup> About 23.8 MWh of electricity could be generated annually from these modules, which is equivalent to the annual consumption of five households. It meets approximately 15% of the school's electricity demand. These examples highlight the potential of organic solar cells in meeting the energy requirements, which comes with exceptionally beautiful aesthetics.

### 1.3. Organic solar cell materials

Organic materials having a delocalized pi-electronic system are capable of absorbing solar energy, generating charge carriers and transporting them to respective electrodes are

---

known as organic semiconductors.<sup>26,27</sup> These materials are having alternating ‘ $\sigma$ ’ and ‘ $\pi$ ’ bonds, which are responsible for the above mentioned properties. The molecules may have heteroatoms such as N, O, S and sometimes halogens, and some of them may also involve in conjugation. Research on OSCs generally focuses on the development of such pi-conjugated materials that can be either solution processable polymers/small molecules or vacuum deposited small molecules.

Organic semiconductors are in general referred to as “intrinsic wide bandgap materials” (bandgaps above 1.4 eV) with negligibly low intrinsic charge carriers at room temperature in the dark. The bandgap of the ground state of these materials is defined as the difference in the energy levels between the Highest Occupied Molecular Orbital (HOMO) and Lowest Unoccupied Molecular Orbital (LUMO) levels. Materials with low bandgap are particularly preferred for solar cell application because a bandgap of 1.1 eV (1100 nm) is capable of absorbing about 77% of the solar irradiation.<sup>28</sup> However, a majority of the semiconducting polymers have a bandgap higher than 2 eV (620 nm), this limits the harvesting capacity of solar cells at 30% or below. Hence, structure engineering on these materials plays a crucial role in lowering the bandgap. Reduction of the intrinsic bandgap in these materials was achieved by incorporating push-pull (donor-acceptor) moieties in the conjugated backbone.<sup>29</sup> Bringing together an electron-rich unit (donor, D) and electron-deficient unit (acceptor, A) to form donor-acceptor (D-A) or acceptor-donor-acceptor (A-D-A) or donor-acceptor-donor (D-A-D) systems, not only help to reduce the bandgap but also broaden the absorption in the UV-Vis region. Apart from

this, electrochemical, photochemical or chemical doping methods were introduced to produce extrinsic charge carriers in the material.<sup>30</sup>

Owing to the requirement in improving the efficiency and stability of OSCs, widespread research is going on ranging from the optimization of device architecture to tuning/controlling the morphology and the design of novel active materials. For the past two decades, the donors have monopolized attention as they are thought to play crucial roles at each step of the photovoltaic process. This thesis mainly focuses on the design of new donor materials and mainstreams the synthesis of thiophene based donor oligomers, particularly of acceptor-donor-acceptor (A-D-A) type systems.

Chemical structures of commonly employed organic semiconductors in OSCs are shown in **Chart 1.1**. Most commonly used donor polymers in OSCs are (i) derivatives of phenylenevinylene backbones like poly[2-methoxy-5-(3',7'-dimethyloctyloxy)-1,4-phenylenevinylene] (**1**; MDMO-PPV), (ii) derivatives of thiophene units such as poly(3-hexylthiophene) (**2**; P3HT) (iii) derivatives of fluorene (**3**; F8T2), (iv) derivatives of triaryl amine (**4**; PTAA), (v) derivatives of benzodithiophenes (**5**; BDT). While, small molecules like alkylated derivatives of thiophene (**6**; DH-5T and **7**; DH-6T), oligothiophene (**8**;  $\alpha$ -sexithiophene), pentacene (**9**) etc. Among the donor materials, thiophene derivatives (both polymers and oligomers) are widely used in OSCs as a donor due to several reasons. Details of these aspects and their application in a solar cell is discussed in **Section 1.7**.

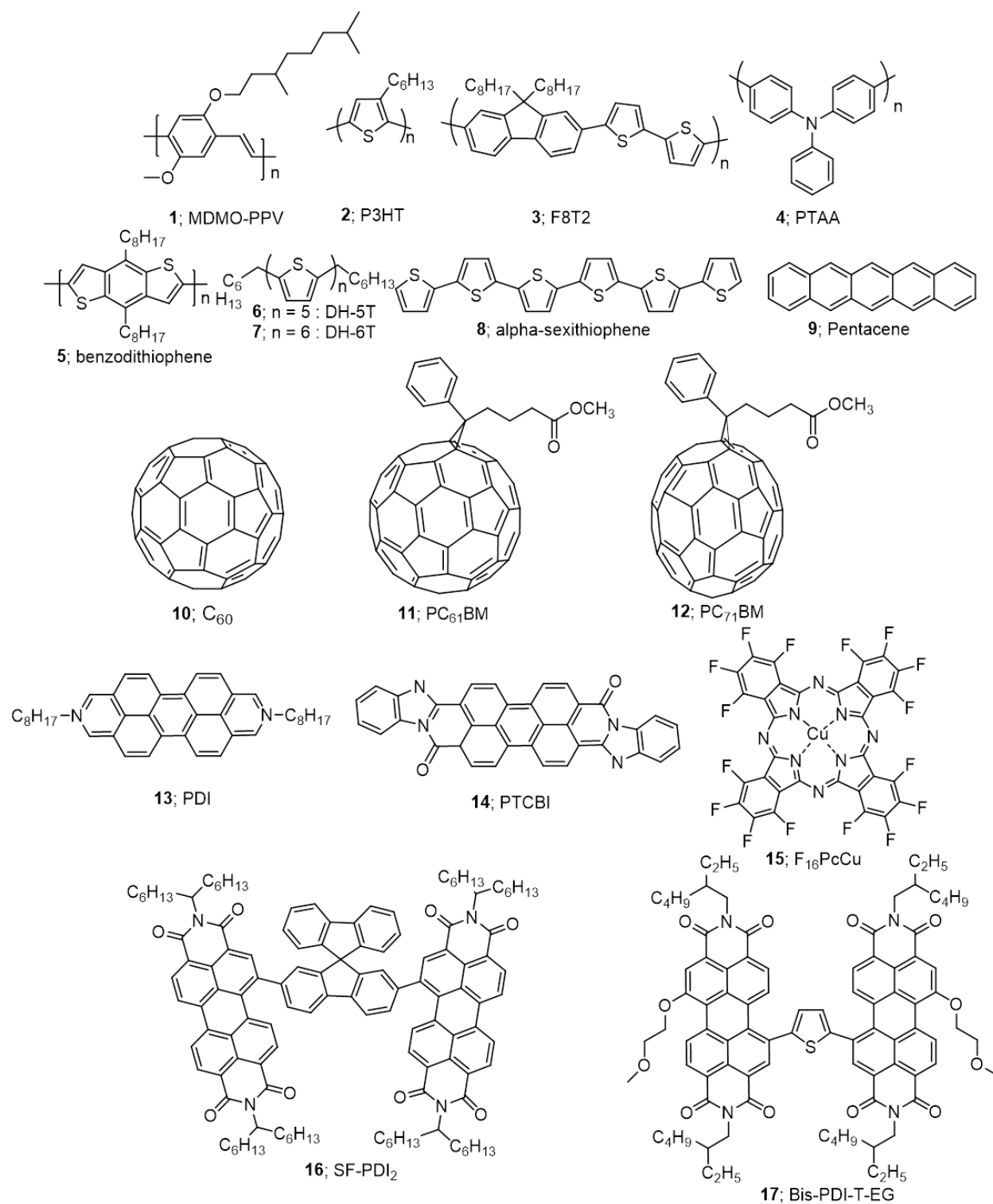


**Chart 1.1.** Examples (1-17) of organic semiconductors used in OSCs.



---

Buckminsterfullerene, C<sub>60</sub> (**10**; **Chart 1.1**) was the commonly used acceptor during the earlier days. It has a unique cage-like, fused ring structure, and has the ability to accept up to 6 electrons. For effective photoinduced electron transfer processes to occur, they need to be mixed with a hole transporting/electron donating material. However, due to the limited solubility of C<sub>60</sub>, their application was limited. In 1992, Wudl *et al.* have synthesized a derivative of fullerene, phenyl-C<sub>61</sub>-butyric acid methyl ester (**11**; PC<sub>61</sub>BM) which gained immense popularity in solar cells due to its enhanced solubility in organic solvents.<sup>31</sup> Another commonly used fullerene derivative is phenyl-C<sub>71</sub>-butyric acid methyl ester (**12**; PC<sub>71</sub>BM). Later, several other functionalized derivatives of fullerenes were also developed. However, PCBM exhibits weak absorption in the visible and near-infrared (NIR) regions, and thus it can only provide a weak channel for charge generation. This drawback of fullerenes led to the development of non-fullerene acceptors (NFAs). The most commonly utilized units for the synthesis of NFA are like naphthalene, perylene, and benzothiadiazole. Some of the well-known examples NFAs are perylene diimide (**13**; PDI), perylene-3,4,9,10-bis-benzimidazole (**14**; PTCBI), fluorinated Cu-phthalocyanine (**15**; F16PcCu), PDI dimer-based NFA (**16**; SF-PDI2 and **17**; bis-PDI-T-EG), etc. Various other examples of NFA in organic solar cells are shown in **Section 1.7**.

## 1. 4. Working principle of an organic solar cell

The aim of an OSC is to convert all the photons from the sunlight into charge carriers and thereby into electrical power. In general, the complete photovoltaic process can be sub-divided into four steps, which are schematically represented in **Figure 1.3**.<sup>32</sup>

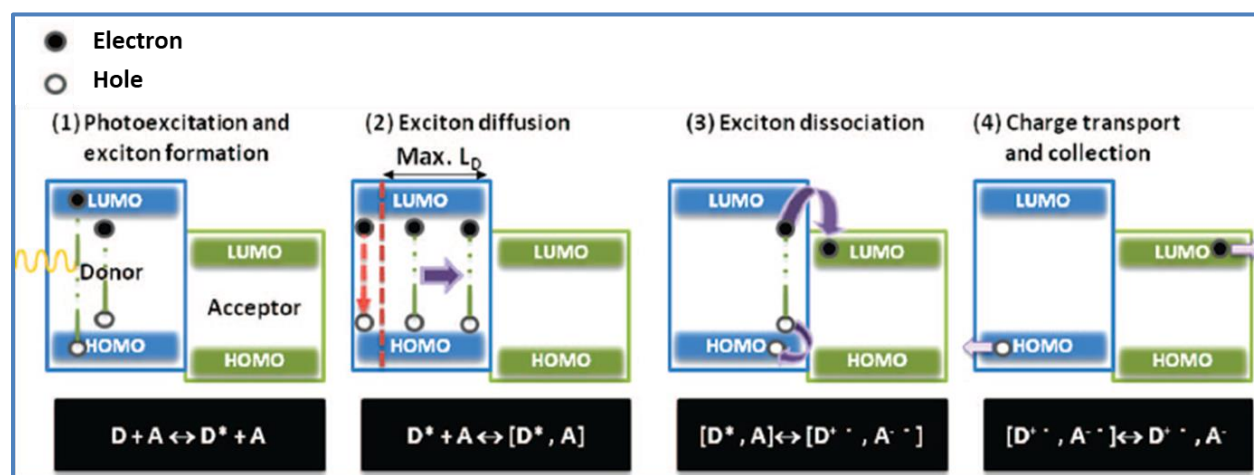


**Figure 1.3.** Schematic representation of the working mechanism for donor-acceptor heterojunction solar cells (Adapted from reference 32).

### 1.4.1. Photoexcitation and exciton formation

The first step involves the light absorption by the active layer (donor or acceptor) after the incident photons penetrate into the device. The efficiency of light absorption depends on the optical absorption coefficient of D and A in the film, which is strictly correlated to their molar absorptivity or molar extinction coefficient (the intrinsic capacity of light absorption by a single molecule), their density (the number of molecules for volume unit) and their absorption cross section (the orientation of the absorbing molecules with respect to the electromagnetic vector of the incident light). It must be noted that the light

absorption is also limited by the bandgap of the organic semiconducting material. For efficient photon absorption, its energy must be equal or greater than the bandgap to excite an electron from the HOMO into higher energy levels.

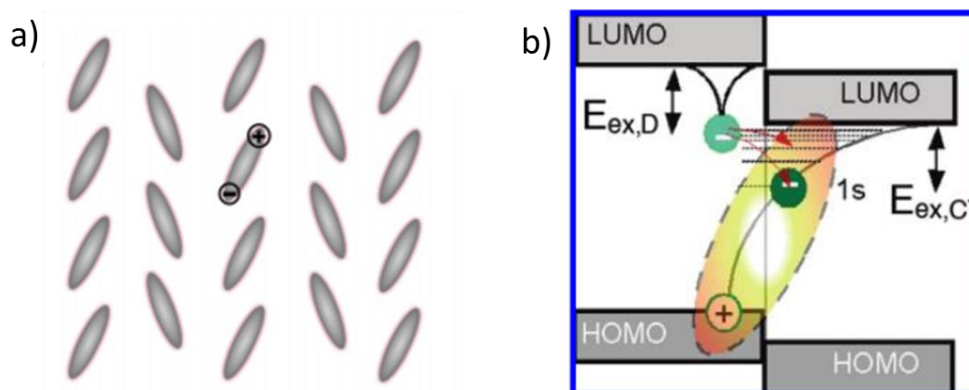


**Figure 1.4.** Schematic representation of a) Frenkel exciton in D molecule and b) CT exciton formation in organic molecules at the D-A interface (Adapted from reference 33 and 34).

Once the light is absorbed by the material, it produces electrostatically coupled electron-hole pairs called excitons. Depending on the strength of the Coulombic attraction, excitons are broadly classified into three major classes. They are the (1) Mott–Wannier exciton, (2) Frenkel exciton, and (3) charge-transfer exciton.<sup>34</sup> When the radius of the electron-hole pair is smaller than the unit cell dimension, it is called Frenkel exciton. On the other hand, if the generated excitons have sizes greater than the unit cell along with delocalized characteristics, it is referred to as Mott–Wannier exciton. In the presence of a donor-acceptor interface, the electrostatically bound electron and hole can get spatially separated across the interface, which is called a charge-transfer exciton. Mott–Wannier exciton is observed particularly in inorganic semiconducting materials

---

having a very small band gap. On the other hand, the Frenkel exciton and the charge-transfer exciton are seen in organic materials. A schematic representation of the Frenkel and a charge-transfer exciton is shown in **Figure 1.4**.

### **1.4.2. Exciton diffusion**

The coulombically bound electron-hole pairs are not capable of producing a photocurrent. In practice, the heterojunctions at donors and acceptors are made use to separate bound charges. The generated excitons should immediately get diffused and converted into charge carriers before getting deactivated to the ground state. The exciton diffusion length  $L_D$  is given by  $L_D = (D\tau)^{1/2}$ , where ' $D$ ' is the diffusion coefficient and ' $\tau$ ' is the exciton lifetime.<sup>35</sup> In general, exciton diffusion lengths in organic semiconductor materials are in the range of 10-20 nm.

### **1.4.3. Exciton dissociation**

At the heterojunction, the diffused photogenerated excitons break apart into free charge carriers by the formation of charge transfer exciton at the donor (D)-acceptor (A) interface.<sup>36</sup> The dissociation occurs due to the energy offset of the LUMO between D and A material at this interface. In this state, the electron finds itself on the acceptor and hole on the donor, this is the charge transfer state ( $D^+A^-$ ). Ultrafast studies have shown that in blends, photoinduced charge transfer takes place on a time scale of femtoseconds (fs). This is faster than the lifetime of photoluminescence (ns). At the charge transfer state,

there is a possibility of the hole and electron on the  $D^+$  and  $A^-$ , respectively to recombine leading to the regeneration of ground state.

#### 1.4.4. Charge transport and collection

Once the excitons have disassociated in the above mentioned process into charge carriers (electrons and holes), they must move efficiently toward the electrodes within their lifetimes. For this, the charge carriers need a driving force to reach the electrodes; this may happen due to various reasons as follows. i) The difference in the energy offset between the HOMO of donor and LUMO of the acceptor contributes to the field-induced drift of charge carriers. ii) Metals of different work function in contact with the active material like one low work function metal for the collection of electrons and one high work function metal for the collection of holes can act as a driving force for the collection of charges. iii) Transportation of charge carriers in the material happens either by drift or by diffusion, where the electric field and the gradient of the particle density are the respective forces driving the current. The drift current,  $j_{\text{Drift}}$  is defined by the charge carrier density ( $n$ ) and the drift velocity ( $V_D$ ),

$$j_{\text{Drift}} = -e(n_e v_{D,e} + n_h v_{D,h})$$

where ' $e$ ' is the elementary charge, ' $n_e$ ' is the density of electrons and ' $n_h$ ' is the density of holes.

The drift current can also be represented in terms of the mobility of electrons ( $\mu_e$ ), holes ( $\mu_h$ ) and the electric field,  $F$ , using the following equation,

$$j_{\text{Drift}} = e(n_e \mu_e + n_h \mu_h) F$$

The faster the electrons and holes can move away from each other, the more efficient their separation will be and eventually, leading to better PCE.

## 1.5. Photovoltaic characteristics

Current-voltage ( $J$ - $V$ ) curves represent an important and direct characterization technique for the evaluation of the efficiency of a solar cell. A schematic representation of the curve under dark and in an illuminated state is shown in **Figure 1.5**. From the illumination  $J$ - $V$  curve, five key parameters can be deduced:

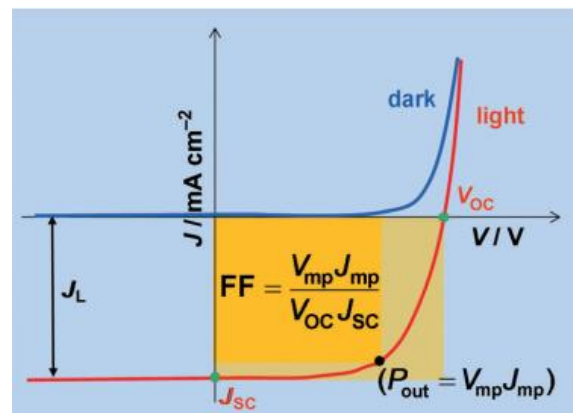


**Figure 1.5.** Current-voltage ( $J$ - $V$ ) characteristics of a typical solar cell. Essential parameters determining the cell performance are shown:  $V_{\text{OC}}$ : open-circuit voltage;  $J_{\text{SC}}$ : short-circuit current density;  $FF$ : fill factor;  $V_{\text{mp}}$  and  $J_{\text{mp}}$  are voltage and current, respectively, at which the power output of a device reaches its maximum (*Adapted from reference 37*).

### 1.5.1. Short circuit current ( $I_{\text{SC}}$ ) and short circuit current density ( $J_{\text{SC}}$ )

The short circuit current ( $I_{\text{SC}}$ ) is the current through the cell at zero applied voltage. It is directly related to the efficiency of free charge carrier generation and collection. The

light harvesting and charge separation also influence  $I_{SC}$ . The photovoltaic community often employs the short circuit current density ( $J_{SC}$ ), to remove the dependence of the solar cell area, which can be obtained by dividing  $I_{SC}$  by the cell surface area.

### 1.5.2. Open circuit voltage ( $V_{OC}$ )

Open circuit voltage ( $V_{OC}$ ) is the voltage at zero current, which represents the maximum photovoltage measured in a solar cell.  $V_{OC}$  is found to depend mainly on the energy level of the frontier orbitals of the donor and acceptor. Brabec *et al.* in 2006 demonstrated that the maximum theoretical ' $V_{OC}$ ' value can be found from HOMO of the donor and LUMO of the acceptor with the following equation,<sup>38</sup>

$$V_{OC} = \frac{1}{e} E_{\text{HOMO}}^{\text{donor}} - \left| E_{\text{LUMO}}^{\text{acceptor}} \right| - 0.3$$

where, ' $e$ ' is the elementary charge, ' $E_{\text{HOMO}}^{\text{donor}}$ ' is the HOMO of the donor material and ' $E_{\text{LUMO}}^{\text{acceptor}}$ ' is the LUMO of the acceptor material. In the above equation, 0.3 eV is the energy required for overcoming the exciton binding energy, it is therefore subtracted from the difference between donor HOMO and acceptor LUMO energy levels. In general, low  $V_{OC}$  is commonly observed for OSCs, largely due to imperfections in the film, by unfavorable morphology or resistances within the device.  $V_{OC}$  can be affected by charge recombination processes too, which cannot be completely avoided, resulting in a lower  $V_{OC}$ .

---

### 1.5.3. Fill factor ( $FF$ )

Fill factor ( $FF$ ) gives a picture of the quality of solar cell, which can be defined as the ratio of the ‘actual’ maximum output power to the ‘possible’ maximum power (where there are no losses due to series resistance and shunt resistance).<sup>37</sup> The  $FF$  can also be referred as a measure of the solar cell’s closeness to an ideal solar cell and depends on the photogenerated charge carriers and the fraction of that reaches the electrode. It is calculated by the following equation:

$$FF = \frac{P_{\max}}{I_{sc} \cdot V_{oc}}$$

where,  $P_{\max}$  is the maximal power corresponds to the orange area in **Figure 1.4**. It is the maximum power that can be supplied by the solar cell device. It follows that an ideal device would exhibit a  $FF$  of one. To date, the best polymer-based solar cells have shown a fill factor of 0.80.<sup>39</sup>

### 1.5.4. Power conversion efficiency

The efficiency of a solar cell is determined as the fraction of incident power which is converted into electricity. It is also referred to as power conversion efficiency (PCE), which represents the ratio where the output electrical power at the maximum power point on the IV curve is divided by the incident light power ( $P_{in}$ ). PCE can be represented by the equation:

$$PCE = \frac{P_{\max}}{P_{in}} = \frac{FF \cdot I_{sc} \cdot V_{oc}}{P_{in}}$$



## 1.6. Device architecture

The device architectures used for developing OSCs are broadly classified into two major categories - planar heterojunction (PHJ) and bulk-heterojunction (BHJ).

### 1.6.1. Planar heterojunction

In PHJ, the active materials are sandwiched in layers between the electrodes. The PHJ is further sub-divided into (i) single-layer, (ii) bilayer, and (iii) multi-layer devices:

#### 1.6.1.1 Single-layer organic solar cell

The preparation of first organic solar cell dates back in 1975 by Prof. C. W. Tang and Prof. A. C. Albrecht using chlorophyll-a (Chl-a) sandwiched between two metal electrodes of different work functions.<sup>40</sup> A layer of Chl-a was deposited by electrodeposition technique on quartz pre-coated by metal, and the cell resulted in a PCE of 0.001%. The solar cell of this kind is called a single layer organic photovoltaic cell. For efficient exciton dissociation in a single molecule, the device requires a potential of  $10^6 \text{ Vcm}^{-1}$  to overcome the Coulombic force of attraction between the electron-hole pair. However, such strong electric fields cannot be generated by the voltages at which organic solar cells normally operate. Another drawback of this architecture is that the photogenerated positive and the negative charges have to travel through the same material, which increases the recombination losses. These disadvantages eventually resulted in the development of bilayer planar heterojunction.

---

### 1.6.1.2. Bilayer planar heterojunction

Bilayer planar heterojunction cell was also first reported by Prof. C. W. Tang, where Cu-phthalocyanine was used as the donor and perylene-3,4,9,10-bis-benzimidazole [PTCBI (**13**); **Chart 1.1**] as the acceptor material sandwiched between two electrodes of different work functions.<sup>41</sup> The thicknesses of the donor and acceptor materials were 30 and 50 nm, respectively. The device architecture was anode/donor/acceptor/cathode. Indium tin oxide (ITO), a transparent conducting electrode, was used as the anode and silver as the cathode. The obtained PCE was 0.95% under  $75 \text{ mWcm}^{-2}$  with an impressive *FF* of 0.65. Later, various developments were made and the architecture was modified by incorporating hole transporting and exciton-blocking layers to the device architecture.

For efficient photoabsorption in a bilayer solar cell, the layers are required to have a thickness of at least 100 nm but the excitons may not be able to travel more than 10–20 nm before recombination.<sup>42</sup> As a result, most of the excitons generated in bilayer devices do not reach the interface and contribute to the charge carrier generation. Therefore, the PCEs of the bilayer solar cells usually lie in the range of 1.0-1.5%,<sup>43,44</sup> and approach a maximum of 2-5% in exceptional cases.<sup>45-49</sup>

### 1.6.1.3 Multilayer devices

In order to have an improved photon absorption by organic solar cells, materials with either broad absorption band were preferred or different narrow-band absorbers were

chosen which can be stacked or mixed in multiple junctions. When two (or more) donor materials with non-overlapping absorption spectra are used in layers, a broader range of the solar spectrum can be covered and such architecture is termed as multilayer (or tandem) solar cell. The voltage at which charges are collected in each sub-cell is closer to the energy of the photons absorbed in that cell. A record-breaking efficiency of 15% was reported by Forrest *et al.* by utilizing this kind of architecture.<sup>23</sup>

### **1.6.2. Bulk heterojunction**

Intermixing of donor and acceptor was proposed as a plausible solution to solve the problems associated with bilayer devices. This kind of active layer architecture is known as bulk-heterojunction (BHJ), which is schematically shown in **Figure 1.6**. In this structure, the thickness of the light absorbing material can be 100 nm or more. The intermixing of donor and acceptor can facilitate the creation of nanodomains in the order of 10-20 nm, which results in efficient dissociation of the generated excitons to charge carriers (holes and electrons). These charges can travel to the respective electrodes (holes to the anode and electrons to the cathode) through the interpenetrating donor/acceptor network with minimum recombination. The first prototype of BHJ was realized and experimentally verified by Heeger and co-workers in 1992.<sup>50</sup> The major requirement of the donor is to have an optical bandgap in the visible range of the solar spectrum. Light falling on the active layer is therefore efficiently absorbed by the donor and leads to the generation of highly energetic excitons (ca. 100 MeV). For the efficient diffusion and

dissociation of excitons and the transport of charge carriers, the active layer should have a bicontinuous interpenetrating network of donors and acceptors with a minimum number of defect sites.<sup>51</sup> The PCEs of BHJ architecture has reached an efficiency as high as 14.4% in a polymer solar cell by utilizing a polymer as a donor and a non-fullerene as acceptor.<sup>52</sup>

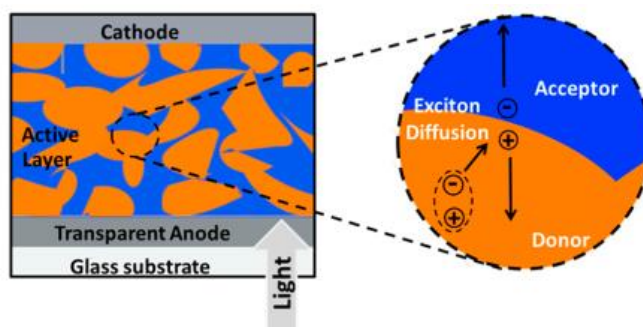


**Figure 1.6.** Simplified schematic representation describing the main processes in a bulk-heterojunction solar cell device. The light absorption by the active layer (predominantly donor) generates exciton, which diffuses towards the donor-acceptor interface where they separate into free charge carriers (holes and electrons). Holes move towards anode and electrons move to the cathode (*Adapted from reference 51*).

### 1.6.3. Conventional OSCs vs inverted OSCs

Conventional architecture is mainly of the type: ITO/PEDOT:PSS/Donor:Acceptor/Ca/Al, where, ITO is coated with PEDOT:PSS (poly(3,4-ethylenedioxythiophene)-poly(styrenesulfonate)) followed by the active layer of BHJ. PEDOT:PSS has an electron blocking behavior along with the ability to control the direction of current flow in conventional-architecture. Role of calcium is mainly to extract electrons from the bulk-heterojunction device. In order to complete the device architecture, a low work function metal electrode (Al) is evaporated as the top electrode. Even though the majority of

---

polymer-based solar cells are fabricated in this architecture, there are some inherent issues with device stability. The conducting ITO electrode when comes in contact with acidic PEDOT:PSS, it can get etched over a period of time.<sup>53</sup> Apart from this, low work function electrode such as Al on exposure to oxygen can lead to oxidation leading to device degradation and failure. Therefore, it was essential to have a device architecture that can remove PEDOT:PSS at the ITO interface and use non-vacuum deposited high work function metal electrodes at the top.

The drawbacks of the conventional device led to the development of inverted architecture.<sup>53</sup> Here, the flow of the charge collection is reversed and is suggested as a good device alternative. Importantly, the device durability and processing advantages compared to the conventional architecture attracted considerable attention of researchers. High work function metals that can be used as the top electrode are Au, Ag, Cu, etc. The use of high work function metals will offer better ambient interface device stability to the device. In this thesis, we have employed an inverted architecture to test the potential of the newly developed donor molecules.

## **1.7. Thiophenes-based conjugated materials**

Thiophenes are one of the most important classes of heterocyclic compounds in the field of material science and have attracted considerable attention of scientist across the globe due to its tunable optical and electronic properties by molecular design. Thiophene is a flat five-membered ring comprising of a sulfur atom, which has two lone-pair of

electrons out of which one participates in ring aromatization. The large size of a sulfur atom also enables high polarizability, which facilitates the electron donating and charge transport properties of thiophene derivatives. Selective modification of thiophene at  $\alpha$ - and  $\beta$ - positions of the ring enable versatile structures. For instance, the incorporation of the  $\alpha$ -linked thiophene units into oligomers render an efficient conjugation along the main chain while attaching long alkyl side-chains at the  $\alpha$ - or  $\beta$ -position guarantees solution processibility and self-assembly capability. Furthermore, multiple short intermolecular S...S nonbonding interactions can bring about highly ordered molecular arrays in the bulk solid state, possessing high charge carrier mobility along the  $\pi$ -stacking direction.

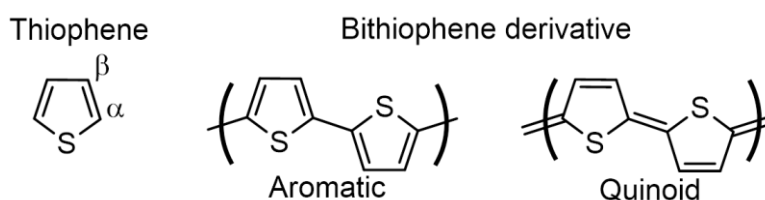


**Figure 1.7.** Schematic representation of thiophene; aromatic and quinoid structures of bithiophene derivatives.

Quinoid resonance structure of thiophene-based conjugated oligomers and polymers lead to an increase in rigidification and planarization of the backbone leading to significant restriction of the rotation between the rings. As a result, quinoid form exhibit higher energy and a lower bandgap compared to its corresponding aromatic form. **Figure 1.7** shows both the aromatic and quinoid form of a bithiophene unit. The degree of  $\pi$ -conjugation determines the electronic properties of thiophene-based oligomers and

polymers, which in turn affect the energy gaps, optical, electrical, and electrochemical properties.

### 1.7.1. Solution-processed thiophene-based polymers

In the class of *pi*-conjugated polymers for OPV applications, polythiophenes (**18**, PTs, **Figure 1.8**)<sup>54</sup> exhibits a unique combination of high thermal stability, electrical conductivity, processability, and possess most synthetic versatility. We can also access to a wide range of properties *via* facile modifications brought on the ring.

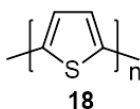


**Figure 1.8.** Chemical structure of *pi*-conjugated polythiophenes (**18**).

In the family of organic semiconductors, poly(3-hexylthiophene) (**2**; P3HT, **Chart 1.1**) is one of the most commonly used donor material investigated for BHJ solar cells. The development of this polymer started with the synthesis of 2,5-polythiophene (**18**), which was first reported by two research groups in the 1980s; Yamamoto *et al.* have synthesized this polymer through the polycondensation of 2,5-dibromothiophene using nickel as a catalyst.<sup>55</sup> Lin *et al.* have described another method for making the same polymer using a metal-catalyzed route.<sup>56</sup> However, due to poor solubility of the polymer, its application in optoelectronic devices was limited. In order to pursuit solubility, new alkylated thiophene polymers were developed. The first stable and soluble alkylated poly(3-alkylthiophene)s including P3HT was reported by Elsenbaumer and co-workers in

1985.<sup>54</sup> The polymerization reaction of 3-hexylthiophene resulted in three different P3HT isomers, hence control on the regioselectivity of the polymer was crucial for studying its optoelectronic properties. Widespread emergence of P3HT as a semiconducting material came with the development of synthetic methods that enable the production of highly regioregular P3HT with good control of the molecular weight.<sup>55</sup>

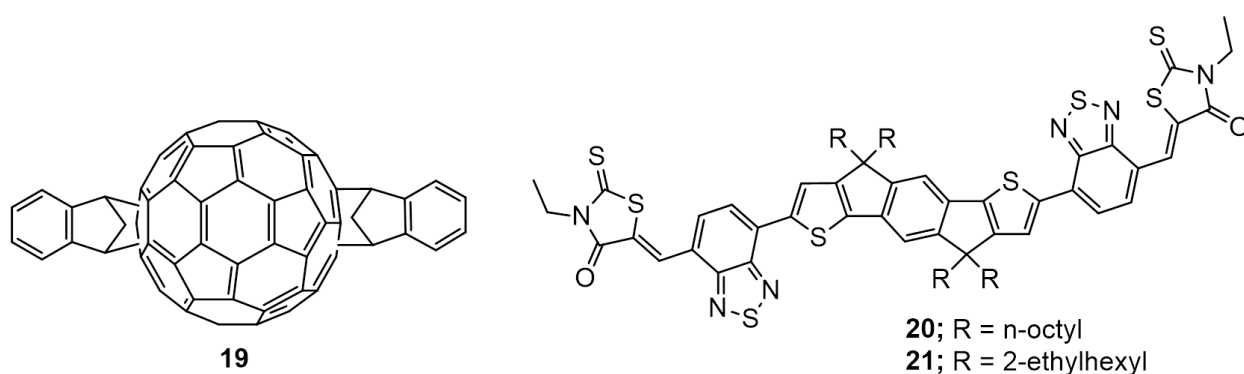


**Figure 1.9.** Chemical structures of fullerene indene- $C_{70}$  bisadduct (**19**) and small molecule acceptors (**20** and **21**) developed by McCulloch *et al.*

The first report of P3HT:PC<sub>61</sub>BM based solar cell gave a PCE of 2.8% under AM 1.5 and 100 mWcm<sup>-2</sup> spectral conditions ( $I_{sc}$ : 8.7 mAcm<sup>-2</sup>,  $V_{OC}$ : 580 mV,  $FF$ : 0.55).<sup>56</sup> The device exhibited a monochromatic external quantum efficiency as high as 76% at the maximum peak (550 nm) and the internal quantum efficiency was found to be close to 100%. Hence, photoinduced charge carrier recombination is negligible or even absent in these devices. In 2012, Li *et al.* have reported a high efficiency for P3HT with a new fullerene indene- $C_{70}$  bisadduct (**19**; **Figure 1.9**) as NFA.<sup>57</sup> A polymer solar cell (PSC) was fabricated with the device architecture as ITO/PEDOT:PSS/P3HT:**19** (1:1,w/w)/Ca/Al. The optimized PSC was based on the active layer blend (1:1, w/w) with



3 vol% 1-chloronaphthalene as an additive. The pre-thermal annealing of the active layer at 150 °C for 10 min, exhibited a PCE of 7.40% ( $V_{OC}$ : 0.87 V,  $J_{SC}$ : 11.35  $\text{mAcm}^{-2}$ ,  $FF$ : 0.75), under the illumination of AM1.5G, 100  $\text{mWcm}^{-2}$ . The high efficiency is ascribed to the strong absorption of the blend and optimized donor/acceptor interpenetrating network. Later in 2016, McCulloch *et al.* synthesized two new NFA derivatives by varying the alkyl chain length, (**20**; *n*-octyl) and (**21**; 2-ethylhexyl) comprised of central indacenodithiophene unit flanked by benzothiadiazole and *N*-ethylrhodanine as end group acceptor (**Figure 1.9**).<sup>58</sup> An inverted device was constructed and the active blends of P3HT:**20** or **21** (1:1) were spin-coated from chlorobenzene solution and the blend films were thermally annealed for 10 min at 130 °C to induce ordering to the polymer. Under simulated AM1.5G illumination at 100  $\text{mWcm}^{-2}$ , **20** gave an efficiency of 6.30% ( $J_{SC}$ : 13.9  $\text{mAcm}^{-2}$ ,  $V_{OC}$ : 0.72 V and  $FF$ : 0.60), whereas, the ethylhexyl derivative (**21**) gave an efficiency of 6.00% ( $J_{SC}$ : 12.1  $\text{mAcm}^{-2}$ ,  $V_{OC}$ : 0.76 and  $FF$ : 0.62). The oxidative stability of these devices was found to be higher than the benchmark P3HT:PCBM blend.

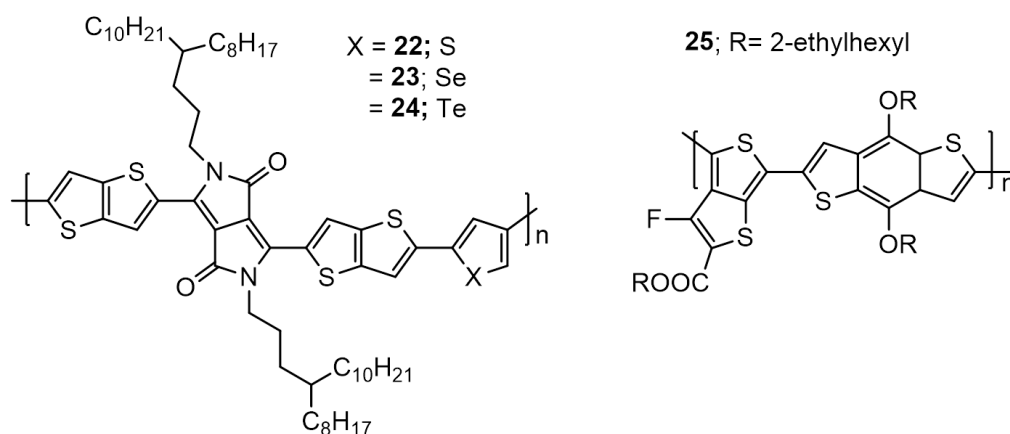


**Figure 1.10.** Chemical structure of polymers, **22-25**.

Apart from P3HT, numerous thiophene-based co-polymers were synthesized that performed equally well or better than that of P3HT. McCulloch and coworkers reported a series of thienothiophene and diketopyrrolopyrrole (DPP) based copolymers with thiophene, selenophene, and tellurophene co-monomers (**22-24**; **Figure 1.10**).<sup>59</sup> Bandgaps of the polymers are narrowed with the increased size of the chalcogen atoms due to LUMO energy level stabilization. The absorption of all three polymers extended up to the near-IR region and a high PCE of 8.8% was achieved in an inverted architecture of **22**:PC<sub>71</sub>BM device. Another important thiophene-based unit is benzodithiophene (BDT); the chemical structure of the unit shown in **Chart 1.1**. Wu and co-workers have reported an efficiency of 9.12% ( $J_{SC}$ : 17.2;  $FF$ : 0.72,  $V_{OC}$ : 0.74) efficiency based on a derivative of BDT, thieno[3,4-*b*]thiophene/benzodithiophene polymer (**25**, **Figure 1.10**).<sup>60</sup> This high efficiency was recorded by a blend of **23** with PC<sub>71</sub>BM in an inverted device structure. Here, poly[(9,9-bis(3'-(*N,N*-dimethylamino)propyl)-2,7-fluorene)-alt-2,7-(9,9-dioctylfluorene)] (PFN), an alcohol-/water-soluble conjugated polymer was used as ITO surface modifier in the device.

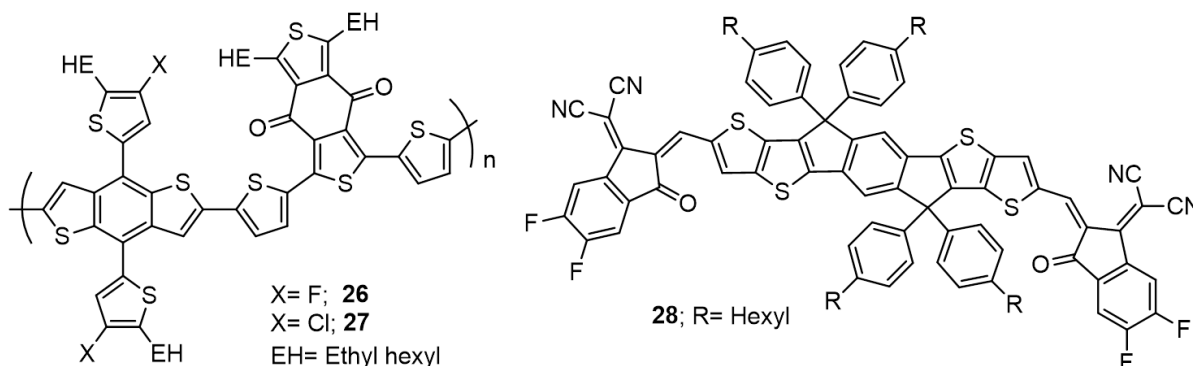


**Figure 1.11.** Chemical structures of donor polymer (**26** and **27**) and acceptor **28**.

Recently, many research groups are reporting modified BDT polymers having two-dimensional pi-conjugated groups. They generate better intermolecular interactions and photovoltaic performance than one-dimensional alkyl/alkoxy chains attached BDT counterparts (as shown above). Two such polymers were reported by the groups of Hao and Yang in 2018.<sup>52,61</sup> Hao *et al.* synthesized two co-polymers comprised of thiophene-substituted benzodithiophene (BDT) and dithiophene-4,8-dione units along with thiophene as pi-spacer (**26** and **27**; **Figure 1.11**). The thiophene side groups on the BDT unit are fluorinated in **26** and chlorinated in **27**. PSC was fabricated using the device architecture, ITO/ZnO/active layer/MoO<sub>3</sub>/Al. The fluorinated polymer gave PCE of 13.2%, while, chlorinated polymer yielded an efficiency of 14.4% when blended with the acceptor **28**. The theoretical calculations of these polymers clearly suggest that the replacement of fluorine with chlorine does not affect backbone but reduced the HOMO energy level of the polymer significantly. This highlights the critical role of chlorine in achieving highly efficient PSCs.

Yang *et al.* have reported highly efficient polymer photovoltaic materials by fine-tuning the side chains of benzodithiophene (BDT) unit (**29** and **30**). With the replacement of alkoxy chains in **29** with alkylthio chains in **30**, great enhancement of PCE was observed from 9.20% to 12.09%. A non-fullerene acceptor (**31**) was used for fabricating devices. The chemical structures of the donor polymers (**29** and **30**) and acceptor is (**31**) is shown in **Figure 1.12**.

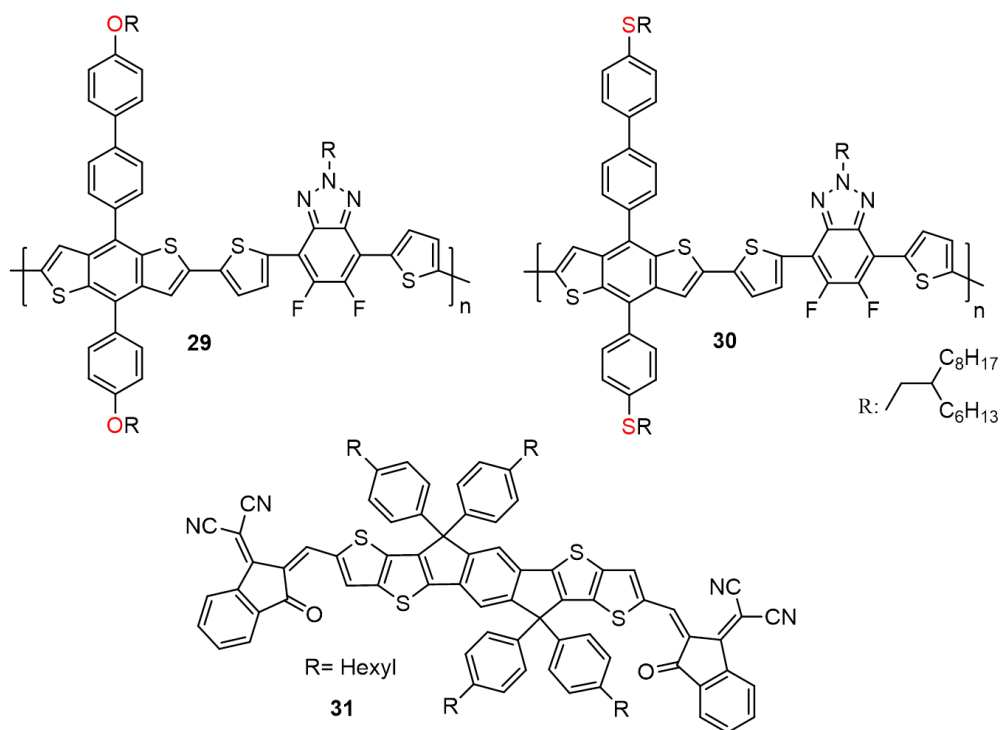


Figure 1.12. Chemical structures of the donor polymers (29 and 30) and acceptor (31).

### 1.7.2 Solution-processed thiophene-based oligomers

Polymers offer excellent solution-processing, film-forming properties and allow devices to be fabricated on plastic substrates for flexible devices. However, the polydispersity of molecular weights and difficulty in the purification of polymer results in batch to batch variation. This hampers the performance of the devices, reproducibility and hence commercialization. Oligomers, on the other hand, are monodisperse with molecular weights generally in the range of thousands, and their sizes are between those of small molecules (generally with molecular weights <1,000) and polymers (generally with molecular weights >10,000). They offer combined advantages such as defined molecular structure, definite molecular weight, easy purification, mass-scale production,

---

good batch-to-batch reproducibility, good solution processability, and film-forming properties.

Oligothiophenes have earned intense scientific interest over polythiophenes in the last few years due to the above mentioned advantages. In addition to that, they exhibit relatively very high stability, also offer excellent charge transport properties, and free from any structural defects. The absence of any twist in the backbone allows these molecules to crystallize, which make them suitable for X-ray single-crystal analysis and hence allow further structural engineering for developing devices with improved efficiencies. The past decade provided a variety of successful methods to prepare polythiophenes and their derivatives. Many of the latest oligothiophene syntheses are borrowed and adapted from these methods. Most of them provide methods for the synthesis of short oligothiophenes of less than 8 units. In this section, we will describe some of the historic and recent development in the area of oligothiophenes based organic solar cells.

In 2006, Bauerle *et al.* reported a low-bandgap oligothiophene,  $\alpha,\alpha'$ -bis(2,2-dicyanovinyl)-quinquethiophene (**32**, **Figure 1.13**) with two terminal electron-withdrawing dicyanovinyl (DCV) groups, resulting in an A–D–A type donor molecule.<sup>62</sup> The bandgap of the material is around 1.77 eV, and when it was blended with C<sub>60</sub> gave a PCE of 3.4% under 118 mWcm<sup>-2</sup> simulated sunlight.

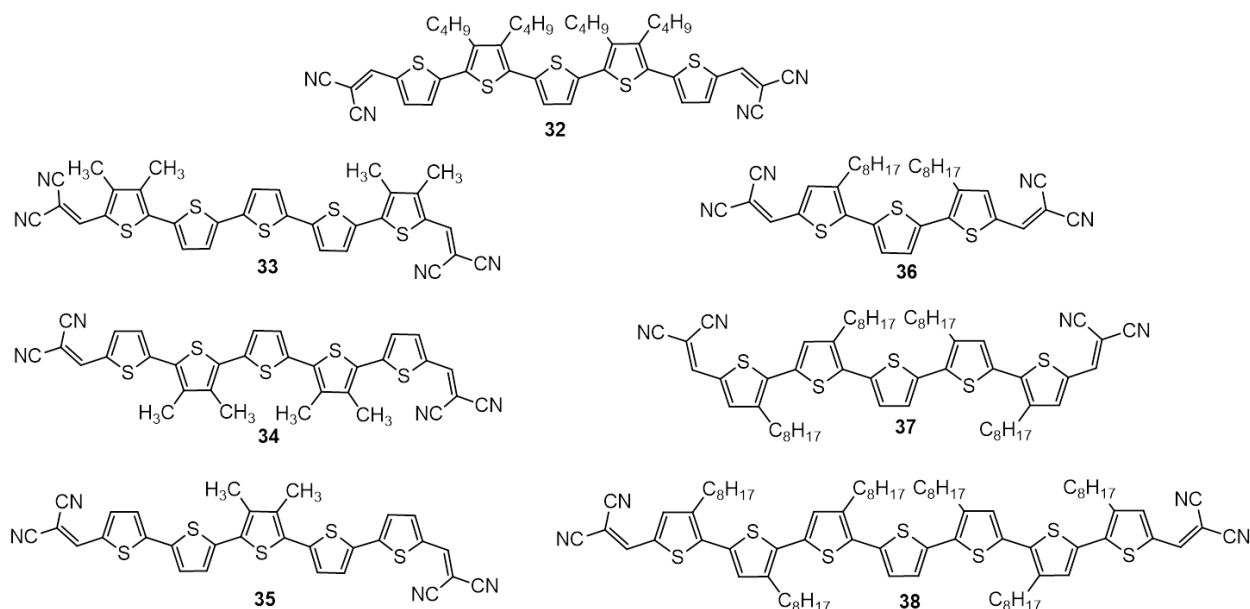


**Figure 1.13.** Chemical structures of A-D-A type oligothiophenes (**32-38**).

The same group later reported a series of molecules analog to that of **32** (**33-35**; **Figure 1.13**).<sup>63</sup> The obtained PCEs were in the range of 4.8-6.9% on blending with C<sub>60</sub>, where the highest was obtained for **35**. Co-deposition under vacuum was employed for coating the active layers of all these molecules due to their poor solubility.

Later, various groups started working for the development of solution processable oligothiophene derivatives substituted with long alkyl chains. The A-D-A type oligomers, **36-38**, reported by Liu *et al.* are typical examples (**Figure 1.13**).<sup>63</sup> The photophysical and electrochemical properties of molecules were studied in detail. It was observed that the bandgap became significantly smaller with increasing the number of thiophene units (1.90, 1.74, and 1.68 eV, respectively). The molecule with the lowest bandgap (**38**) was used as the donor to fabricate solution processed BHJ cells with PC<sub>61</sub>BM, and a PCE of 2.45% ( $J_{SC}$ : 10.23 mAcm<sup>-2</sup>;  $V_{OC}$ : 0.82 V and  $FF$ : 0.29) was obtained.<sup>64</sup> Further, device

optimization gave a PCE of 3.7% with a high  $J_{SC}$  of  $12.4 \text{ mAcm}^{-2}$  and  $V_{OC}$  of 0.88 V, but a low  $FF$  of 0.34. The low  $FF$  was attributed to the poor film quality caused by lower solubility of the molecule.

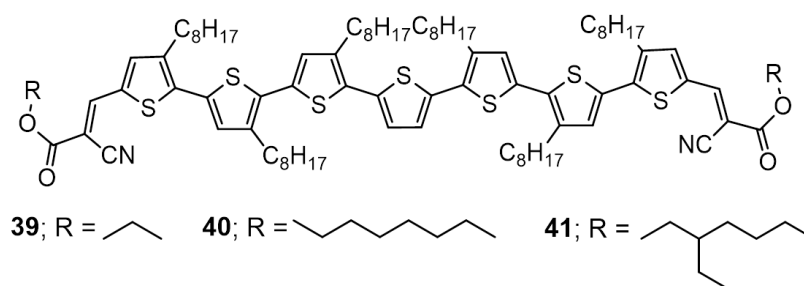


**Figure 1.14.** Chemical structures of the oligomers (**39-41**).

In order to improve the solubility and solution processability, electron-withdrawing groups like alkyl cyanoacetate were used instead of DCV as the terminal unit in oligothiophenes (**Figure 1.14, 39-41**).<sup>65</sup> Rational designing and control on the position and density of different alkyl chains on the acceptor unit not only increase the solubility of materials in various organic solvents for spin-casting devices but also enhance their packing ability as well as solid-state miscibility with fullerenes. All the three derivatives obtained efficiencies between 4-5% using a conventional architecture using  $\text{PC}_{61}\text{BM}$  as acceptor.

To obtain a stronger absorption of the solar spectrum, dye chromophores such as *N*-ethylrhodanine (**42**), 1,3-dimethylpyrimidine-2,4,6(1*H*,3*H*,5*H*)-trione (**43**), rhodanine derivative (**44**), 1,3-indanedione (**45**) and its derivatives (**46-47**) are introduced as end groups (**Figure 1.15**).<sup>63</sup>

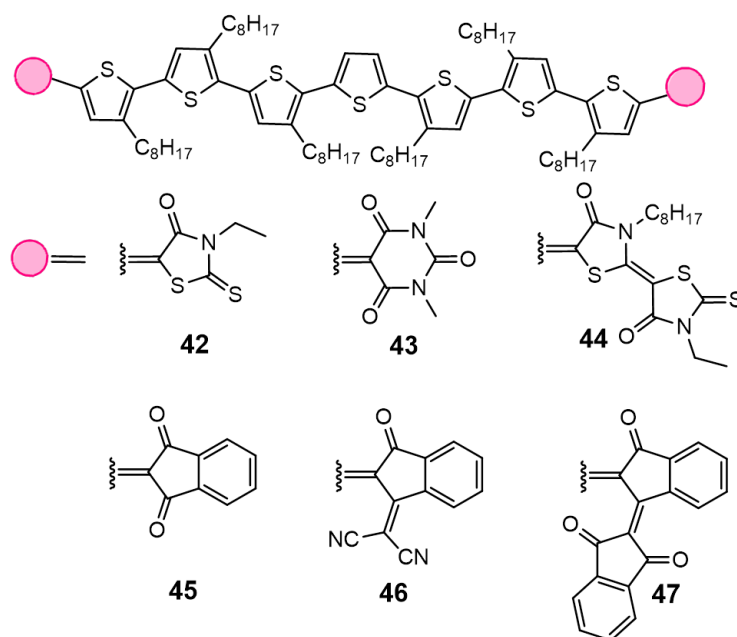


**Figure 1.15.** Chemical structures of small molecules; **42-47**.

All these oligomers exhibited red-shifted absorption and a higher absorption coefficient due to extended conjugation. **42** showed stronger solar absorption in addition to good film quality. A conventional device was fabricated with PC<sub>61</sub>BM as acceptor and resulted in a PCE of 6.10% ( $V_{OC}$ : 0.92 V,  $J_{SC}$ : 13.98 mA cm<sup>-2</sup>,  $FF$ : 0.47). **43** exhibited an efficiency of 4.05% ( $V_{OC}$ : 0.90 V,  $J_{SC}$ : 7.54 mA cm<sup>-2</sup>,  $FF$ : 0.60), while **44** gave a PCE of 2.46% ( $V_{OC}$ : 0.92 V,  $J_{SC}$ : 6.77 mA cm<sup>-2</sup>,  $FF$ : 0.39). The low PCEs of these compounds were believed to be due to their lower hole mobilities. Chen *et. al.* synthesized **45-47**, among them **45** exhibited the highest efficiency of 4.93% with a high  $FF$  of 0.72, under illumination of AM.1.5, 100 mWcm<sup>-2</sup>. **46** had an unexpected low solubility which limited its application in BHJ. The twisted molecular architecture of **47** leads to poor solid-state packing and low lying LUMO molecule, which gave a very low efficiency of 0.66%.



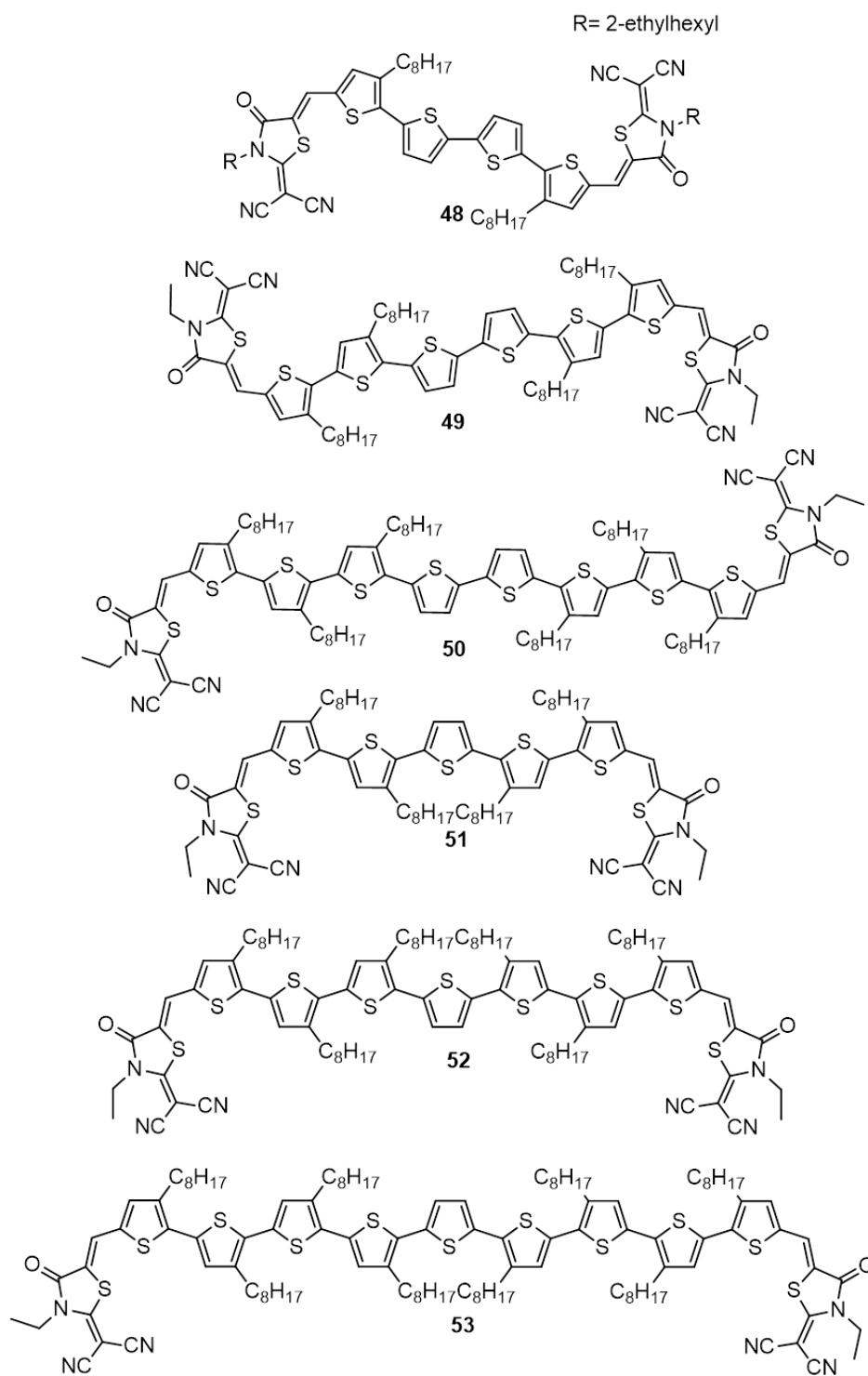
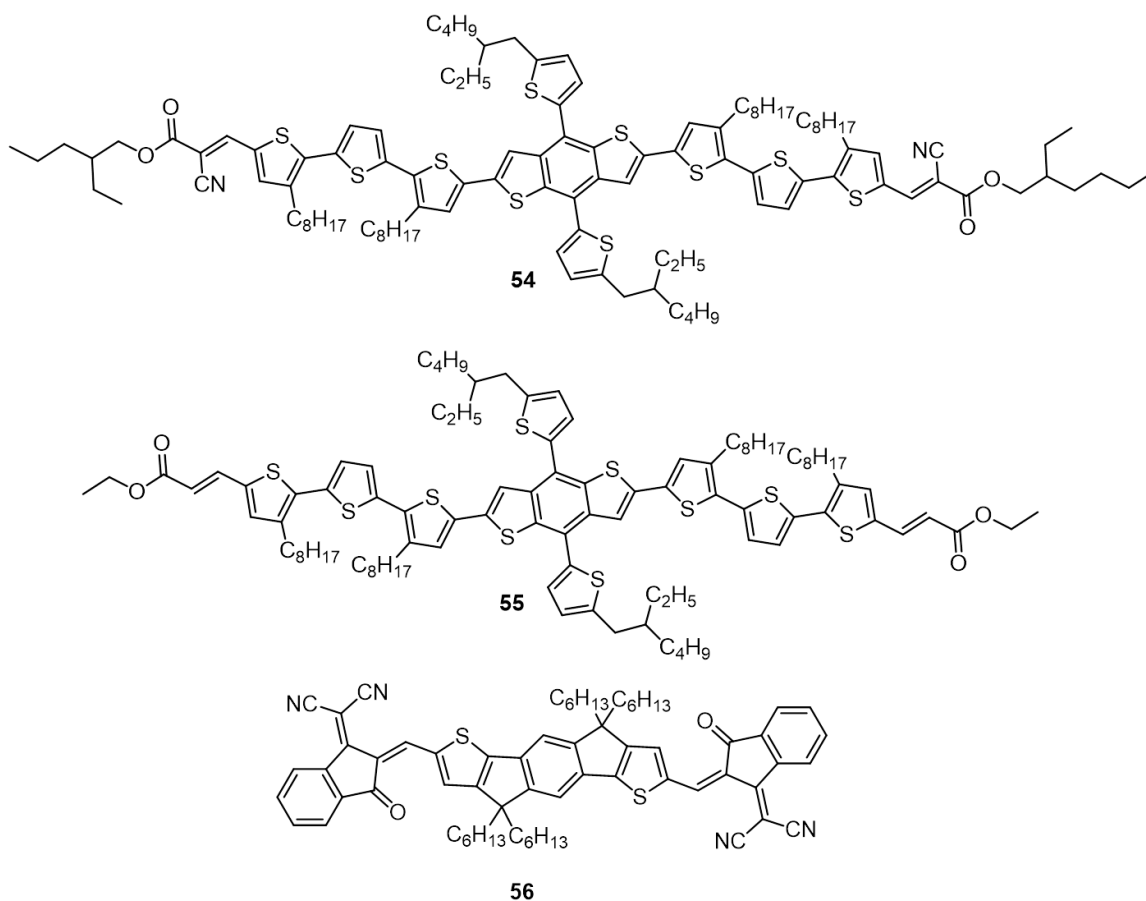


Figure 1.16. Chemical structures of oligothiophenes (48-53) synthesized by *Chen et al.*

---

In 2015, Chen *et al.* have reported another series of simple oligomers of the type A-D-A (**48-53**; **Figure 1.16**) having linear thiophenes as the donor unit and 2-(1,1-dicyanomethylene)rhodanine as the end group acceptor.<sup>64</sup> All are made of similar backbones but different conjugation lengths and spatial symmetry. Except **48**, all other compounds (**49-53**) yielded good photovoltaic performances with efficiencies over 6.0%. **48** exhibited poor PCE of 0.24%, which could be attributed to a narrow absorption in the UV-vis region when compared to other derivatives. This was due to the shorter conjugation length and a large bandgap (1.77 eV). Interestingly, among the other derivatives, an odd-even effect was observed in the  $J_{SC}$  and PCE. Relatively, higher PCE was observed for oligomers which are composed of an odd number of thiophene units (**49**, **51** and **53**; 7.8 to 9.8%). These oligomers have an axisymmetric structure and therefore exhibited larger dipole moment differences between the ground and excited states. The large dipole moment change when going from the ground to the excited state can lower the Coulombic binding energy of the exciton. This facilitates intramolecular charge dissociation and contributes to the high  $J_{SC}$ . A notably high PCE of 10.10% was achieved for the devices based on molecule **51** ( $J_{SC}$ : 15.88 mAcm<sup>-2</sup>;  $V_{OC}$ : 0.92 V;  $FF$ : 0.69).

In 2017, Zhang and co-workers reported donors (**54**, **55**) of the type A-D-A.<sup>65</sup> They are composed of two-dimensional benzodithiophene central core flanked by alkylated terthiophene units as pi-spacers but different end groups (**Figure 1.17**).



**Figure 1.17.** Chemical structures of small-molecule donors **54**, **55** and low bandgap small molecule, **56** as acceptor.

A non-fullerene small molecules acceptor, 2,2'-((2Z,2'Z)-((4,4,9,9-tetrahexyl-4,9-dihydro-s-indaceno[1,2-*b*:5,6-*b'*]dithiophene-2,7-diyl)bis(methanylylidene))bis(3-oxo-2,3-dihydro-1H-indene-2,1-diylidene))dimalo-nitrile (IDIC; **56**) was used for making devices. The donors and acceptor possess complimentary absorption spectra. A conventional device of the structure, ITO/PEDOT:PSS/donor:IDIC/PDINO/Al was fabricated to investigate the photovoltaic properties. PDINO is a perylenediimide based electron transporting layer. The as-cast device of **54:56** exhibited a PCE of 5.45%, while it enhanced to 8.48% after thermal annealing at 100 °C for 10 min. After being annealed

at 115 °C for 10 min, PCE was further improved to 10.11% ( $J_{SC}$ : 15.18 mA cm<sup>-2</sup>;  $V_{OC}$ : 0.91 V;  $FF$ : 0.73). The as-cast OSCs based on **55:56** gave a PCE below 1%. After heating at 110 °C for 10 min, the PCE was further improved to 5.32% ( $J_{SC}$ : 10.77 mAcm<sup>-2</sup>;  $V_{OC}$ : 0.76 V;  $FF$ : 0.64).

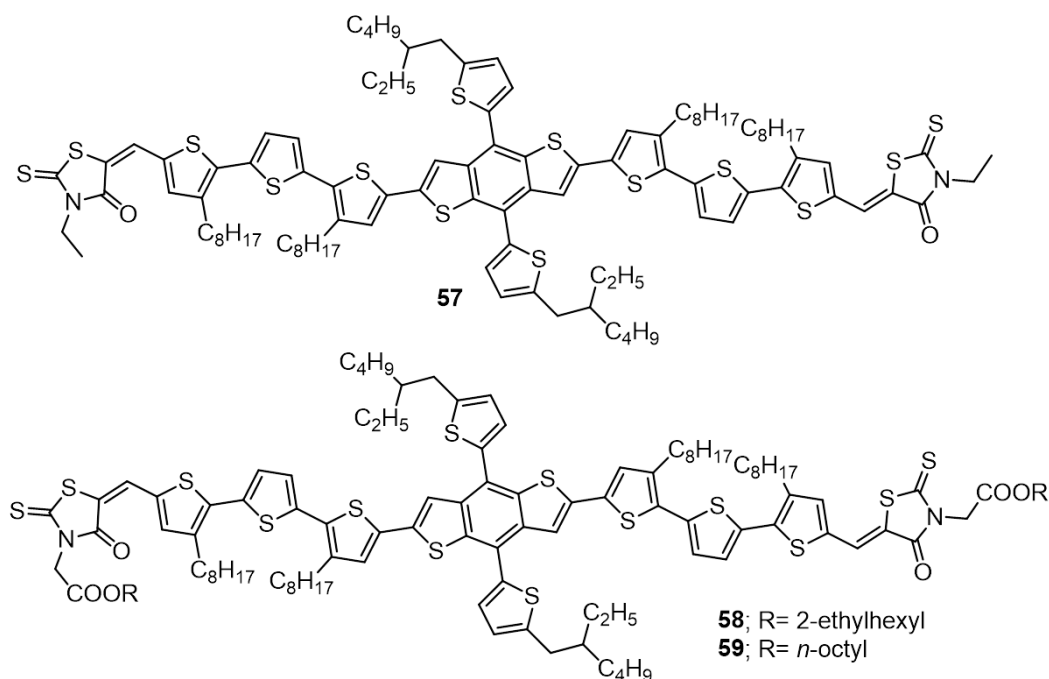


**Figure 1.18.** Structures of small molecule donors, **57-59**.

Very recently, Liang and co-workers reported another set of donors (**57-59**; **Figure 1.18**) having BDT central core and a backbone similar to the above mentioned examples.<sup>66</sup> The acceptor end groups were rhodanine (**57**) and esterified rhodanine isomers (**58** and **59**). These oligomers were blended with the acceptor, **56** and the photovoltaic parameters were compared. The conventional devices of esterified rhodanine isomers (**58** and **59**) gave an efficiency of 9.01% and 8.36%, respectively. However, the devices of **57** gave an efficiency of 7.61%. The results suggest that the

rhodanine-esterified donors are promising candidates than rhodanine. The carrier recombination analyses through light intensity-dependent studies suggested that devices based on **59** exhibited low bimolecular recombination losses but pronounced trap-induced recombination. On the other hand, both bimolecular and trap-assisted recombination losses in the devices of **58** was low. This might be the reason behind higher efficiency for **58** than **59**.

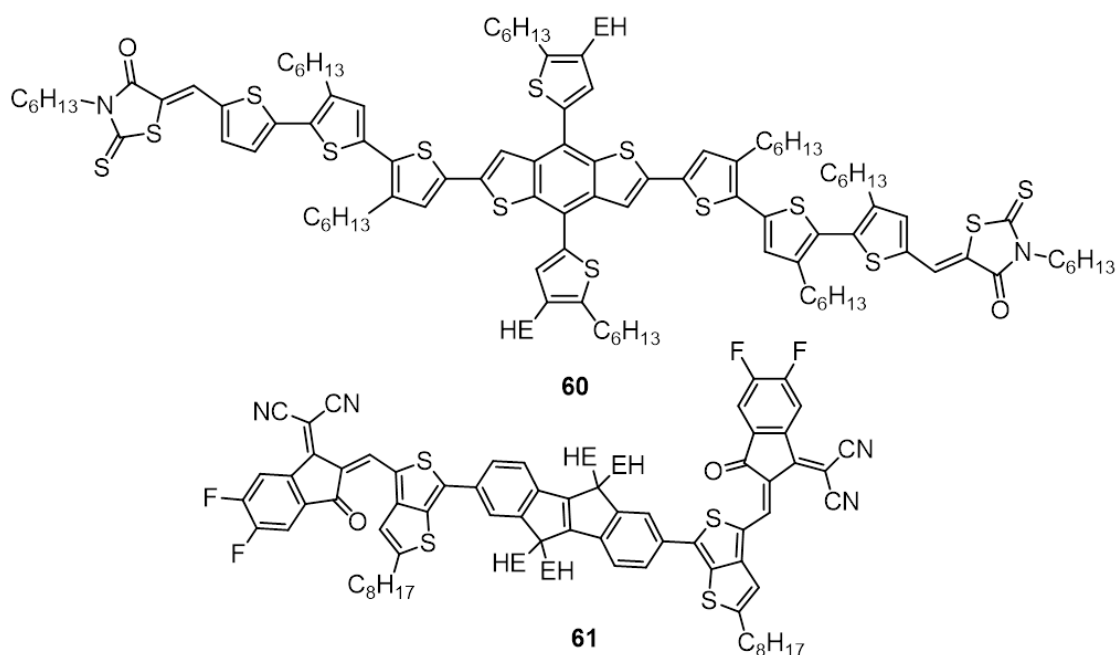


**Figure 1.19.** Chemical structure of small molecules, **60** and **61**.

In 2018, Zhu *et al.* reported a highly efficient ternary solar cell using combinatory photoactive blends.<sup>67</sup> The concept of employing multiple light-absorbing materials to broaden the absorption spectrum has now been recognized as an efficient approach to realize high PCE in ternary organic photovoltaics (TOPVs). Authors have made use of this concept to fabricate ternary solar cells, for comparison purpose, they have also made

binary solar cells. They have utilized **60** as a donor composed of benzodithiophene as the central core, terthiophene as the pi-spacer and end-functionalized with rhodanine as acceptor, a low bandgap small molecule (**61**) and PC<sub>71</sub>BM were used as acceptors (**Figure 1.19**). A conventional device structure consisting of **60**:PC<sub>71</sub>BM (1:1) exhibited an efficiency of 9.03%, while, **60**:**61** (1:1) showed a PCE of 6.82%. The ternary blend of **60**:**61**:PC<sub>71</sub>BM (1:0.4:1) after solvent vapour annealing (tetrahydrofuran) showed a very high PCE of 13.63% ( $J_{SC}$ : 19.50 mAcm<sup>-2</sup>;  $V_{OC}$ : 0.94V;  $FF$ : 0.73). This device had the combined advantage of both fullerene and non-fullerene acceptor and hence exhibited a high PCE.

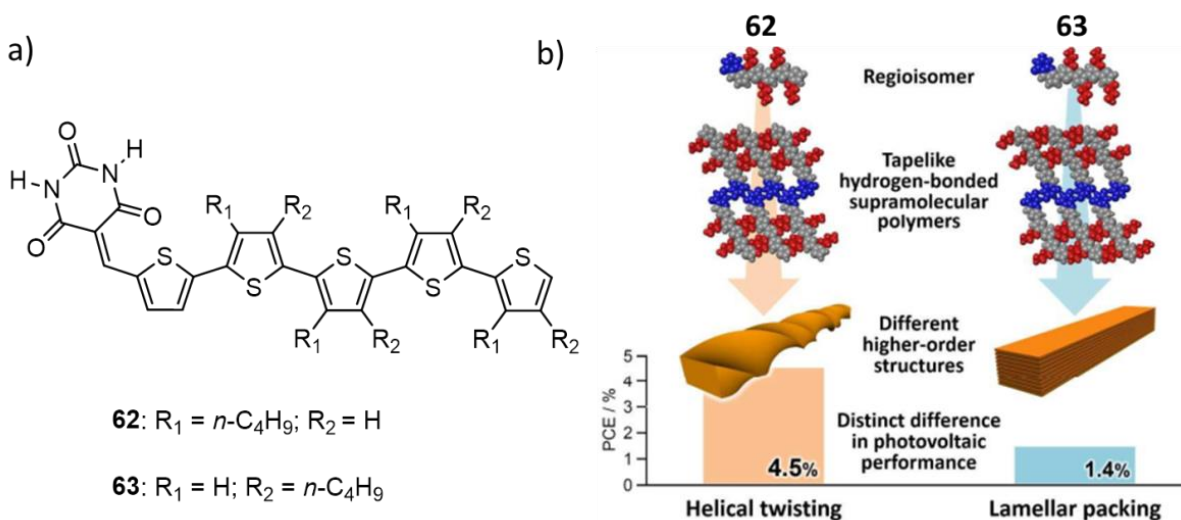


**Figure 1.20.** a) Molecular structures of barbiturated oligothiophenes, **62** and **63**, and b) their hydrogen-bonded motifs and self-assembled nanostructures with the best PCEs of the optimized BHJ solar cells (*Adapted from reference 64*).

In 2018, Yagai *et al.* have studied the impact of the helical organization of thiophene oligomers on photovoltaic properties. For this purpose, the authors have synthesized barbiturated oligothiophene supramolecular polymers with the only difference in the

---

position of the alkyl chain (**62** and **63**; **Figure 1.20**).<sup>68</sup> A tape-like organization was observed for **62**, that was hierarchically organized into helical nanofibers as confirmed by scanning tunneling microscope (STM), transmission electron microscopy (TEM) and atomic force microscopy (AFM) analysis. **63** also formed tape-like supramolecular polymer but it further reorganizes into 3D lamellar agglomerates. Due to a notable difference in the hierarchical organization, a remarkable difference in the PCE of these oligomers in BHJ solar cells was observed. The blends of **62**:PC<sub>71</sub>BM gave a PCE of 4.50%, while **63**: PC<sub>71</sub>BM gave a PCE of 1.39%. Hence, this study demonstrated that control on primary molecular arrays as well as regulating higher order structure is of paramount importance to utilize molecular organization in practical devices.

## 1.8. Objective of the present investigation

Literature has clearly outlaid that thiophene-based donors represent one of the best classes of donor materials for organic solar cell application due to their relatively good stability, light harvesting property, and ease of functionalization. Inspired by the recent progresses in the design of thiophene systems for OSCs, we have set our objective to explore the controlled self-assembling properties of custom designed thiophene derivatives and study their structure-property-device performance relationship. Our first objective was to explore how small structural modification in thiophene oligomers can bring about an effect on the molecular and supramolecular properties as well as on the photovoltaic properties. We were also interested to study how this could, in turn, control

---

the intrinsic and fundamental properties such as the p/n-polarity of organic semiconductors in a BHJ solar cell. To study this aspect, we have designed two acceptor–donor–acceptor type semiconducting thiophene oligomers end-functionalized with oxazolone/isoxazolone derivatives. The second objective of our study is to find the fundamental reasons for the improvement in device performance upon solvent engineering in detail. For this purpose, we have planned to synthesize oligomers having *N*-ethylrhodanine as acceptor, but different central core like thiophene, bithiophene, and thienothiophene connected through thiophene pi-linker (alkylated terthiophene). From the literature background, we have envisaged that precise supramolecular organization of the materials play a crucial role in the device efficiency. In this line, we have planned to study the preferential packing of thiophene oligomers induced through rational molecular designing and self-assembly. To study this, we have designed two acceptor-donor-acceptor type oligothiophene derivatives, with similar central part (thienothiophene), which is flanked by dioctyl terthiophenes on either side but with different acceptor end groups, 2-(1, 1-dicyanomethylene)rhodanine or *N*-octyl rhodanine. Such supramolecular control over the chromophore packing not only help to tune the direction of charge carrier transport in organic semiconductors but also helpful in developing functional and efficient photovoltaic and thin-film transistor devices.

## 1.9. References

1. Y.-B. Cheng, *Nature* **2016**, 539, 488–489.



2. M.K. Nazeeruddin, *Nature* **2016**, 538, 463–464.
3. N. Banerji, *Nat. Mater.* **2017**, 16, 503–505.
4. J.D. Major, R.E. Treharne, L.J. Phillips, K. Durose, *Nature* **2014**, 511, 334–337.
5. C. Battaglia, A. Cuevas, S. De Wolf, *Energy Environ. Sci.* **2016**, 9, 1552–1576.
6. J.D. Poplawsky, W. Guo, N. Paudel, A. Ng, K. More, D. Leonard, Y. Yan, *Nat. Commun.* **2016**, 7, 12537.
7. S.B. Darling, F. You, *RSC Adv.* **2013**, 3, 17633–17648.
8. R.F. Service, *Science* **2011**, 332, 293.
9. M. Kaltenbrunner, M.S. White, E.D. Głowacki, T. Sekitani, T. Someya, N.S. Sariciftci, S. Bauer, *Nat. Commun.* **2012**, 3, 770.
10. D. Angmo, T.T. Larsen-olsen, F.C. Krebs, *Mater. Today* **2012**, 15, 36–49.
11. J.-S. Wu, S.-W. Cheng, Y.-J. Cheng, C.-S. Hsu, *Chem. Soc. Rev.* **2014**, 44, 1113–1154.
12. H. Youn, H.J. Park, L.J. Guo, *Small* **2015**, 11, 2228–2246.
13. C. Brabec, U. Scherf, V. Dyakonov, *Organic Photovoltaics: Materials, Device Physics, and Manufacturing Technologies*, 2nd ed.; Willey: New York, NY, USA, **2014**.
14. D. Liu, Q. Zhu, C. Gu, J. Wang, M. Qiu, W. Chen, X. Bao, M. Sun, R. Yang, *Adv. Mater.* **2016**, 28, 8490–8498.
15. H. Bin, L. Gao, Z. Zhang, Y. Yang, Y. Zhang, C. Zhang, S. Chen, L. Xue, C. Yang, M. Xiao, *Nat. Commun.* **2016**, 7, 13651.
16. D. Deng, Y. Zhang, J. Zhang, Z. Wang, L. Zhu, J. Fang, B. Xia, Z. Wang, K. Lu, W. Ma, *Nat. Commun.* **2016**, 7, 13740.
17. S. Holliday, R.S. Ashraf, A. Wadsworth, D. Baran, S.A. Yousaf, C.B. Nielsen, C. Tan, S.D. Dimitrov, Z. Shang, N. Gasparini, *Nat. Commun.* **2016**, 7, 11585.
18. A. Zhang, C. Li, F. Yang, J. Zhang, Z. Wang, Z. Wei, W. Li, *Angew. Chem. Int. Ed.* **2017**, 56, 2694–2698.

- 
19. T.D. Nielsen, C. Cruickshank, S. Foged, J. Thorsen, F.C. Krebs, *Sol. Energy Mater. Sol. Cells* **2010**, *94*, 1553–1571.
  20. The future is light: Organic solar film by Heliatek. Available online: <http://www.heliatek.com>.
  21. Konark.com. Available online: <http://www.konarka.com>.
  22. NREL Transforming ENERGY: <https://www.nrel.gov/pv/>
  23. X. Che, Y. Li, Y. Qu, S. R. Forrest, *Nat. Energy* **2018**, *3*, 422–427.
  24. Heliatek- The future is light: <https://www.heliatek.com/en/press/press-releases/details/new-heliatek-solar-energy-facade>
  25. [https://www.photonics.com/Articles/Heliatek\\_Integrated\\_Organic\\_Photovoltaic\\_Project/a62857](https://www.photonics.com/Articles/Heliatek_Integrated_Organic_Photovoltaic_Project/a62857)
  26. V. Coropceanu, A. Demetrio, S. Filho, Y. Olivier, R. Silbey, J. Bredas, *Chem. Rev.* **2007**, *107*, 926–952.
  27. M. V Jacob, *Electronics*, **2014**, *3*, 594–597.
  28. L. Dou, Y. Liu, Z. Hong, G. Li, Y. Yang, *Chem. Rev.* **2015**, *115*, 12633–12665.
  29. F. Bures, *RSC Advances*, **2014**, *4*, 58826–58851.
  30. S. Gunes, H. Neugebauer, N. S. Scariciftci, *Chem. Rev.* **2007**, *107*, 1324–1338.
  31. F. Wudl, *Acc. Chem. Res.* **1992**, *25*, 157161.
  32. Y.-J. Cheng, S.-H. Yang, C.-S. Hsu, *Chem. Rev.* **2009**, *109*, 5868–923.
  33. D. Qi, H. Su, M. Bastjan, O. D. Jurchescu, T. M. Palstra, A. T. S. Wee, M. Rubhausen, A. Ruydy, *Appl. Phys. Lett.* **2013**, *103*, 113303.
  34. X. Zhu, Q. Yang, M. Muntwiler, *Acc. Chem. Res.* **2009**, *42*, 1779–1787.
  35. Y. Tamai, H. Ohkita, H. Benten, S. Ito, *J. Phys. Chem. Lett.* **2015**, *6*, 3417–3428.
  36. J. Singh, M. Narayan, D. Ompong, F. Zhu, *J. Mater. Sci. Mater. Electron* **2017**, *28*, 7095–7099.
  37. A. Mishra, P. Bäuerle, *Angew. Chemie Int. Ed.* **2012**, *51*, 2020–2067.
  38. M.C. Scharber, D. Mühlbacher, M. Koppe, P. Denk, C. Waldauf, A. J. Heeger, C. J. Barbec, *Adv. Mater.* **2006**, *18*, 789–794.

- 
39. X. Guo, N. Zhou, S.J. Lou, J. Smith, D. B. Tice, J. W. Hennek, R. P. Ortiz, J. T. L. Navarrete, S. Li, J. Strzalka, L. X. Chen, R. P. H. Chang, A. Facchetti, T.J. Marks, *Nat Photonics* **2013**, 7, 825–833.
  40. C. W. Tang, A. C. Albrecht, C. W. Tang, A. C. Albrecht, *J. Chem. Phys.* **1975**, 62, 2139–2149.
  41. C. W. Tang, *Appl. Phys. Lett.* **1986**, 48, 183–185.
  42. B. Aldo, T. Wagner, *Synth. Met.* **2014**, 190, 20–26.
  43. B. D. Wöhrle, D. Meissner, *Adv. Mater.* **1991**, 3, 129–138.
  44. J. J. M. Halls, K. Pichler, R. H. Friend, S. C. Moratti, A. B. Holmes, *Appl. Phys. Lett.* **2012**, 68, 3120–3122.
  45. R. Fitzner, E. Reinold, A. Mishra, E. Mena-osteritz, H. Ziehlke, C. Körner, K. Leo, M. Riede, M. Weil, O. Tsaryova, A. Weiß, C. Urich, M. Pfeiffer, P. Bäuerle, *Adv. Energy Mater.* **2011**, 21, 897–910.
  46. J. Xue, B. P. Rand, S. Uchida, S. R. Forrest, J. Xue, B. P. Rand, S. Uchida, S. R. Forrest, *J. Appl. Phys.* **2005**, 12, 1249031–1249039.
  47. C. Lin, S. Liu, C. Lee, J. Hunag, W. Su, T. Chiu, C. Chen, J. Lee, *Sol. Energy Mater. Sol. Cells* **2012**, 103, 69–75.
  48. J. Xue, S. Uchida, B. P. Rand, S. R. Forrest, *Appl. Phys. Lett.* **2004**, 84, 3013–3015.
  49. P. Peumans, S. R. Forrest, *Appl. Phys. Lett.* **2001**, 79, 126–128.
  50. N. S. Sariciftci, L. Smilowitz, A. J. Heeger, F. Wudi, *Science* **1988**, 258, 1474–1476.
  51. T. Ghosh, J. S. Panicker, V. C. Nair, *Polymer* **2017**, 9, 1–40.
  52. S. Zhang, Y. Qin, J. Zhu, J. Hou, *Adv. Mater.* **2018**, 30, 1800868.
  53. S. K. Hau, H.-L. Yip, A. K.-Y. Jen, *Polym. Rev.* **2010**, 50, 474–510.
  54. A. Marrocchi, D. Lanari, A. Facchetti, L. Vaccaro, *Energy Environ. Sci.* **2012**, 5, 8457–8474.
  55. T. Yamamoto, K. Sanechika, A. Yamamoto, *J. Polym. Science: Polym. Lett. Ed.* **1980**, 18, 9–12.

- 
56. P. Schilinsky, C. Waldauf, C. J. Brabec, *Appl. Phys. Lett.* **2002**, *81*, 3885–3887.
  57. X. Guo, C. Cui, M. Zhang, L. Huo, Y. Huang, Y. Li, *Energy Environ. Sci.* **2012**, *5*, 7943–7949.
  58. S. Holliday, R. S. Ashraf, A. Wadsworth, D. Baran, S. A. Yousaf, C. B. Nielsen, C. Tan, S. D. Dimitrov, Z. Shang, N. Gasparini, M. Alamoundi, F. Laquai, C. J. Brabec, A. Salleo, J. R. Durrant, I. McCulloch, *Nat. Commun.* **2016**, *7*, 11585.
  59. R. S. Ashraf, I. Meager, M. Nikolka, M. Kirkus, M. Planells, B. C. Schroeder, S. Holliday, M. Hurhangee, C. B. Nielsen, H. Sirringhaus, I. McCulloch, *J. Am. Chem. Soc.* **2015**, *137*, 1314–1321.
  60. Z. He, C. Zhong, S. Su, M. Xu, H. Wu, Y. Cao, *Nat. Photonics* **2012**, *6*, 591–595.
  61. W. Chen, G. Huang, X. Li, H. Wang, Y. Li, H. Jiang, N. Zheng, R. Yang, *ACS Appl. Mater. Interfaces* **2018**, *10*, 42747–42755.
  62. R. Fitzner, E. Mena-osteritz, A. Mishra, G. Schulz, E. Reinold, M. Weil, C. Ko, H. Ziehlke, C. Elschner, K. Leo, M. Riede, M. Pfeiffer, C. Urich, P. Bauerle, *J. Am. Chem. Soc.* **2012**, *134*, 11064–11067.
  63. Y. Chen, X. Wan, G. Long, *Acc. Chem. Res.* **2013**, *46*, 2645–2655.
  64. B. Kan, M. Li, Q. Zhang, F. Liu, X. Wan, Y. Wang, W. Ni, G. Long, X. Yang, H. Feng, Y. Zuo, M. Zhang, F. Huang, Y. Cao, T. P. Russell, Y. Chen, *J. Am. Chem. Soc.* **2015**, *137*, 3886–3893.
  65. B. Qiu, L. Xue, Y. Yang, H. Bin, Y. Zhang, C. Zhang, M. Xiao, K. Park, W. Morrison, Z.-G. Zhang, Y. Li, *Chem. Mater.* **2017**, *29*, 7543–7553.
  66. T. Duan, H. Tang, R.-Z. Liang, J. Lv, Z. Kan, R. Singh, M. Kumar, Z. Xiao, S. Lu, F. Laquai, *J. Mater. Chem. A* **2019**, DOI: 10.1039/C8TA11420J.
  67. Z. Zhou, S. Xu, J. Song, Y. Jin, Q. Yue, Y. Qian, F. Liu, F. Zhang, X. Zhu, *Nat. Energy* **2018**, *3*, 952–959.
  68. H. Ouchi, T. Kizaki, M. Yamato, X. Lin, N. Hoshi, F. Silly, T. Kajitani, T. Fukushima, K. Nakayama, S. Yagai, *Chem. Sci.* **2018**, *9*, 3638–3643.

## Chapter 2

---

### Molecular and Supramolecular Effects on p/n-Polarity of Thiophene Oligomers in Photovoltaic Cells

---

#### 2.1. Abstract

*Molecular and supramolecular properties play crucial roles in the optoelectronic properties and photovoltaic performances of organic semiconducting materials. In this chapter, we have discussed how minimal changes in the chemical structure affect such properties, which in turn control the intrinsic and fundamental properties such as the p/n-polarity of organic semiconductors in bulk-heterojunction solar cells. To study this aspect, we have designed and synthesized two acceptor–donor–acceptor (A-D-A) type semiconducting thiophene oligomers end-functionalized with oxazolone and isoxazolone derivatives (OT1 and OT2, respectively). The HOMO–LUMO energy levels of both derivatives were found to be positioned in such a way that they can act as electron acceptors to P3HT and electron donors to PCBM. However, OT1 functions as a donor (with PCBM) and OT2 as an acceptor (with P3HT) in BHJ solar cells, and their reverse roles results in either no or poor performance of the cells. Detailed studies proved that both molecular and supramolecular properties contributed equally but in a contrasting manner to the above mentioned observation. The results obtained from the experiments conducted were further validated by flash-photolysis time-resolved microwave conductivity studies which showed an excellent correlation between the structure, property, and device performances of the materials.*

---

## 2.2. Introduction

Thiophene-based polymers and fullerene-based small molecules are a typical combination of donors and acceptor, respectively, used in BHJ OSCs.<sup>1-4</sup> It is well established that molecular properties of polymers such as absorption characteristics, the highest occupied molecular orbital (HOMO) and the lowest unoccupied molecular orbital (LUMO) energy levels play important roles in the device performances. Such properties could be easily controlled by suitable structural changes in the conjugated backbone.<sup>5-9</sup> In addition to the molecular properties, supramolecular interactions among and between donor polymers and fullerene acceptors also play a key role in the functionality and device performances of a bulk-heterojunction assembly.<sup>10-13</sup> The rational choice of solvents, solvent additives, and processing conditions was found to affect the supramolecular interactions, and hence the optoelectronic properties and device performances significantly.<sup>14-19</sup>

Small molecules and oligomers have gained huge popularity over their polymer counterparts for photovoltaic applications due to several advantages as discussed in **Chapter 1**. Due to these advantages and recent findings, oligomers are now considered as a potential replacement for polymers in solution processed OSCs. However, dependence on supramolecular interactions is more pronounced in oligomers when compared to that in polymers, which demands careful molecular designing and rational fabrication techniques for obtaining optimum performances. This effect could be attributed to the limited pathways available for oligomers for charge transport; unlike polymers, where

inter- and intra-polymer routes are available for charge transport,<sup>20,21</sup> oligomers depend exclusively on intermolecular routes. This may result in significant variations in optoelectronic properties of comparable oligomers even when the structural differences between them are minimal.

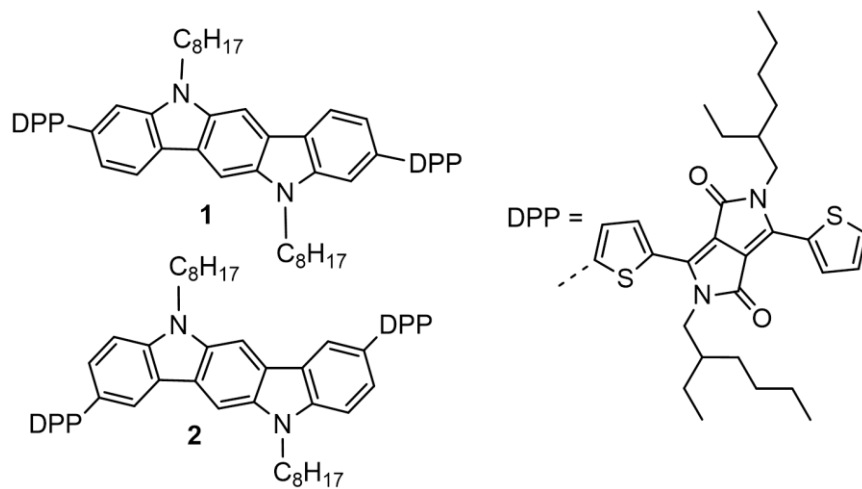


**Figure 2.1.** Chemical structures of regioisomers of indolo[3,2-*b*]carbazole derivatives, **1** and **2**.

Yagai *et al.* have reported the effect of regioisomerism on the solid state properties and BHJ solar cell performance of two indolo[3,2-*b*]carbazoles end-substituted with diketopyrrolopyrrole derivatives (**1** and **2**, **Figure 2.1**).<sup>22</sup> They have observed different packing behavior and inverse structural ordering upon thermal annealing in these regioisomers. The regioisomer **1** has a linear molecular geometry and showed stronger diffraction in XRD, while **2** with S-shaped molecular structure displayed no notable diffraction, ascribes to the higher crystallinity in the former in comparison to the latter. Thermal annealing was found to decrease the degree of phase separation in the blend of **1** with PC<sub>61</sub>BM, while it increased in **2**. As a result, a distinct effect of thermal annealing on

the device parameters of the solar cell was observed for these compounds. A pronounced increase in the  $J_{SC}$  value of **2** (from 1.73 to 2.86  $\text{mAcm}^{-2}$ ) was observed upon heating at 130 °C compared to **1** (from 3.50 to 3.83  $\text{mAcm}^{-2}$ ). This implies that compound **2** undergoes a certain degree of reorientation on heating. Though, there is a distinct effect on  $J_{SC}$ , the optimized devices of both the isomers exhibited similar PCE in the range of 0.70-0.74%.

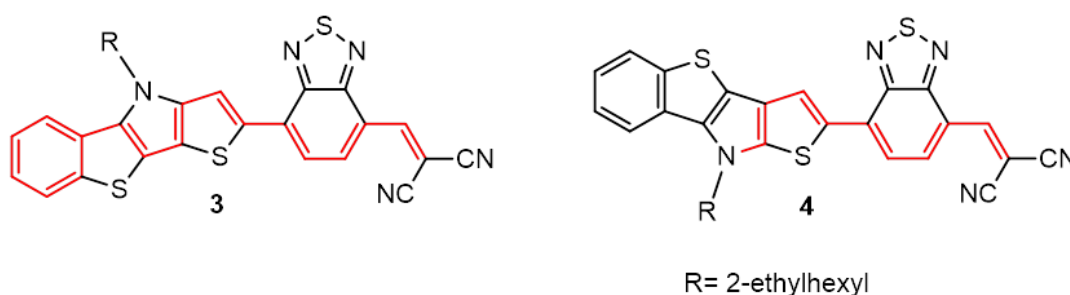


**Figure 2.2.** Chemical structures of regioisomers, **3** and **4**.

Forrest and co-workers synthesized regioisomeric D-A-A' type small molecules (**3** and **4**; **Figure 2.2**) and studied their structure-property-performance relationships.<sup>23</sup> Both molecules pack in an antiparallel arrangement to achieve a centrosymmetric dimer, leading to a net dipole moment of zero. The molecule **3** exhibited more compact crystal packing and when mixed with  $C_{70}$ , achieved a PCE of 7.2% ( $J_{SC}$ : 14.2  $\text{mAcm}^{-2}$ ;  $V_{OC}$ : 0.91V;  $FF$ : 0.56). While in the case of isomer **4**, the effective conjugation length is reduced due to the interruption by the *N*-bridge atom as indicated by the highlighted red colored bonds in the chemical structure. As a result, blue-shifted absorption with a lower extinction coefficient was observed. Its absorption cutoff does not extend deeply into the near IR region which in turn resulted in a lower  $J_{SC}$ . However, the HOMO of **4** was



stabilized when compared to **3**, resulted in an increased  $V_{OC}$  (1.01 V) yielding a PCE of 6.1% ( $J_{SC}$ :  $11.6 \text{ mAcm}^{-2}$  and  $FF$ : 0.52).

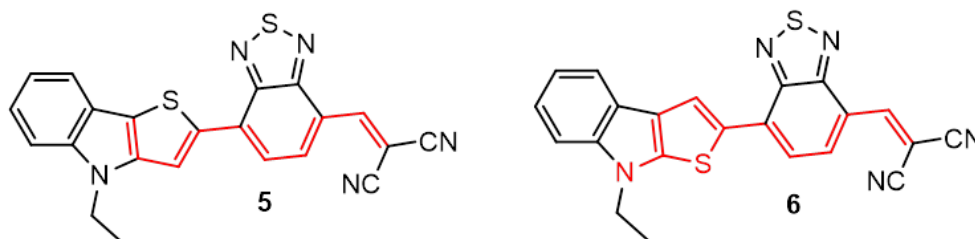


**Figure 2.3.** Molecular structures of **5** and **6**.

Another promising D-A-A type electron-donor regioisomers based on coplanar thieno[3,2-*b*]/[2,3-*b*]indole, benzo[*c*][1,2,5]thiadiazole, and dicyanovinylene was reported by Wong *et al.* (**5** and **6**; **Figure 2.3**).<sup>24</sup> They have studied the role of the regioisomeric electron-donating thienoindole moiety on the photophysical and structural properties. They exhibited broadband absorption with high extinction coefficients. In **6**, the lone-pair of electrons on syn-positioned nitrogen (*vs* S atom) is effectively delocalized with benzo[*c*][1,2,5]thiadiazole ring, leading to increased conjugation and lower oxidation potential in comparison to **5**. Also, the external quantum efficiency for the device containing **6** extends further into the near-IR region compared to the device of **5**. As a result, the optimized **6**-C<sub>70</sub> BHJ solar cells gave a higher PCE of 5.0% in comparison to **5**-C<sub>70</sub> cells (3.7%).

Very recently, Wu *et al.* have studied the effect of isomeric small-molecule acceptors, with varied oxygen position in the benzodi(thienopyran) core (**7** and **8**; **Figure 2.4**).<sup>25</sup>

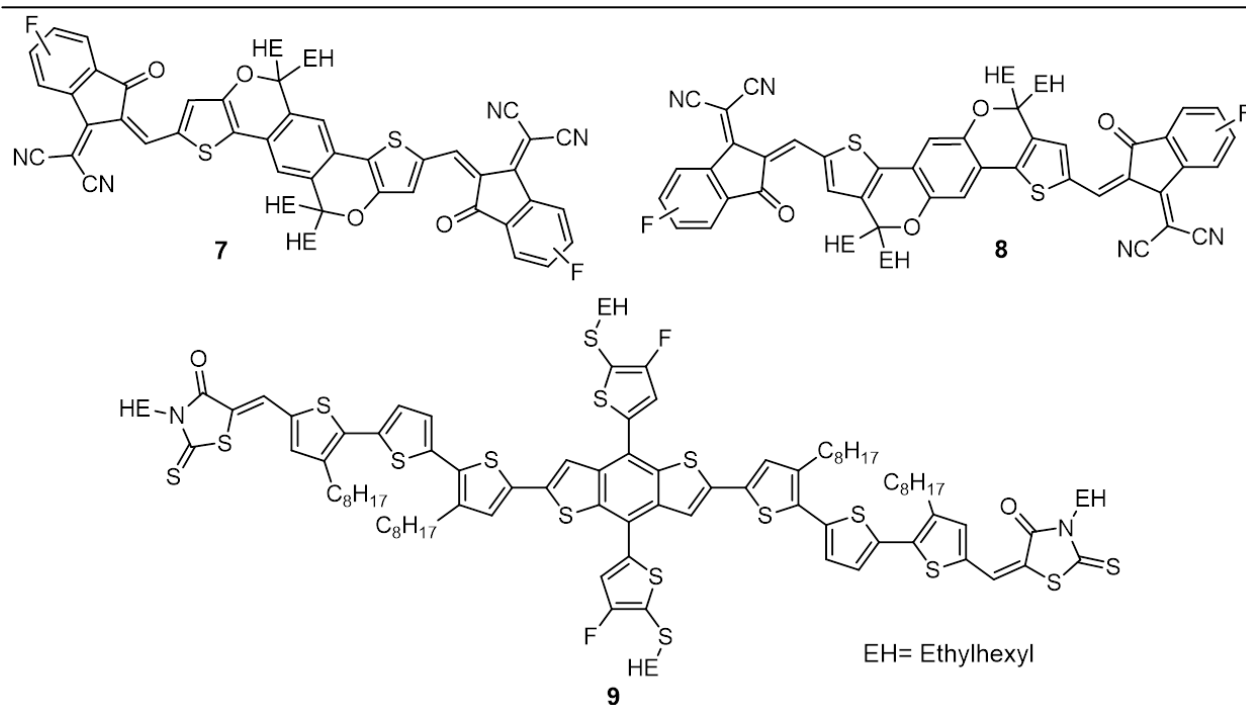


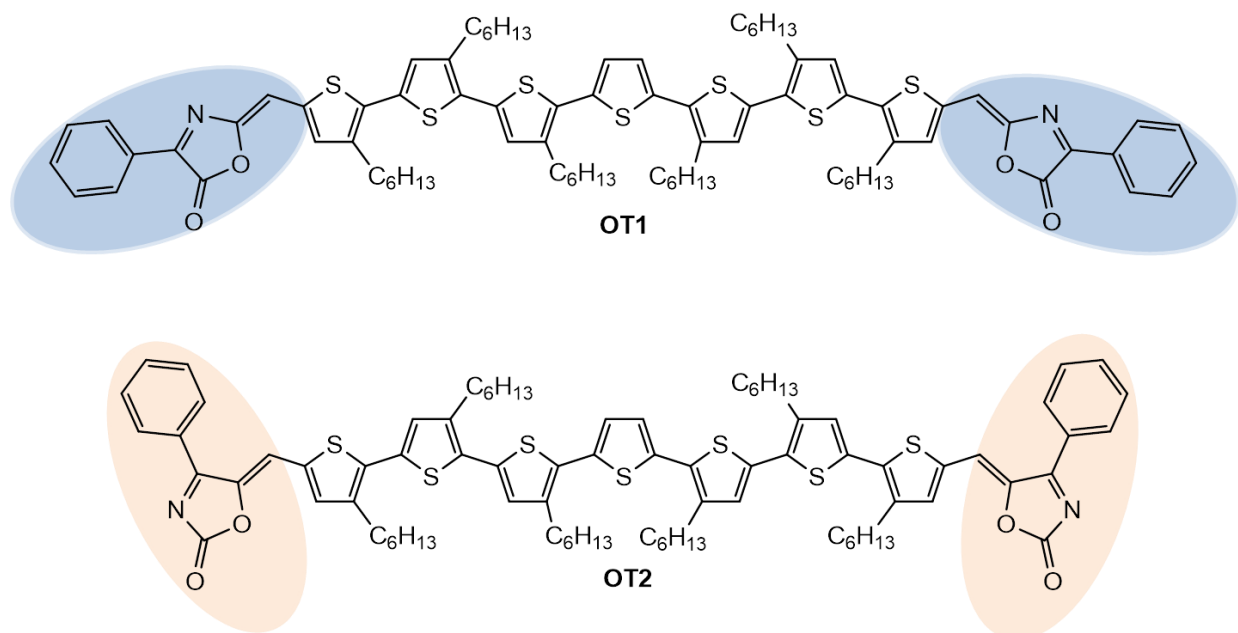
**Figure 2.4.** Molecular structures of donors (**7** and **8**) and acceptor **9**.

When blended with the donor (**9**), devices based on the two isomeric acceptors showed disparate photovoltaic performance. Conventional devices when fabricated using this blend (**7:9**) delivered a high PCE of 11.2%. On the other hand, (**8:9**) blend showed almost no photovoltaic response (0.02%). Detailed investigations on inherent optoelectronic processes as well as morphological evolution were carried out; this performance disparity was correlated to the interfacial tension and miscibility of the two combinations. Compared to **8**, the acceptor **7** exhibits stronger non-covalent intermolecular interactions, which induces higher surface tension and larger interfacial tension when blended with **9**. This phenomenon lowers the miscibility and contributes to the formation of favourable phase separation. Conversely, the blend of **8:9** lacks such driving force, which resulted in excessively miscible behaviour, poor phase separation,

and inefficient charge carrier transport. Based on these results, it was concluded that proper interfacial tension is a key factor for effective phase separation, optimal blend morphology, and superior performance, which can be achieved by the “isomerization” design on molecular acceptors.

## 2. 3. Results and discussion

In this chapter, we describe an excellent example illustrating the effect of small structural changes on the molecular and supramolecular properties of conjugated oligomers, which in turn affect their p/n polarity and photovoltaic performance in a bulk-hetero-junction solar cell. We have designed and synthesized two thiophene oligomers consisting of seven thiophene rings connected with each other at 2,5-positions, and end-functionalized with oxazolone (**OT1**) or isoxazolone (**OT2**) derivatives (**Scheme 1**).



**Scheme 2.1.** Chemical structures of the thiophene oligomers **OT1** and **OT2** under study.

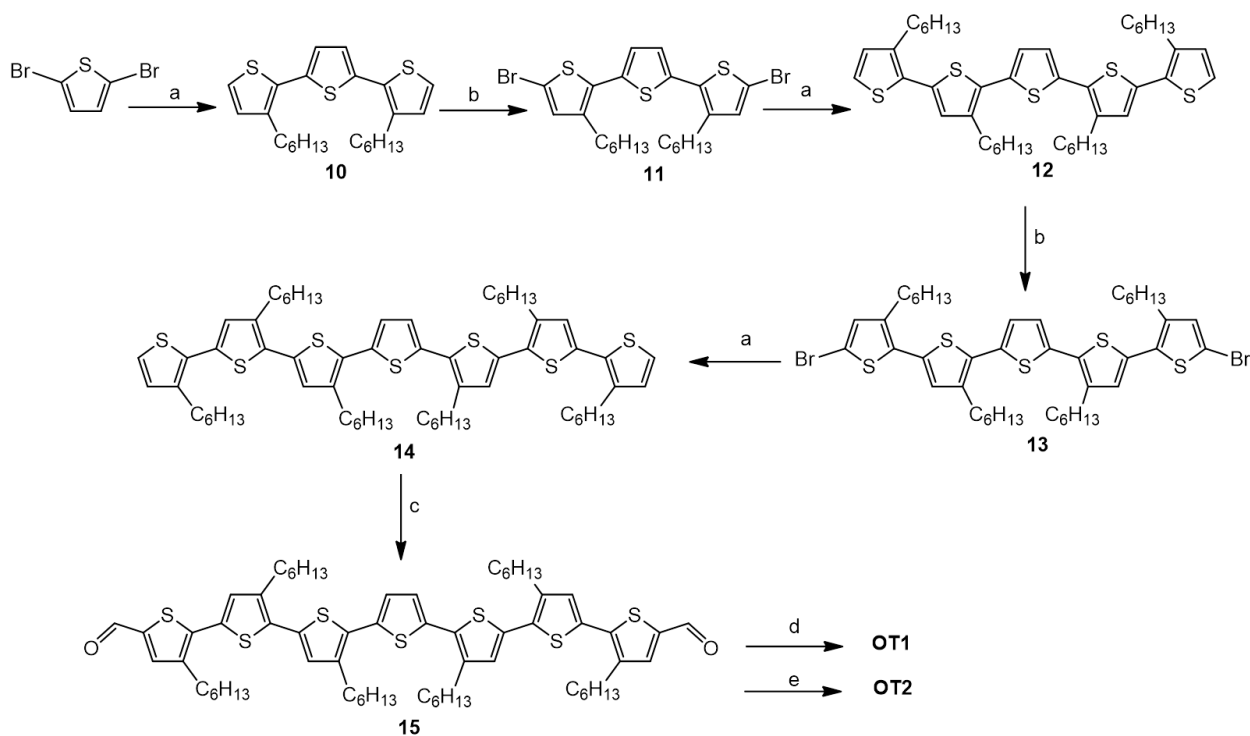
---

Oxazolone and isoxazolone are positional isomers which differ in the respective positions of nitrogen atoms and the phenyl group on the 5-membered heterocyclic ring. Both of them are good electron acceptors because of the presence of electronegative heteroatoms and an electron withdrawing carbonyl group in conjugation. All thiophenes in **OT1** and **OT2**, except the middle one, are attached with *n*-hexyl chains for solution processability.

### 2. 3. 1. Synthesis and characterization

The oligothiophene derivatives **OT1** and **OT2** were synthesized according to methods reported in the literature as shown in **Scheme 2.2**. Suzuki coupling of 2,5-dibromothiophene and 3-hexylthiophene-2-boronic acid pinacol ester afforded dihexylterthiophene derivative (**10**) in 74% yield. Subsequent dibromination of terthiophene was carried out using *N*-bromosuccinimide in chloroform–acetic acid mixture provided **11** with a 98% yield. Compound **11** on Suzuki coupling with 3-hexylthiophene-2-boronic acid pinacol ester, gave **12** with a yield of 83%, which was again brominated with the same reagents as before yielded 89% of **13**. Suzuki coupling of **13** with 3-hexylthiophene-2-boronic acid pinacol ester was conducted to achieve thiophene oligomers with seven thiophene units, **14** with a yield of 70%. **14** was then functionalized with aldehyde groups at both ends by treating with a Vilsmeier reagent by mixing POCl<sub>3</sub> and DMF in anhydrous 1,2-dichloroethane gave bis-aldehyde **15** as brown solid with a yield of 70%. Finally, incorporation of oxazolone/isoxazolone acceptors into

the thiophene backbone was carried out by the Knoevenagel condensation method in the presence of base triethylamine. Both derivatives **OT1** and **OT2** were obtained in good yields (88%) and characterized by using various analytical techniques such as  $^1\text{H}$  NMR,  $^{13}\text{C}$  NMR, IR, and MALDI-TOF mass spectrometry. They were found to be soluble in common organic solvents such as toluene, chloroform, chlorobenzene, tetrahydrofuran, *N,N*-dimethylformaldehyde, etc.



**Scheme 2.2.** Synthetic route to the preparation of **OT1** and **OT2**. Reagents and conditions: (a) 3-hexylthiophene-2-boronic acid pinacol ester, 2 M aq.  $\text{K}_2\text{CO}_3$ ,  $\text{Pd}(\text{PPh}_3)_4$ , Aliquat 336, toluene, reflux, Ar, 24 h; (b) NBS, AcOH,  $\text{CHCl}_3$ ; (c)  $\text{POCl}_3$ , DMF, 1,2-dichloroethane; (d) 2-phenyl-5-oxazolone,  $\text{NEt}_3$ , dry  $\text{CHCl}_3$ ; (e) 3-phenyl-5-isoxazolone,  $\text{NEt}_3$ , dry  $\text{CHCl}_3$ .

### 2.3.2. Photophysical properties in the solution state

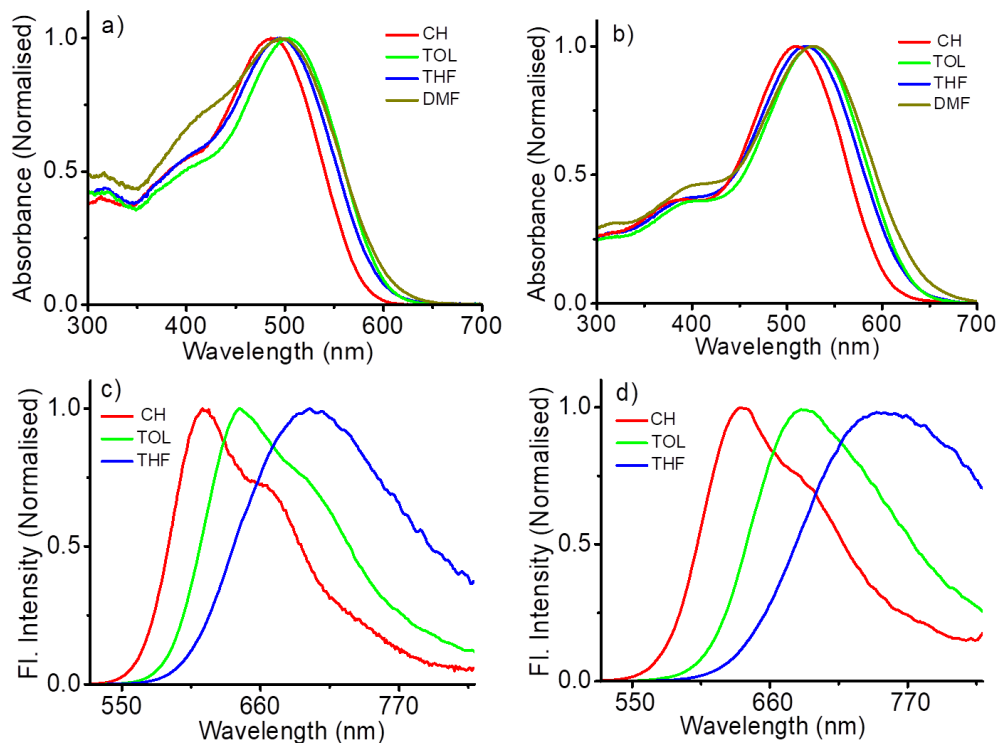


**Figure 2.5.** UV-vis absorption spectra of a) **OT1** and b) **OT2**; fluorescence emission spectra of c) **OT1** and d) **OT2** in cyclohexane (CH), toluene (Tol), tetrahydrofuran (THF) and *N,N*-dimethyl formamide (DMF;  $c = 1 \times 10^{-5}$  M,  $l = 1$  cm,  $\lambda_{\text{ex}} = 490$  nm).

The UV-vis absorption and fluorescence properties of **OT1** and **OT2** were studied in solvents such as cyclohexane, toluene, tetrahydrofuran (THF), and *N,N*-dimethylformamide (DMF) at a concentration of  $1 \times 10^{-5}$  M (**Figure 2.5**), and the details are summarized in **Table 2.1**. The solvent polarity increases from cyclohexane to DMF. In general, both molecules exhibited an intense broad absorption in the UV-visible region, which is typically observed for conjugated thiophene oligomers. The most intense band observed in the visible region could be attributed to the  $\pi$ - $\pi^*$  transition. Although the trend is not regular with the solvent polarity, the absorption maximum of both

molecules was fairly sensitive to the solvent polarity indicating that the ground state of the molecules is slightly polarized. This could be attributed to the conjugation of electron donating thiophenes with electron withdrawing oxazolone/isoxazolone derivatives, resulting in the localization of electron clouds towards the latter. This was evident from the DFT results, which showed that HOMO is localized on the thiophene backbone, whereas, the LUMO is biased towards the oxazolone/isoxazolone acceptors (**Figure 2.6**). It should be noted that the absorption maximum of **OT2** is about 20 nm red-shifted, and the extinction coefficient is almost double in any solvent when compared to that of **OT1** in the same solvent. Both these observations indicate that the isoxazolone derivative is a stronger acceptor than the oxazolone derivative, leading to the red-shifted absorption peak of the latter.

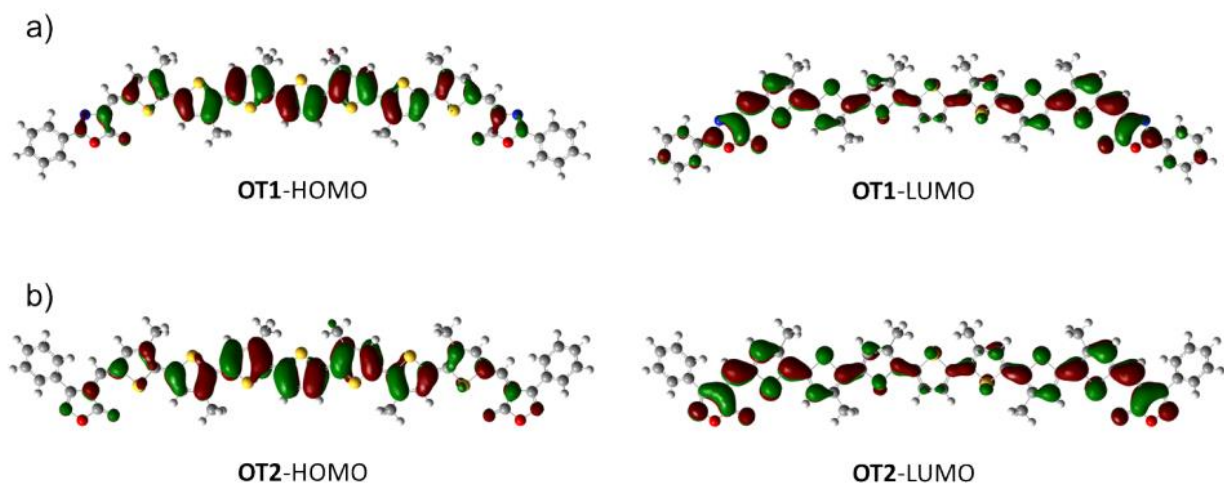


**Figure 2.6.** HOMO and LUMO distribution of a) **OT1** and b) **OT2** obtained by density functional theory calculation with B3LYP 6-31G(d,p).

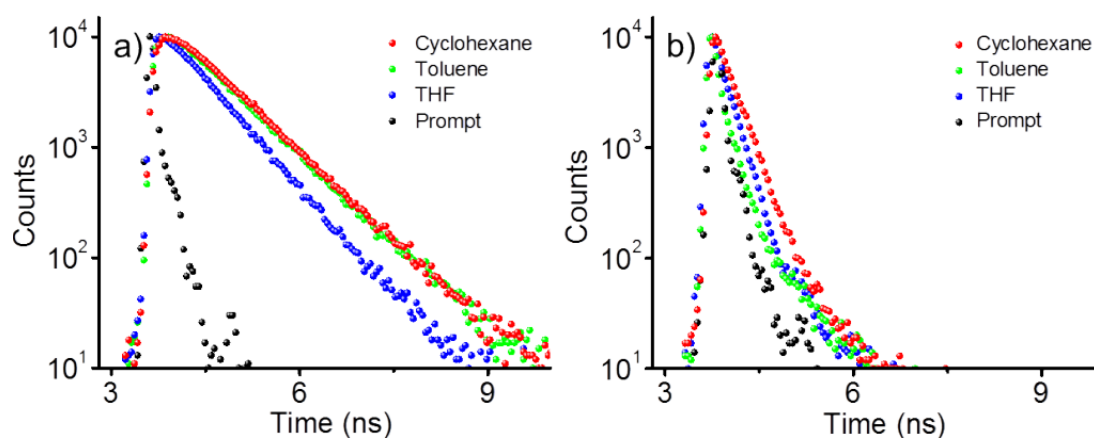


**Figure 2.7.** Fluorescence decay profiles of a) **OT1** and b) **OT2** in different solvents. ( $c = 1 \times 10^{-5}$  M,  $l = 1$  cm,  $\lambda_{\text{ex}} = 440$  nm).

Emission spectra were also recorded in cyclohexane, toluene, THF, and DMF. However, in contrast to absorption, fluorescence showed high sensitivity towards the solvent polarity, as evident from the significant red-shift of the emission maximum with increasing solvent polarity. This observation revealed that the excited states of both molecules are highly polar (compared to the ground state) in nature. Both molecules were found to be non-emissive in DMF, which is the highest polar solvent among the four. In the other three solvents, **OT1** exhibited good emission quantum yields, whereas **OT2** was poorly emissive. Similarly, the average fluorescence lifetime was higher for **OT1** than that for **OT2**. Similar to the absorption properties, **OT2** showed more red-shift than **OT1** in the same solvents. Moreover, **OT2** exhibited an emission maximum shift of 106 nm when going from cyclohexane to THF, whereas **OT1** showed a shift of only 86 nm under similar conditions. These observations reiterate that the isoxazolone derivative is a stronger acceptor than the oxazolone derivative. **OT1** showed the decrease in



fluorescence quantum yield as well as lifetime (negligible in the case of cyclohexane and toluene solutions) with an increase in solvent polarity which is expected for donor-acceptor systems exhibiting charge transfer (**Figure 2.7**). However, such trends were not clear in **OT2** due to poor emission.

**Table 2.1.** Photophysical parameters such as absorption maxima, emission maxima, extinction coefficients ( $\epsilon$ ) and fluorescence quantum yields ( $\phi_f$ ) of **OT1** and **OT2** in various solvents.

| Compound   | Solvent     | Absorption               |  | Emission                 |                   |                |
|------------|-------------|--------------------------|--|--------------------------|-------------------|----------------|
|            |             | $\lambda_{\max}$<br>(nm) | $\epsilon \times 10^5$<br>( $M^{-1} \text{ cm}^{-1}$ ) | $\lambda_{\max}$<br>(nm) | $\phi_f^a$<br>(%) | $\tau$<br>(ns) |
| <b>OT1</b> | Cyclohexane | 487                      | 0.35   | 614                      | 52                | 0.90           |
|            | Toluene     | 504                      | 0.34   | 643                      | 33                | 0.88           |
|            | THF         | 496                      | 0.35   | 700                      | 15                | 0.74           |
|            | DMF         | 497                      | 0.24   | -                        | -                 | -              |
| <b>OT2</b> | Cyclohexane | 510                      | 0.78   | 639                      | 1.2               | 0.21           |
|            | Toluene     | 527                      | 0.82   | 685                      | 2.3               | 0.19           |
|            | THF         | 519                      | 0.84   | 745                      | 2.5               | 0.20           |
|            | DMF         | 529                      | 0.78   | -                        | -                 | -              |

<sup>a</sup>Rhodamine B in ethanol ( $\phi_f=0.5$ ) was used as the standard for quantum yield measurements, error limit  $\pm 5\%$ .

### 2. 3. 3. HOMO–LUMO levels and optical band-gap

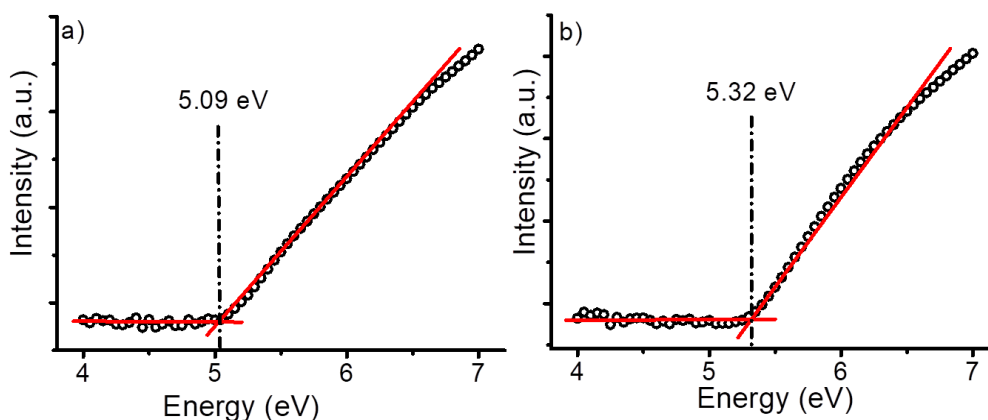


**Figure 2.8.** PYS spectra of a) **OT1** and b) **OT2** in the film state.

The HOMO levels of the oligomers were measured in the film state as ionization threshold energies using ultraviolet photoelectron yield spectroscopy (PYS, **Figure 2.8a** and **2.8b**). PYS measurements showed that the HOMO energy levels of **OT1** and **OT2** were at -5.09 and -5.32 eV, respectively. The LUMO levels were obtained by adding the value of the HOMO to the optical band gap ( $E_g^{\text{opt}}$ ), which is obtained from the onset of UV-vis absorption of the oligomers in the film state (details of film state absorption are given in the following section). The optical band gap of **OT1** and **OT2** was found to be 1.65 and 1.67 eV, respectively. Accordingly, the LUMO levels were found to be -3.44 and -3.65 eV for **OT1** and **OT2**, respectively. The deeper HOMO and LUMO values for **OT2** reiterate better delocalization of  $\pi$ -electrons due to the presence of a stronger electron withdrawing isoxazolone derivative in it.



**Figure 2.9.** Scheme showing the comparison of the HOMO–LUMO levels of the oligomers with that of P3HT and PCBM.

The comparison of the HOMO and LUMO of the oligomers with those of P3HT (a standard donor material; HOMO: -4.9 eV, LUMO: -2.7 eV) and PCBM (a standard

acceptor material; HOMO: -6.0 eV, LUMO: -4.2 eV, where the latter is varied by the method and calibration equation) is shown in **Figure 2.9**. It shows that the HOMO and LUMO levels of the oligomers are lower than the corresponding energy levels of P3HT, whereas those are higher than the corresponding energy levels of PCBM. Furthermore, the energy offset between the LUMOs of oligomers and P3HT/PCBM is high enough for exciton splitting at the interfaces. Hence, it could be assumed that both oligomers can act as donors to PCBM and acceptors to P3HT in a photovoltaic cell.

#### 2.3.4. Photovoltaic properties

Though the electrochemical properties revealed that both **OT1** and **OT2** can act as donors to PCBM and acceptors to P3HT, the p/n-polarity of material in BHJ solar cells depends on not only the ability to donate/accept electrons but also the ability to transport holes/electrons. To check the p/n-polarity of **OT1** and **OT2** in a photovoltaic cell, bulk-heterojunction organic solar cells were fabricated in the presence of P3HT or PCBM. An inverted device structure consisting of ITO/ZnO/BHJ/MoO<sub>x</sub>/Ag was used for this analysis.

The active layer consisting of **OT1**:P3HT, **OT1**:PCBM, **OT2**:P3HT, or **OT2**:PCBM in a 1:1 weight ratio was prepared from chlorobenzene solution. The **OT1**:P3HT solar cell showed a power conversion efficiency (PCE) of only 0.07% ( $J_{SC}$ : 0.69 mA cm<sup>-2</sup>;  $V_{OC}$ : 0.36 V;  $FF$ : 0.28; **Figure 2.10c**). On the other hand, the **OT1**:PCBM cell exhibited a PCE of 0.75% ( $J_{SC}$ : 3.25 mA cm<sup>-2</sup>;  $V_{OC}$ : 0.62 V;  $FF$ : 0.37).

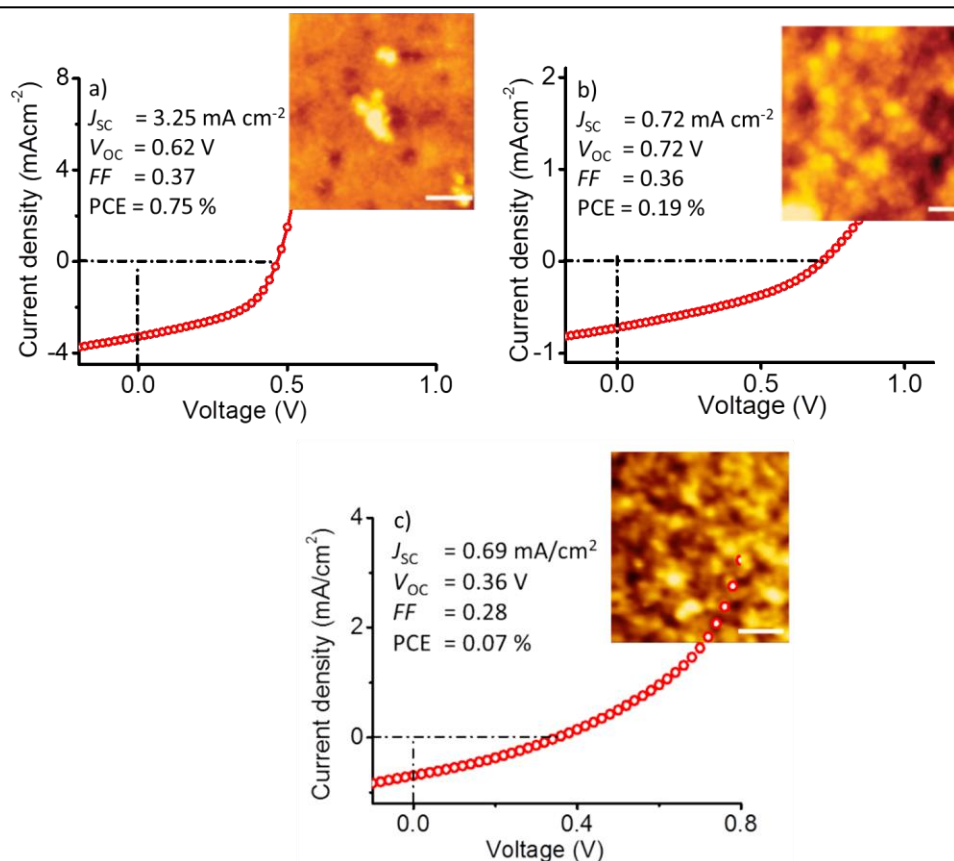


**Figure 2.10.**  $J$ - $V$  characteristics of photovoltaic devices fabricated from a solution of a) **OT1**:PCBM and b) **OT2**:P3HT (1:1 blend) and c) **OT1**:P3HT (1:1 blend) in chlorobenzene (device structure: glass/ITO/ZnO/BHJ/MoO<sub>x</sub>/Ag). AFM height images of the corresponding active layers are shown in the inset (scale bar corresponds to 500 nm).

Under identical conditions, **OT2**:P3HT exhibited an efficiency of 0.19% ( $J_{SC}$ : 0.72 mAcm<sup>-2</sup>;  $V_{OC}$ : 0.71V;  $FF$ : 0.36), whereas, **OT2**:PCBM exhibited no diode characteristics.  $J$ - $V$  curves of the **OT1**:PCBM and **OT2**:P3HT cells are shown in **Figure 2.10a** and **2.10b**, respectively. The atomic force microscopy images of the corresponding films are shown in the insets. Though the oligomers showed relatively low photoconversion efficiencies, the observed difference in the p/n-polarity of **OT1** and **OT2** in the presence of P3HT/PCBM was noteworthy. It is clear that **OT1** has shown more p-type characteristics, whereas **OT2** exhibited n-type characteristics. This could be partially

---

explained by the difference in the relative HOMO–LUMO levels of the molecules. The shallower HOMO and LUMO of **OT1** (compared to **OT2**) provide the better driving force for it to donate electrons and make it function as a donor. Similarly, deeper HOMO and LUMO of **OT2** are suitable for accepting electrons and make it function as an acceptor. The effect of energy offset difference between the oligomers is particularly visible when they are blended with P3HT, i.e., **OT2**, which has the higher energy offset showed better photoconversion efficiency than **OT1**. However, such logics could not explain the observed difference in photoconversion efficiency when the oligomers are blended with PCBM. **OT1** showed an efficiency of 0.75% in the presence of PCBM, whereas **OT2** exhibited no diode characteristics under identical conditions.

### 2.3.5. Energy minimized structure

It is well known that the supramolecular interactions and packing of the molecules in the film state play a very important role in the charge carrier generation, charge carrier transport and photovoltaic properties.<sup>25–29</sup> Planarity of the conjugated backbone is a key factor that decides the packing ability of conjugated oligomers. In order to get an insight into the planarity of the molecules, the energy minimized structures of the oligomers were calculated using density functional theory (DFT) at the B3LYP/6-31G(d,p) level (**Figure 2.11**).

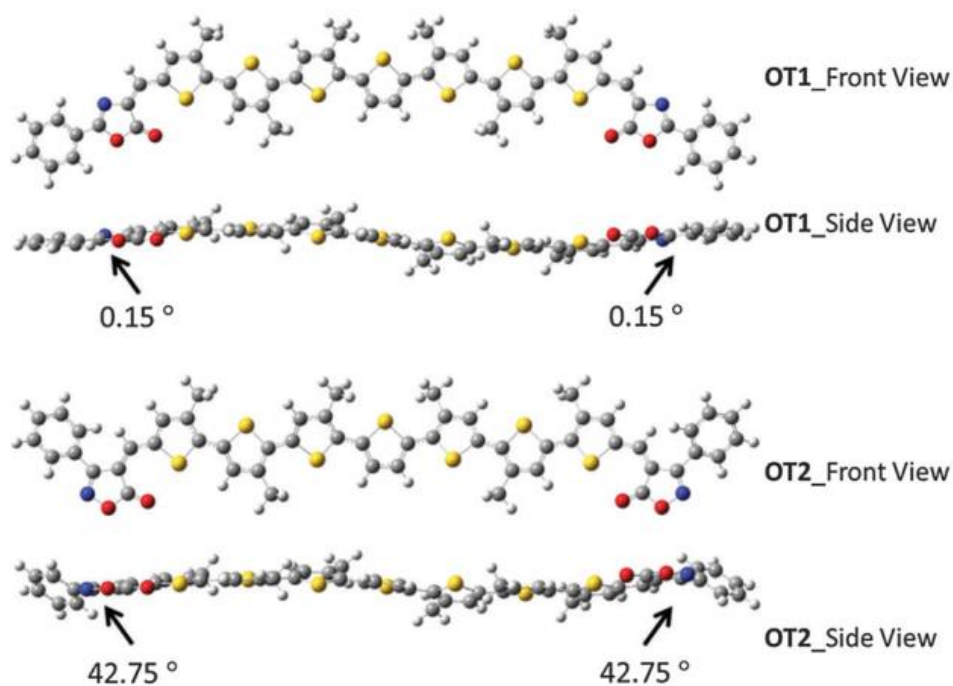


**Figure 2.11.** Energy minimized structures of the oligomers obtained by DFT calculation.

The conjugated thiophene backbones of both molecules looked similar and were relatively planar. The major difference between the molecules was seen at the ends. The oxazolone derivative of **OT1** was found to be coplanar with the thiophene backbone, whereas, the phenyl group on the isoxazolone derivative in **OT2** was found to be out of the plane. The dihedral angle between the isoxazolone and the attached phenyl ring in **OT2** was about 42.75°. The out of plane geometry of the phenyl ring in **OT2** could have a detrimental effect on the packing of the oligomers in the film state.

### 2.3.6. Film state absorption properties

The steady-state photoabsorption spectra of both oligomers were recorded in the film state by spin-casting from chlorobenzene (1 wt%) solution (**Figure 2.12a** and **2.12b**). For

comparison, the corresponding absorption in the solution state in chlorobenzene was also recorded.

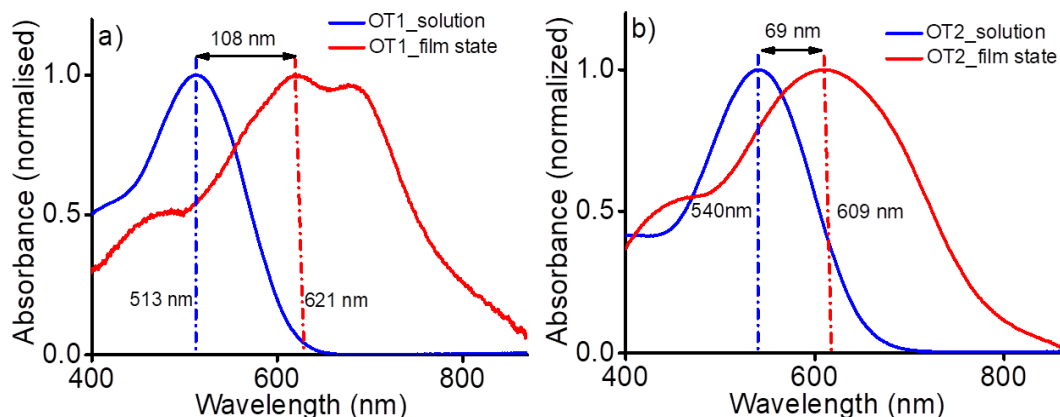


**Figure 2.12.** Normalized absorption spectra of (a) **OT1** and (b) **OT2** in chlorobenzene solution (blue line,  $c = 1 \times 10^{-5}$  M,  $l = 1$  cm) and in the film state (red line, spin-cast from 1 wt% chlorobenzene solution).

**OT1** in chlorobenzene solution exhibits an absorption maximum at 513 nm, which was red-shifted to 621 nm in the film state. On the other hand, the absorption maximum of **OT2** was at 540 nm in the solution state and 609 nm in the film state. As explained in the previous section, the higher relative red-shift of the absorption maximum for **OT2** than that for **OT1** in the same solvents could be attributed to the better electron accepting ability of the isoxazolone derivative. The red-shift exhibited by both molecules when going from the solution to film state indicates the planarization of the conjugated backbone. However, **OT1** and **OT2** exhibited a significant difference in this aspect; the relative red-shift was higher for **OT1** ( $\Delta\lambda = 108$  nm) when compared to that for **OT2** ( $\Delta\lambda = 69$  nm). Moreover, an additional shoulder band also appeared for **OT1** at around 683 nm, which is absent in the case of **OT2**. These observations correlate well with the results

obtained from DFT calculations. **OT1** with a coplanar oxazolone acceptor is able to form highly ordered aggregates through supramolecular interactions, mainly pi–pi stacking, which is evident from the shoulder peak seen at 683 nm. Such ordering further improves the planarity of the conjugated backbone and electronic communication between the molecules leading to the significant red-shift in the film state. On the other hand, **OT2** with an out-of-plane isoxazolone acceptor is unable to form well-ordered aggregates because of weaker pi–pi stacking, which is reflected from the absence of such features as well as a lesser red-shift in the film state absorption.

### 2.3.7. Solid state packing and thermal stability

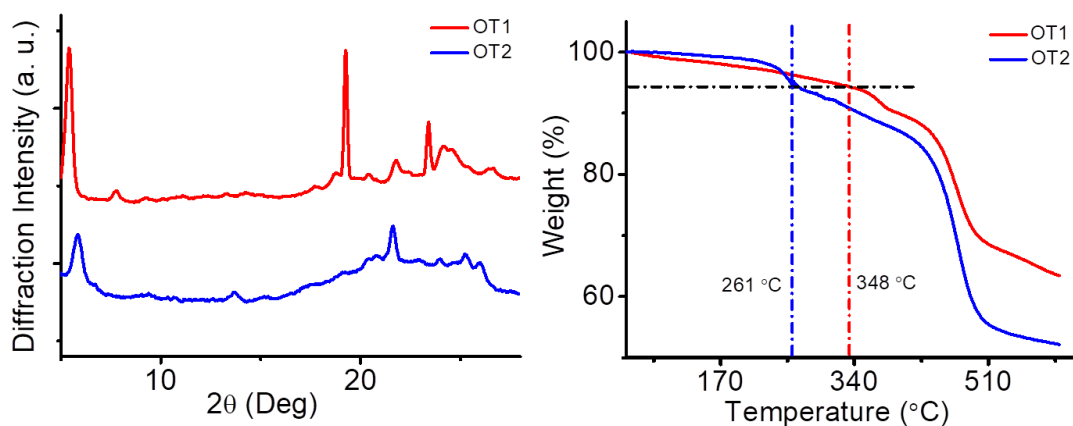


**Figure 2.13.** a) X-ray diffraction patterns of **OT1** and **OT2** in the self-assembled powder state; b) TGA profiles of **OT1** and **OT2**; the black line indicates the temperature at which the material loses 5% of its initial weight.

In order to get a better insight into the supramolecular packing, we have carried out wide-angle X-ray scattering (WAXS) studies in the self-assembled powder state (**Figure 2.13a**). **OT1** showed sharp and intense WAXS peaks, which indicates that the molecules are relatively ordered in the aggregated state. The sharp reflection at  $2\theta = 5.42^\circ$



corresponds to 16.3 Å, which is well correlated with the lamellar distance. The mean size of the **OT1** crystallites was estimated to be 21 nm using Scherrer's relation.<sup>30</sup> On the other hand, **OT2** exhibited less intense and broad peaks, particularly in the higher angle region (corresponding to intermolecular stacking distances). The reflection at  $2\theta = 5.86^\circ$  corresponds to 15.1 Å, which is slightly lower than the lamellar distance. The intensity of this peak is six-fold less when compared to that of the corresponding peak of **OT1**. Since the integrated intensity is directly proportional to the volume of nanodomains, the crystallinity of **OT2** is less than that of **OT1**. Hence it could be confirmed that the positional isomerism exhibited by the acceptors significantly affects the supramolecular interactions, which is reflected in the bulk packing. Relatively disordered packing in **OT2** may provide higher free volume for the alkyl chains thus reducing the spacing between the oligomers through slight intercalation of the alkyl chains.

The thermal stability of the molecules was investigated by thermogravimetric analysis (TGA), which was conducted at a heating rate of 10 °C min<sup>-1</sup> in the presence of nitrogen (**Figure 2.13b**). The temperature at which **OT1** loses 5% of its weight ( $T_5$  value) was 348 °C while that at which **OT2** loses its weight was 261 °C. Comparison of the  $T_5$  values of **OT1** and **OT2** reveals that **OT1** is thermally more stable than **OT2**, which reiterates the higher crystallinity in the former. Based on these observations, the supramolecular packing in the oligomers could be schematically represented as shown in **Figure 2.14**.

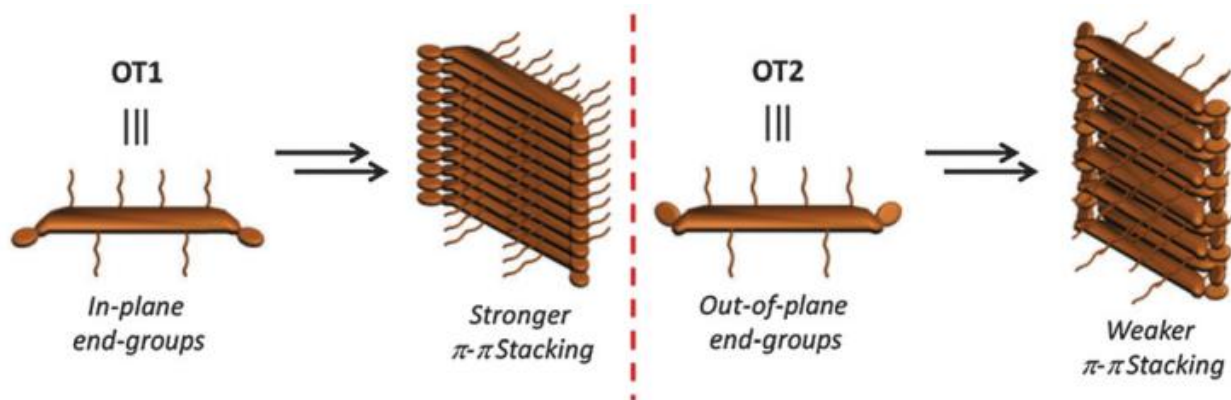


**Figure 2.14.** Simplified schematic representation of the supramolecular organization of **OT1** and **OT2** in the self-assembled state.

### 2.3.8. Blend with P3HT and PCBM

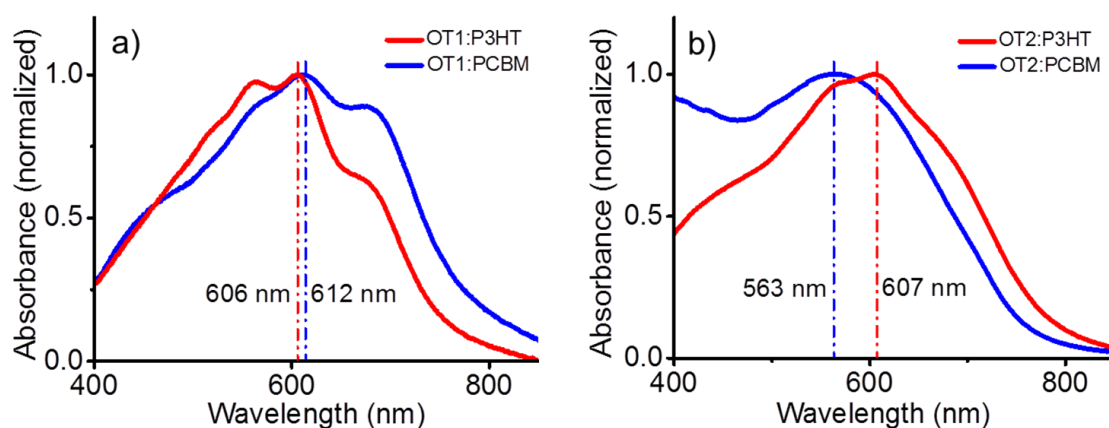


**Figure 2.15.** Normalized absorption spectra of (a) **OT1** and (b) **OT2** blend films (1:1 w/w) with P3HT and PCBM spin-cast from chlorobenzene solution.

In an attempt to study the effect of PCBM and P3HT on the film state packing of **OT1** and **OT2**, 1:1 (w/w) mixture of these compounds with PCBM/P3HT were prepared in chlorobenzene and the photoabsorbance of the blend films was recorded (**Figure 2.15**). The absorption maximum ( $\lambda_{\text{max}}$ ) of the **OT1**/P3HT blend film was observed at 606 nm while that of **OT1**/PCBM was at 612 nm. It should be noted that the vibronic features of

the **OT1** absorption were intact even in the blend state which indicates that the supramolecular interactions in **OT1** is strong enough and remains stable upon addition of P3HT or PCBM. The film state absorbance of **OT2** with P3HT and PCBM was measured under identical conditions. The absorption maximum of the **OT2**/P3HT blend film was at 607 nm, while that of **OT2**/PCBM was at 563 nm. It could be assumed that the spherically shaped PCBM completely destroys the packing in **OT2** resulting in the blue-shift of the absorption maximum by 48 nm when compared to the pristine film. This further proves that the supramolecular interactions in **OT2** are weaker. However, no such blue-shift was observed upon addition of P3HT, but some vibrational features were observed between 500 and 700 nm in the spectrum. The vibrational features could be attributed to the crystallite formation of P3HT,<sup>31</sup> which may not interfere with the stacking of **OT2**. In other words, **OT2** molecules might be pushed away during the formation of P3HT crystallites in the film development process, resulting in the pure **OT2** domains.

### 2.3.9. Photoconductivity analysis

Photoconductivity measurements using flash-photolysis time-resolved microwave conductivity (FP-TRMC) is an excellent method to understand the charge carrier generation and transport dynamics of organic semiconducting materials.<sup>26-29,32</sup> In literature, it is shown that it has been employed to study the transfer, transport, recombination, and trapping of photogenerated charges in organic dyes, organic thin

---

films, conjugated polymers, inorganic quantum dots, semiconductor single crystals, and nanostructures in devices such as BHJ solar cells, organic light emitting diodes, and photocatalysts. Photoconductivity transients obtained from FP-TRMC usually reflect the molecular as well as supramolecular properties, and hence are helpful for correlating the structure, property and device performance relationship. FP-TRMC is an electrode-less technique, which gives information about the short-range (nanometer scale) intrinsic charge carrier transport properties. Use of the photoexcitation process allows us to cover a larger variety of materials and to determine their carrier mobility using quite a small amount of samples. Free carriers in semiconductors are able to strongly absorb microwave radiation in accordance with the relations given by Drude–Zener<sup>33</sup> or Drude–Smith,<sup>34</sup> and upon irradiation; their contributions to the relative change in microwave power dominate largely in comparison to the much less mobile impurity ions, dipoles, and trapped species. Therefore, the relative change in microwave power ( $\Delta P_r/P_r$ ) as a function of time due to the injection of excess carriers can also be studied. And eventually, it could be quantified in terms of  $\phi\Sigma\mu$  values where  $\phi$  is the charge carrier generation quantum yield obtained upon excitation with laser light and  $\Sigma\mu$  is the sum of charge carrier mobilities, i.e., the sum of electron and hole mobilities ( $\mu_e$  and  $\mu_h$ , respectively), other details related to this experiment is discussed in the experimental **Section 2.5**. We have therefore employed this technique to study the photoinduced charge carriers and further provide support to our observation discussed in the photovoltaic properties **Section 2.3.4**.

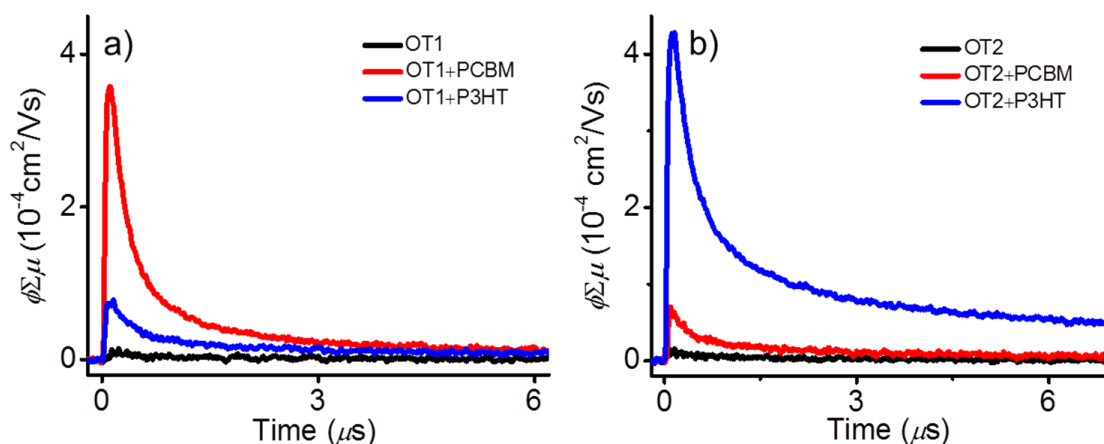


**Figure 2.16.** TRMC transients of a) **OT1** and b) **OT2** films and their blends (1:1 w/w) with PCBM and P3HT drop-cast from chlorobenzene solution.

The photoconductivity transients of **OT1** and **OT2** and their blends with P3HT and PCBM in the film state are shown in **Figure 2.16**. Both **OT1** and **OT2** exhibited comparable values of  $\phi \Sigma \mu_{\text{max}}$  ( $1.4 \times 10^{-5} \text{ cm}^2 \text{ V}^{-1} \text{ s}^{-1}$  and  $1.7 \times 10^{-5} \text{ cm}^2 \text{ V}^{-1} \text{ s}^{-1}$ , respectively) upon excitation using a 500 nm laser.  $\phi \Sigma \mu_{\text{max}}$  of **OT1** showed a 5-fold enhancement in the presence of P3HT (1:1 w/w) and a 24-fold increase in the presence of PCBM (1:1 w/w). This is consistent with the  $J_{\text{SC}}$  of the relevant OPV devices (**OT1**:P3HT– $0.69 \text{ mA cm}^{-2}$  and **OT1**:PCBM– $3.25 \text{ mA cm}^{-2}$ ). Significant enhancement of the photoconductivity in the presence of PCBM reiterated the p-type characteristics of **OT1**. On the other hand, under identical conditions,  $\phi \Sigma \mu_{\text{max}}$  of **OT2** increased by only 4 times in the presence of PCBM, and that of 25 times upon the addition of P3HT. This gave further proof for the n-type characteristics of **OT2**. We emphasize again that the FP-TRMC results are in line with the OPV devices (**OT2**:PCBM showed no diode output and **OT2**:P3HT– $0.72 \text{ mA cm}^{-2}$ ).

---

From the above studies, it is evident that the observed p/n-polarity of **OT1** and **OT2** in the bulk heterojunction assembly with P3HT/PCBM could be correlated with their molecular as well as supramolecular properties. The n-polarity of the molecules in the presence of P3HT could be mainly correlated with the relative HOMO–LUMO levels, which is a molecular property. However, the supramolecular effect is not completely ruled out either. In the presence of crystalline polymeric materials such as P3HT, amorphous **OT2** has an advantage over crystalline **OT1** due to effective nanoscale miscibility. This effect might help the former to perform well in the presence of P3HT. On the other hand, the p-polarity exhibited by the molecules could be exclusively dependent on the supramolecular interactions. **OT1** with a planar geometry formed a stable assembly, whereas **OT2** containing non-planar end-groups formed a weak assembly. As a result, the former assembly remained stable upon the addition of spherically shaped PCBM and functioned as an efficient p-type material in the presence of PCBM. On the other hand, **OT2** got dis-assembled in the presence of PCBM and hence failed to function as a p-type material.

Though these molecules illustrate an interesting example of the effect of the molecular structure on the supramolecular properties and thereby their p/n-polarity in bulk-heterojunction solar cells, the device performance fell short of expectation. This could be mainly attributed to the low value of  $J_{SC}$ , probably due to the lack of continuity in the oligomer phase resulting in hindered charge transport. As mentioned earlier, unlike polymers, oligomers exclusively depend on the intermolecular route for charge transport.

---

Lack of continuity is detrimental to efficient charge carrier transport to the electrodes and results in poor device performances. This may also result in imbalanced charge carrier mobility and lowers the  $FF$  value.

## 2.4. Conclusions

In summary, two thiophene oligomers with an acceptor–donor–acceptor structure consisting of oxazolone/isoxazolone derivatives as acceptors have been designed and synthesized. The isoxazolone derivative (**OT2**) was found to be a stronger electron-withdrawing unit than the oxazolone derivative (**OT1**), as evident from the photoabsorption and emission spectroscopy. Importantly, we have shown that the positional isomerism had a significant effect on the supramolecular properties. The suitable HOMO–LUMO energy levels of **OT2** favoured it to act as a better n-type material in the presence of P3HT in bulk-heterojunction solar cells. On the other hand, better supramolecular interaction in **OT1** helped it to form a stable bicontinuous network with PCBM and hence acted as a p-type material, which is consistent with the FP-TRMC evaluations. Though the dependence of molecular and supramolecular properties on device performances is well established, this work clearly illustrates how delicate changes in the basic molecular structure affect the ordering and p/n-polarity of organic semiconducting materials in bulk-heterojunction photovoltaic cells.

---

## 2. 5. Experimental section

### 2. 5. 1. Materials

The reagents and chemicals for synthesis were purchased either from local suppliers or from Sigma Aldrich, Alfa Aesar or TCI. Air- and water-sensitive synthetic steps were performed in an argon atmosphere using standard Schlenk techniques. Indium Tin Oxide (ITO)-coated glass substrates ( $<15 \Omega \text{ square}^{-1}$ ) was purchased from H. C. Stark and Sanyo Shinku Corp., respectively. [6,6]-Phenyl-C<sub>61</sub>-butyric acid methyl ester (PCBM) and regio-regular poly(3-hexylthiophene-2,5-diyl) (P3HT) were purchased from Frontier Carbon Inc. and Sigma Aldrich respectively.

Melting points were determined using a Mel-Temp-II melting point apparatus and are uncorrected. <sup>1</sup>H and <sup>13</sup>C NMR spectra were recorded on a 600 MHz Bruker Avance DRX-600 Spectrometer and a DPX 500 MHz spectrometer. All the chemical shifts were referenced to (CH<sub>3</sub>)<sub>4</sub>Si (TMS;  $\delta = 0$  ppm) for <sup>1</sup>H or residual CHCl<sub>3</sub> ( $\delta = 77$  ppm) for <sup>13</sup>C. High-resolution LCMS-TOF and MALDI-TOF mass spectra were recorded on a KRATOS ANALYTICAL SHIMADZU mass spectrometer using a-cyano-4-hydroxy cinnamic acid as the matrix. Absorption spectra were recorded on a Shimadzu UV-3101 spectrophotometer using quartz cuvettes with 1 cm path length. Fluorescence spectra were recorded using a Fluorolog HORIBA JOBINYVON. Fluorescence quantum yields were determined relative to standard compounds (rhodamine B in ethanol;  $\phi_F = 0.5$ ) using optically matching solutions. Fluorescence lifetimes were measured using an IBH FluoroCube time correlated picosecond single photon counting (TCSPC) system.



---

Samples were excited using a pulsed diode laser (<100 ps pulse duration) at a wavelength of 375 nm (NanoLED-11) with a repetition rate of 1 MHz. PYS measurements were performed on a Sumitomo Heavy Industry Co. PCR-202. For this measurement, thin films of the oligomers were spin-cast on an ITO-coated glass surface from chlorobenzene solution. The solvent was completely removed under vacuum before mounting onto the spectrometer. Photoelectrons emitted from the films were detected after illuminating the film with UV radiation. By increasing the photon energy at an interval of 0.1 eV, the photoelectron counts were measured. DFT calculations were performed using Gaussian 09 to obtain the energy minimized structures of the molecules.<sup>34</sup> The B3LYP functions with the 6-31G(d,p) basis set were used and for simplicity, the *n*-hexyl side chains were replaced by methyl groups. XRD analysis was done by using a Xeuss Simultaneous WAXS with Ni-filtered Cu K<sub>α</sub> radiation ( $\lambda = 0.154$  nm). Thermal gravimetric analysis was carried out using a Perkin Elmer STA 6000 simultaneous thermal analyzer. Platinum pans were used for the measurement and as reference samples. The analysis was conducted between 50 and 600 °C at 10 °C min<sup>-1</sup> under dry N<sub>2</sub>. Transient conductivity was measured by the FP-TRMC technique. A resonant cavity was used to obtain a high degree of sensitivity in the measurement. The resonant frequency and the microwave power were set at ~9.1 GHz and 3 mW, respectively, so that the electric field of the microwave was sufficiently small not to disturb the motion of charge carriers. The value of conductivity is converted to the product of the quantum yield ( $\phi$ ) and the sum of charge carrier mobilities ( $\Sigma\mu$ ), by the following equation.

---

$$\phi \sum \mu = \frac{1}{e \cdot A \cdot I_0 \cdot F_{light}} \cdot \frac{\Delta P_r}{P_r}$$

where  $e$ ,  $A$ ,  $I_0$ ,  $F_{light}$ ,  $\Delta P_r$ , and  $P_r$  are the unit charge of a single electron, a sensitivity factor  $[(S/m)^{-1}]$ , incident photon density of the excitation laser (photons per  $m^2$ ), a correction (or filling) factor ( $/m$ ), a change in reflected microwave power, and a power of reflected microwave, respectively. The change in conductivity is equivalent to  $\Delta P_r/(AP_r)$ . 500 nm laser light with a photon density of  $6.4 \times 10^{15}$  photons per  $cm^2$  was used as the excitation source. The sample was set at the highest electric field in a resonant cavity. The experiments were carried out at room temperature.

## 2.5.2. Synthesis and characterization

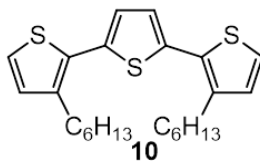
### 2.5.2.1. General procedure for Suzuki coupling

The dibromothiophene derivative and 3-hexylthiophene-2-boronic acid pinacol ester were weighed accurately into a two-necked round bottom flask and dissolved in degassed toluene. 2 M aq.  $K_2CO_3$  and a few drops of Aliquat 336 were added to the mixture and the flask was equipped with a reflux condenser and a septum. Air was removed from the setup and replaced by Ar three times by using the freeze-pump-thaw method, then  $Pd(PPh_3)_4$  was added under Ar counter flow. The reaction mixture was heated and stirred in Ar for 24 h, then poured into water and extracted with  $CH_2Cl_2$ . The combined organic layers were washed with brine and water, dried over  $Na_2SO_4$  and evaporated to dryness under vacuum.

### 2. 5. 2. 2. General procedure for bromination

The thiophene derivative was dissolved in chloroform–acetic acid mixture (1:1 v/v). The reaction mixture was kept in the dark and cooled to 0 °C by using a salt-ice bath. *N*-Bromosuccinimide (NBS) was added in several portions, and the reaction mixture was stirred at room temperature for 6 h followed by stirring at 50 °C for 4 h. The reaction mixture was then added to water and extracted with CH<sub>2</sub>Cl<sub>2</sub>. The combined organic layers were washed with aq. NaHCO<sub>3</sub>, brine, and water, dried over anhydrous Na<sub>2</sub>SO<sub>4</sub> and evaporated to dryness under vacuum.

#### *Synthesis of 3,3''-dihexyl-2,2':5,2''-terthiophene (10).*

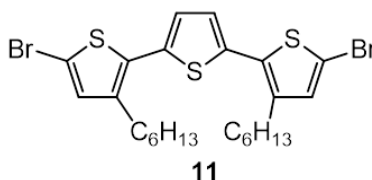


**10** was prepared by Suzuki coupling using 2,5-dibromothiophene (3.20 g, 13.23 mmol, 1 eq.), 3-hexylthiophene-2-boronic acid pinacol ester (8.17 g, 27.78 mmol, 2.1 eq.), 2 M aq. K<sub>2</sub>CO<sub>3</sub> (30 mL), Aliquat 336 (4 drops), Pd(PPh<sub>3</sub>)<sub>4</sub> (0.92 g, 0.79 mmol, 0.06 eq.) and toluene (100 mL). The crude product was purified by column chromatography (silica gel, hexane) to provide **10** as a viscous pale yellow liquid. Yield: 74%.

$\delta_{\text{H}}$  (600 MHz, CDCl<sub>3</sub>, ppm): 7.20 (d, 2H,  $J = 5.4$  Hz), 7.08 (s, 2H), 6.96 (d, 2H,  $J = 5.4$  Hz), 2.80 (t, 4H,  $J = 7.8$  Hz), 1.63–1.68 (m, 4H), 1.22–1.35 (m, 12H), 0.87 (t, 6H,  $J = 7$  Hz).  $\delta_{\text{C}}$  (150 MHz, CDCl<sub>3</sub>, ppm): 139.69, 136.07, 130.27, 126.07, 123.72, 31.73, 30.78, 29.31, 29.25, 22.64, 14.12.

---

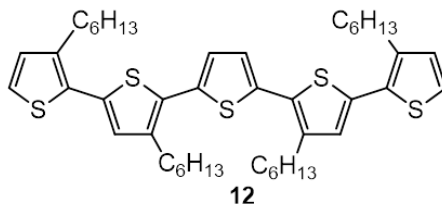
**Synthesis of 5,5''-dibromo-3,3''-dihexyl-2,2':5',2''-terthiophene (11)**



Bromination of terthiophene **10** (2.00 g, 4.80 mmol, 1.0 eq.) was carried out using *N*-bromosuccinimide (1.79 g, 10.08 mmol, 2.1 eq.), in a chloroform–acetic acid mixture (100 mL). The crude product was purified by column chromatography (silica gel, 50% CHCl<sub>3</sub>–hexane). A pure product **11** was obtained as light yellow oil. Yield: 98%.

$\delta_{\text{H}}$  (600 MHz, CDCl<sub>3</sub>, ppm): 6.97 (s, 2H), 6.89 (s, 2H), 2.69 (t,  $J = 7.8$  Hz, 4H), 1.65–1.54 (m, 4H), 1.29–1.27 (m, 12H), 0.87 (t,  $J = 3.6$  Hz, 6H).  $\delta_{\text{C}}$  (150 MHz, CDCl<sub>3</sub>, ppm): 140.47, 135.15, 132.68, 131.57, 126.44, 110.65, 31.59, 30.55, 29.20, 29.11, 22.62, 14.09.

**Synthesis of 3,3',3'',3'''-quadrihexyl-2,5':2',5'':2'',2''':5''',2''''-quinquethiophene (12).**

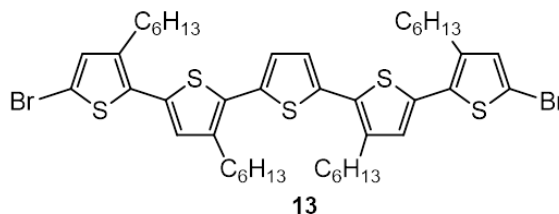


**12** was synthesized through Suzuki coupling using dibromoterthiophene **11** (1.90 g, 3.31 mmol, 1.0 eq.), 3-hexylthiophene-2-boronic acid pinacol ester (2.04 g, 6.95 mmol, 2.1 eq.), 2 M aq. K<sub>2</sub>CO<sub>3</sub> (16.5 mL), Aliquat 336 (2 drops), Pd(PPh<sub>3</sub>)<sub>4</sub> (191 mg, 0.17 mmol, 0.05 eq.), and toluene (30 mL). The crude product was purified using column

chromatography (silica gel, hexane). A pure product was obtained as viscous golden yellow oil. Yield: 83%.

$\delta_{\text{H}}$  (600 MHz,  $\text{CDCl}_3$ , ppm): 7.16 (d,  $J = 4.8$  Hz, 2H), 7.08 (s, 2H), 6.95 (s, 2H), 6.93 (d,  $J = 4.8$  Hz, 2H), 2.78 (t,  $J = 9.6$  Hz, 8H), 1.70–1.63 (m, 8H), 1.37–1.29 (m, 24H), 0.88 (m, 12H).  $\delta_{\text{C}}$  (150 MHz,  $\text{CDCl}_3$ , ppm): 139.85, 139.65, 135.72, 134.24, 130.44, 130.22, 130.09, 128.74, 125.89, 123.61, 31.68, 31.66, 30.65, 30.58, 29.44, 29.28, 29.26, 29.21, 22.63, 22.62, 14.09.

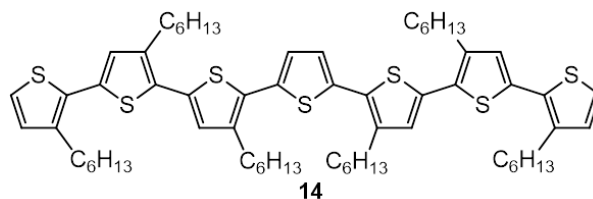
**Synthesis of 5,5''''-dibromo-3,3',3''',3''''-quadrihexyl-2,5':2',5'':2'',2''':5''',2''''-quinquethiophene (13)**



**12** (1.20 g, 1.60 mmol, 1.0 eq.) was brominated using *N*-bromosuccinimide (0.60 g, 3.36 mmol, 2.1 eq.), in a chloroform–acetic acid mixture (75 mL) at 0 °C. The crude product was purified by column chromatography (silica gel, 50%  $\text{CHCl}_3$ –hexane) to yield the pure product of **13** as yellow oil. Yield: 89%.

$\delta_{\text{H}}$  (600 MHz,  $\text{CDCl}_3$ , ppm): 7.08 (s, 2H), 6.88 (s, 2H), 6.89 (s, 2H), 2.77 (t,  $J = 7.8$  Hz, 4H), 2.71 (t,  $J = 7.8$  Hz, 4H), 1.68–1.54 (m, 8H), 1.42–1.28 (m, 24H), 0.88 (m, 12H).  $\delta_{\text{C}}$  (150 MHz,  $\text{CDCl}_3$ , ppm): 140.23, 139.95, 135.62, 132.90, 132.70, 131.92, 130.67, 129.09, 126.07, 110.33, 31.66, 31.60, 30.54, 30.51, 29.39, 29.23, 29.21, 29.09, 22.62, 22.58, 14.08.

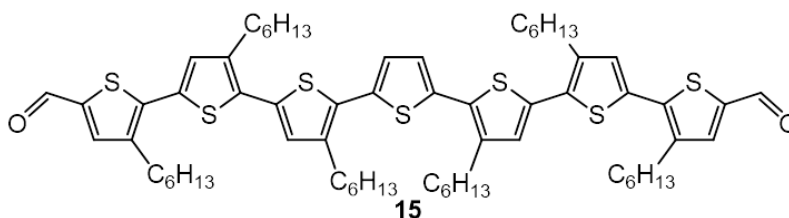
**Synthesis of 3,3',3'',3''',3''''',3''''''-sexihexyl-2,5':2',5'':2'', 2''':5''',2''''':5''''', 2''''''':5''''''',2''''''''-septithiophene (14)**



**14** was synthesized through Suzuki coupling of dibromo quinquethiophene **13** (907 mg, 1.00 mmol, 1.0 eq.), 3-hexylthiophene-2-boronic acid pinacol ester (617 mg, 2.10 mmol, 2.1 eq.), 2 M aq.  $K_2CO_3$  (5 mL), Aliquat 336 (1 drop),  $Pd(PPh_3)_4$  (57 mg, 0.05 mmol, 0.05 eq.), and toluene (8 mL) were used. The crude product obtained after reaction was purified using column chromatography (silica gel, hexane). Product was obtained as a brick red solid. Yield: 70%.

$\delta_H$  (600 MHz,  $CDCl_3$ , ppm): 7.16 (d,  $J = 4.4$  Hz, 2H), 7.10 (s, 2H), 6.97 (s, 2H), 6.94 (d,  $J = 4.2$  Hz, 4H), 2.78 (m, 12H), 1.67 (m, 12H), 1.33 (m, 36H), 0.89 (m, 18H).  $\delta_C$  (150 MHz,  $CDCl_3$ , ppm): 139.93, 139.82, 139.62, 135.78, 134.10, 133.99, 130.54, 130.33, 130.10, 128.75, 128.56, 125.91, 123.58, 31.68, 31.57, 31.67, 30.67, 30.60, 30.50, 29.28, 29.24, 29.21, 22.63, 14.10.

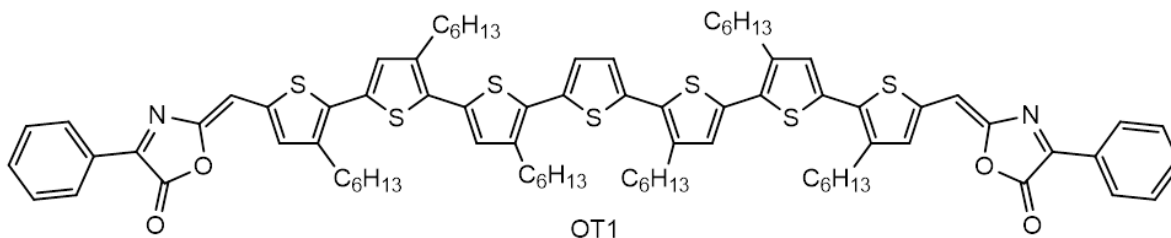
**Synthesis of 5,5''''''-diformyl-3,3',3'',3''',3''''',3''''''-sexihexyl-2,5':2',5'':2'',2''':5''',2''''':5''''', 2''''''':5''''''',2''''''''-septithiophene (15)**



A Vilsmeier reagent was prepared by mixing POCl<sub>3</sub> (0.16 mL, 1.81 mmol, 3.01 eq.) and DMF (0.66 mL, 9.0 mmol, 15.0 eq.) under inert ice-cold condition. In another two-necked flask, septithiophene **14** (650 mg, 0.60 mmol, 1.0 eq.) was dissolved in anhydrous 1,2-dichloroethane (7 mL) by stirring and cooled to 0 °C using an ice bath under an Ar atmosphere. To this solution, the Vilsmeier reagent was added dropwise, the reaction mixture was then heated to 60 °C, and stirred for 12 h. The mixture was poured into ice water (200 mL), neutralized with Na<sub>2</sub>CO<sub>3</sub>, and then extracted with CH<sub>2</sub>Cl<sub>2</sub>. The combined organic layer was washed with brine, water, and dried over Na<sub>2</sub>SO<sub>4</sub>. After removal of solvent, the crude product was purified using column chromatography (silica gel, 70% CH<sub>2</sub>Cl<sub>2</sub>-hexane) to afford **15** as a brown solid. Yield: 80%.

$\delta_{\text{H}}$  (600 MHz, CDCl<sub>3</sub>, ppm): 9.82 (s, 2H), 7.58 (s, 2H), 7.14 (d,  $J = 3.6$  Hz, 4H), 7.01 (s, 2H), 2.81 (m, 12H), 1.70 (m, 12H), 1.35 (m, 36H), 0.90 (m, 18H).  $\delta_{\text{C}}$  (150 MHz, CDCl<sub>3</sub>, ppm): 181.88, 141.21, 140.43, 140.34, 140.25, 140.06, 139.15, 135.82, 133.31, 132.79, 132.65, 130.94, 130.52, 129.23, 126.18, 31.90, 30.98, 30.81, 30.65, 30.46, 29.99, 29.64, 29.58, 29.52, 22.62, 14.11.

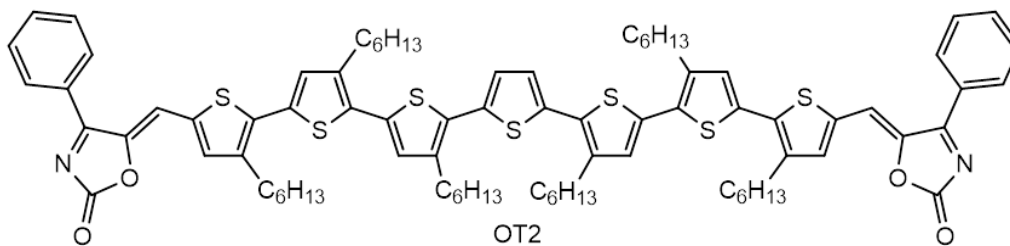
### Synthesis of OT1



**OT1** was prepared by dissolving diformylseptithiophene derivative **15** (50 mg, 0.04 mmol, 1 eq.) and 2-phenyl-5-oxazolone (54 mg, 0.34 mmol, 8.0 eq.) in dry chloroform (10 mL) by stirring under an argon atmosphere. Three drops of triethylamine was added to the reaction mixture, stirred for 8 h at room temperature, and for 1 h at 60 °C. The reaction mixture was then diluted with CHCl<sub>3</sub>, washed with water and brine. The combined organic layer was dried over Na<sub>2</sub>SO<sub>4</sub>, and evaporated to dryness under vacuum. The crude product was purified by column chromatography (silica gel, CHCl<sub>3</sub>) to afford **OT1** as a blackish brown solid. Yield: 88%; Melting Point: 193–194 °C.

$\delta_{\text{H}}$  (500 MHz, CDCl<sub>3</sub>, ppm): 8.20 (d,  $J = 8$  Hz, 4H), 7.61 (t,  $J = 8.4$  Hz, 2H), 7.55 (t,  $J = 9$  Hz, 4H), 7.42 (s, 2H), 7.39 (s, 2H), 7.18 (s, 2H), 7.14 (s, 2H), 7.05 (s, 2H), 2.86–2.82 (m, 12H), 1.72 (d,  $J = 6$  Hz, 12H), 1.45 (s, 12H), 1.36 (t,  $J = 4.8$  Hz, 24H), 0.92 (t,  $J = 3.6$  Hz, 18H).  $\delta_{\text{C}}$  (125 MHz, CDCl<sub>3</sub>, ppm): 167.01, 161.93, 141.32, 140.27, 138.85, 135.73, 135.00, 133.55, 133.01, 132.30, 130.79, 130.31, 128.91, 128.27, 126.09, 125.69, 124.58, 31.66, 30.49, 30.18, 30.11, 29.76, 29.68, 29.43, 29.22, 29.17, 22.63, 14.09. IR (KBr)  $\nu_{\text{max}}$ : 2920, 2848, 1785, 1639, 1555, 1441, 1326, 1263, 1149, 1086, 1013, 815, 690, 576 cm<sup>-1</sup>; MALDI-TOF-MS:  $m/z = 1423.15$  (calcd = 1422.56).

### Synthesis of OT2





**OT2** was synthesized by following a similar procedure employed for preparing **OT1** using diformylseptithiophene derivative **15** (50 mg, 0.04 mmol, 1.0 eq.), 3-phenyl-5-isoxazolone (54 mg, 0.34 mmol, 8.0 eq.), and dry chloroform (10 mL). The crude product was purified by column chromatography (silica gel, CHCl<sub>3</sub>) to afford the **OT2** as a dark brown solid. Yield: 88%; Melting Point: 74–75 °C.

$\delta_{\text{H}}$  (500 MHz, CDCl<sub>3</sub>, ppm): 7.75 (s, 2H), 7.62–7.58 (m, 12H), 7.324 (s, 2H), 7.13 (s, 2H), 7.05 (2H), 2.86–2.80 (m, 12H), 1.74–1.68 (m, 12H), 1.42 (t,  $J = 6$  Hz, 12H), 1.34 (m, 24H), 0.90 ppm (t,  $J = 3.6$  Hz, 18H).  $\delta_{\text{C}}$  (125 MHz, CDCl<sub>3</sub>, ppm): 173.89, 164.93, 149.82, 143.18, 138.45, 138.13, 138.02, 137.11, 136.62, 133.13, 131.67, 131.05, 129.25, 128.77, 128.28, 126.17, 124.61, 31.65, 30.58, 30.52, 30.06, 29.70, 29.51, 29.37, 29.31, 29.22, 22.65, 14.12. IR (KBr)  $\nu_{\text{max}}$ : 2924, 2846, 1789, 1635, 1545, 1429, 1324, 1262, 1147, 1095, 1022, 814, 689, 564 cm<sup>-1</sup>; MALDI-TOF-MS:  $m/z = 1422.89$  (calcd = 1422.56).

## 2.6. Reference

1. F. Martini, S. Borsacchi, S. Spera, C. Carbonera, A. Cominetti, M. Geppi, *J. Phys. Chem. C* **2013**, *117*, 131–139.
2. B. C. Thompson, J. M. J. Fréchet, *Angew. Chem., Int. Ed. Engl.* **2008**, *47*, 58–77.
3. Y. Kim, S. Cook, S. M. Tuladhar, S. A. Choulis, J. Nelson, J. R. Durrant, D. D. C. Bradley, M. Giles, I. McCulloch, C.-S. Ha, M. Ree, *Nat. Mater.* **2006**, *5*, 197–203.
4. J. L. Segura, N. Martin, D. M. Guldi, *Chem. Soc. Rev.* **2005**, *34*, 31–47.
5. Y. Koizumi, M. Ide, A. Saeki, C. Vijayakumar, B. Balan, M. Kawamoto, S. Seki, *Polym. Chem.* **2013**, *4*, 484–494.

- 
6. C. Vijayakumar, A. Saeki, S. Seki, *Chem. – Asian J.* **2012**, *7*, 1845–1852.
  7. H. Zhou, L. Yang, W. You, *Macromolecules*, **2012**, *45*, 607–632.
  8. Y.-J. Cheng, S.-H. Yang, C.-S. Hsu, *Chem. Rev.*, **2009**, *109*, 5868–5923.
  9. K. R. Graham, C. Cabanetos, J. P. Jahnke, M. N. Idso, A. El Labban, G. O. N. Ndjawa, T. Heumueller, K. Vandewal, A. Salleo, B. F. Chmelka, A. Amassian, P. M. Beaujuge, M. D. McGehee, *J. Am. Chem. Soc.* **2014**, *136*, 9608–9618.
  10. F. Li, K. G. Yager, N. M. Dawson, Y. Jiang, K. J. Malloy, Y. Qin, *Chem. Mater.* **2014**, *26*, 3747–3756.
  11. K. Yao, L. Chen, F. Li, P. Wang, Y. Chen, *J. Phys. Chem. C*, **2012**, *116*, 714–721.
  12. G. Li, V. Shrotriya, J. Huang, Y. Yao, T. Moriarty, K. Emery, Y. Yang, *Nat. Mater.* **2005**, *4*, 864–868.
  13. L. Chang, H. W. A. Lademann, J.-B. Bonekamp, K. Meerholz, A. J. Moulé, *Adv. Funct. Mater.* **2011**, *21*, 1779–1787.
  14. D. H. Wang, P.-O. Morin, C.-L. Lee, A. K. Ko Kyaw, M. Leclerc, A. J. Heeger, *J. Mater. Chem. A* **2015**, *2*, 15052–15057.
  15. K. R. Graham, J. Mei, R. Stalder, J. W. Shim, H. Cheun, F. Ste, F. So, B. Kippelen, J. R. Reynolds, *ACS Appl. Mater. Interfaces* **2011**, *3*, 1210–1215.
  16. J. S. Moon, C. J. Takacs, S. Cho, R. C. Coffin, H. Kim, G. C. Bazan, A. J. Heeger, *Nano Lett.* **2010**, *10*, 4005–4008.
  17. A. L. Ayzner, D. D. Wanger, C. J. Tassone, S. H. Tolbert, B. J. Schwartz, *J. Phys. Chem. C*, **2008**, *112*, 18711–18716.
  18. E. Verploegen, R. Mondal, C. J. Bettinger, S. Sok, M. F. Toney, Z. Bao, *Adv. Funct. Mater.* **2010**, *20*, 3519–3529.
  19. B. Balan, C. Vijayakumar, A. Saeki, Y. Koizumi, S. Seki, *Macromolecules*, **2012**, *45*, 2709–2719.
  20. P. Carbone, A. Troisi, *J. Phys. Chem. C* **2014**, *5*, 2637–2641.
  21. R. Noriega, J. Rivnay, K. Vandewal, F. P. V Koch, N. Stingelin, P. Smith, M. F. Toney, A. Salleo, *Nat. Mater.* **2013**, *12*, 1038–1044.

- 
22. X. Lin, Y. Tani, R. Kanda, K.-I. Nakayama, S. Yagai, *J. Mater. Chem. A* **2013**, *1*, 14686–14691.
  23. X. Che, C. Chung, X. Liu, S. Chou, Y. Liu, K. Wong, S. R. Forrest, *Adv. Mater.* **2016**, *28*, 8248–8255.
  24. T. Zhang, H. Han, Y. Zou, Y. Lee, H. Oshima, K. Wong, R. J. Holmes, *Appl. Mater. Interface* **2017**, *9*, 25418–25425.
  25. H. Wu, H. Fan, S. Xu, L. Ye, Y. Guo, Y. Yi, H. Ade, X. Zhu, *Small* **2019**, *15*, 1804271.
  26. S. Prasanthkumar, S. Ghosh, V. C. Nair, A. Saeki, S. Seki, A. Ajayaghosh, *Angew. Chem. Int. Ed.* **2015**, *54*, 946–950.
  27. M. Tsuji, A. Saeki, Y. Koizumi, N. Matsuyama, C. Vijayakumar, S. Seki, *Adv. Funct. Mater.* **2014**, *24*, 28–36.
  28. A. Saeki, S. Yoshikawa, M. Tsuji, Y. Koizumi, M. Ide, C. Vijayakumar, S. Seki, *J. Am. Chem. Soc.*, **2012**, *134*, 19035–19042.
  29. A. Saeki, Y. Koizumi, T. Aida, S. H. U. Seki, *Acc. Chem. Res.* **2012**, *45*, 1193–1202.
  30. T. Erb, U. Zhokhavets, G. Gobsch, S. Raleva, B. Stühn, P. Schilinsky, C. Waldauf, C. J. Brabec, *Adv. Funct. Mater.* **2005**, *15*, 1193–1196.
  31. S. D. Dimitrov, J. R. Durrant, *Chem. Mater.* **2014**, *26*, 616–630.
  32. S. Prasanthkumar, A. Seki, S. Seki, A. Ajayaghosh, *J. Am. Chem. Soc.* **2010**, *132*, 8866–8867.
  33. B. Donovan, N. H. March, *Proc. Phys. Soc., Sect. B* **1956**, *69*, 528.
  34. N. V. Smith, *Phys. Rev. B* **2001**, *64*, 155106.
  35. M. J. Frisch, *et al.*, Gaussian 09, Revision A02, Gaussian Inc., Wallingford, CT, **2009**.

---

### Optimization of Photovoltaic Efficiency and Structure-Property Correlation of Thiophene Oligomers

---

#### 3.1 Abstract

*In this chapter, semiconducting conjugated oligomers having same end group (N-ethylrhodanine) but different central core (thiophene: **OT-3**, bithiophene: **OT-4**, thienothiophene: **OT-5**) connected through alkylated terthiophene were synthesized. The effect of the incorporation of extra thiophene to the central thiophene unit either through C–C bond linkage to form bithiophene or by fusing two thiophenes together to form thienothiophene on the optoelectronic properties and photovoltaic performances of the oligomers were studied in detail. FP–TRMC shows **OT-5** has significantly higher photoconductivity than **OT-3** and **OT-4** implying that the former can outperform the latter two derivatives by a wide margin under identical conditions in a BHJ solar cell device. However, the initial photovoltaic devices fabricated from all three oligomers (with PC<sub>71</sub>BM as the acceptor) gave PCEs of about 0.7%, which was counterintuitive to the TRMC observation. By using TRMC results as a guiding tool, solution engineering was carried out; no remarkable changes were seen in the PCE of **OT-3** and **OT-4**. On the other hand, 5-fold enhancement in the device efficiency was achieved in **OT-5** (PCE: 3.52%, V<sub>OC</sub>: 0.80 V, J<sub>SC</sub>: 8.74 mA cm<sup>-2</sup>, FF: 0.50), which was in correlation with the TRMC results. The structure-property correlation and the fundamental reasons for the improvement in device performance upon solvent engineering were studied in detail.*

## 3.2. Introduction

One of the major progress seen in the donor molecular design strategy was the breakthrough of push-pull organic semiconductors. Bringing together electron-deficient terminal units (acceptor) and an electron-rich central unit (donor) to form an acceptor-donor-acceptor structure helped to tune the absorption as well as energy levels to achieve high PCEs in oligothiophenes.<sup>1-4</sup> Among a variety of acceptor dye units, *N*-ethylrhodanine is being used extensively to develop donor-acceptor and acceptor-donor-acceptor type semiconducting small molecules and oligomers for photovoltaic applications.<sup>5-7</sup> Due to its electron withdrawing abilities, *N*-ethylrhodanine is capable of reducing the optical band gap of associated molecules resulting in better absorption in the visible region. Moreover, it can contribute significantly toward the overall absorption of the molecules.

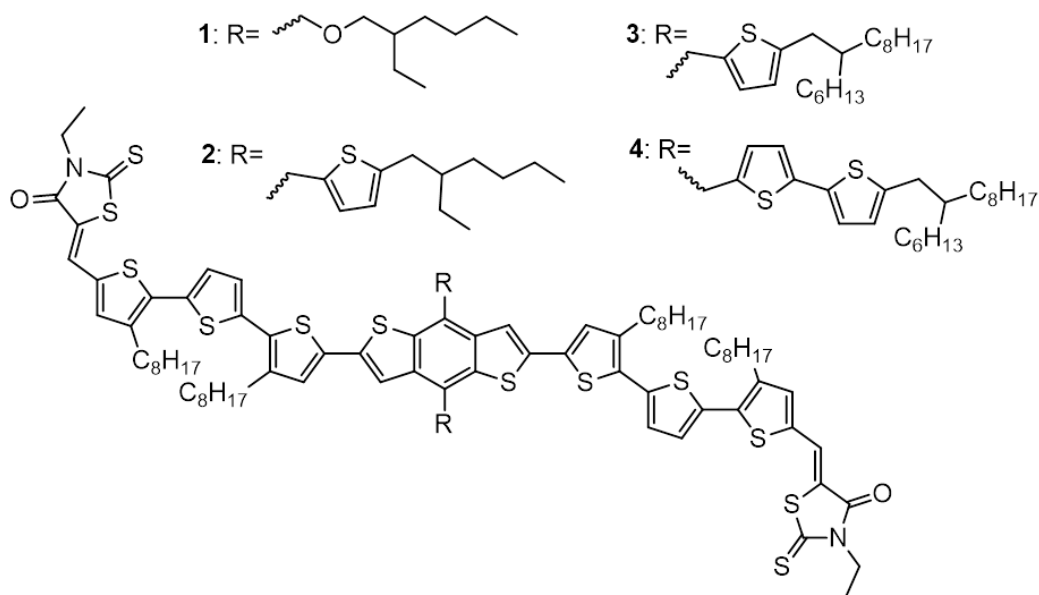


Figure 3.1. Chemical structures of the small molecules (1-4).

---

In 2013, Chen *et al.* have designed and synthesized four A-D-A type small molecules with a benzo[1,2-*b*:4,5-*b'*]dithiophene (BDT) unit as the central building block and *N*-ethylrhodanine as the acceptor unit (**1-4**; **Figure 3.1**).<sup>8</sup> *N*-ethylrhodanine was selected as the end group after a systematic screening of all the available end groups. The increased conjugation length with the introduction of extra thiophene unit in the BDT core resulted in redshifts in solution absorption spectra of **2-4** when compared to **1**. A conventional BHJ device consisting of the structure, ITO/PEDOT:PSS/blend/LiF/Al, was adopted for the analysis of solar cell performance. Authors have tried many additives, out of which addition of polydimethylsiloxane to the active-material in chloroform was found to be best for the device fabrication. All the oligomers showed an improved efficiency upon careful solution engineering. The efficiency of **2** enhanced from 7.51 to 8.12% which is the highest PCE among all the molecules. On the other hand, the efficiency of **1** improved from 6.92 to 7.38%, while that of **3** from 6.32 to 6.79% and **4** from 7.58 to 8.02%. The optimum size of the domains and improved D-A interpenetrating networks resulted in the improved efficiency in all these cases on solution engineering.

Fullerene derivatives such as PC<sub>61</sub>BM and PC<sub>71</sub>BM are generally used as electron acceptors, the latter of which is preferred over the former due to its better photoabsorption in a broad wavelength region. As the solvent evaporates, donor and acceptor phase-separate to form nanoscale domains throughout the photoactive layer. The best solar cells are those composed of domains that are about ten nanometers in size.<sup>9,10</sup> But both PC<sub>61</sub>BM and PC<sub>71</sub>BM would tend to aggregate and form large domains with the

size of  $\sim 100\text{-}200$  nm.<sup>11-13</sup> In order to prevent the formation of large domains, solution engineering through varying the solvent and by incorporating solvent additives was found to be an effective strategy.<sup>14-15</sup> Selection of solvent depends on the optimum solubility of the semiconductor in that solvent. For the selection of additives, two major requirements should be met, (1) the boiling point should be higher than that of the solvent used for processing the device in order to increase the interaction time between the additive and the active layer components during thin film formation; (2) one component (donor or acceptor) of the active layer must be more soluble in the additive than the other one.

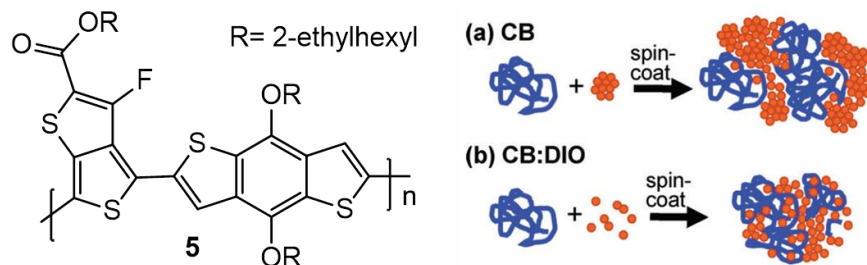


**Figure 3.2.** Schematic representation of donor (polymer: **5**) and PC<sub>71</sub>BM aggregation in (a) CB and (b) CB:DIO, and the resulting film morphology (*Adapted from reference 16*).

Lou *et al.* have shown that the addition of diiodooctane (DIO) to a solution of active layer completely dissolves the PC<sub>71</sub>BM aggregates and promotes the formation of smaller domains and greater interpenetrating donor-acceptor networks within the film.<sup>16</sup> To study this aspect, they have utilized a polymer donor (**5**) and PC<sub>71</sub>BM as acceptor (**Figure 3.2**). They have confirmed their observation by small-angle X-ray scattering (SAXS) investigation on active layer of polymer:PC<sub>71</sub>BM solutions. A plausible explanation for this observation was the presence of strong interaction between DIO and PC<sub>71</sub>BM. The

presence of the negative charge on the iodine of DIO and the electron deficient nature of PC<sub>71</sub>BM could be attributed to the strong interaction.

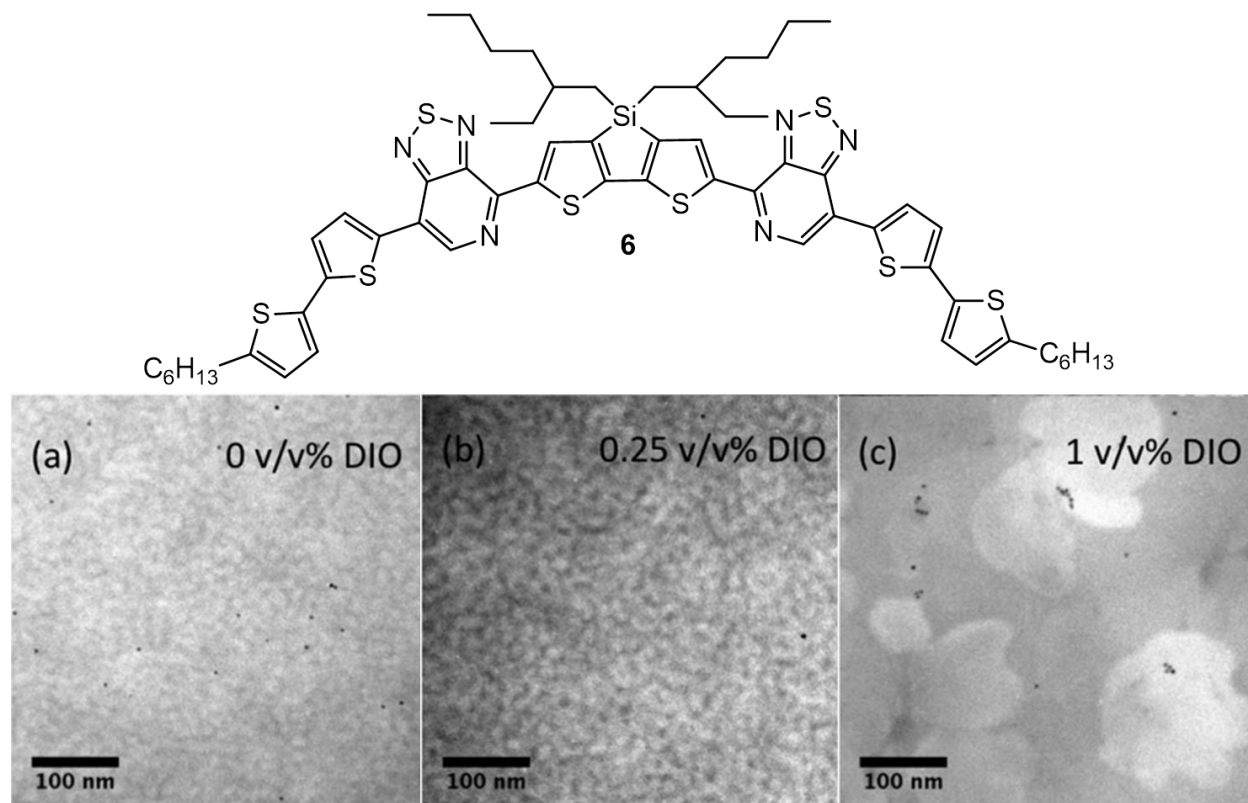


**Figure 3.3.** Chemical structure of small molecule **6** in the upper panel and the lower panel shows the EF-TEM images of active layers of a) 0, b) 0.25, and c) 1.0 v/v% DIO added to the film casting solution. The light regions in each image represent donor-rich domains (*Adapted from reference 17*).

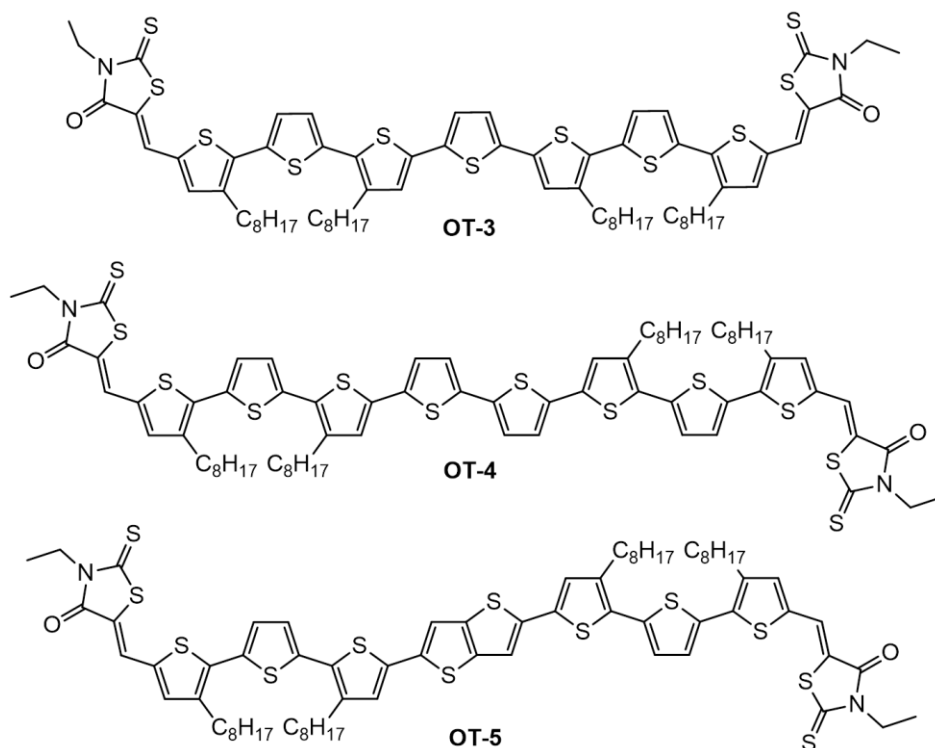
Bazan and co-workers in 2014 studied the effect of the addition of small volumes of DIO on the BHJ solar cell efficiency.<sup>17</sup> For this study, they have used the oligomer **6** (**Figure 3.3**) as the donor and PC<sub>71</sub>BM as the acceptor. Devices fabricated using an active layer without solvent additive treatment had a PCE of 4.5%. When 0.25 v/v % DIO was added to the active layer (**6**:PC<sub>71</sub>BM) several parameters of the solar cell got improved and resulted in a high PCE of 6.70%. The energy filtered transmission electron



microscopy (EF-TEM) images (**Figure 3.3**) have shown how the domain size changes due to the presence of DIO. It was also observed that the nanostructures of the polymer have enhanced connectivity when 0.25 v/v% DIO was used. When 1 v/v% was used, retention of DIO was observed in the active films as evident from the dynamic secondary ion mass spectrometry. This resulted in poor PCE of 0.43%.

Apart from solution engineering, proper design of the donor molecules is also very crucial. Ideally, the donor molecules should have good solubility, broad absorption over the entire UV–visible region, suitable HOMO–LUMO energy levels with respect to acceptor molecules, good redox properties, and appreciable hole mobility.

### 3. 3. Results and discussion



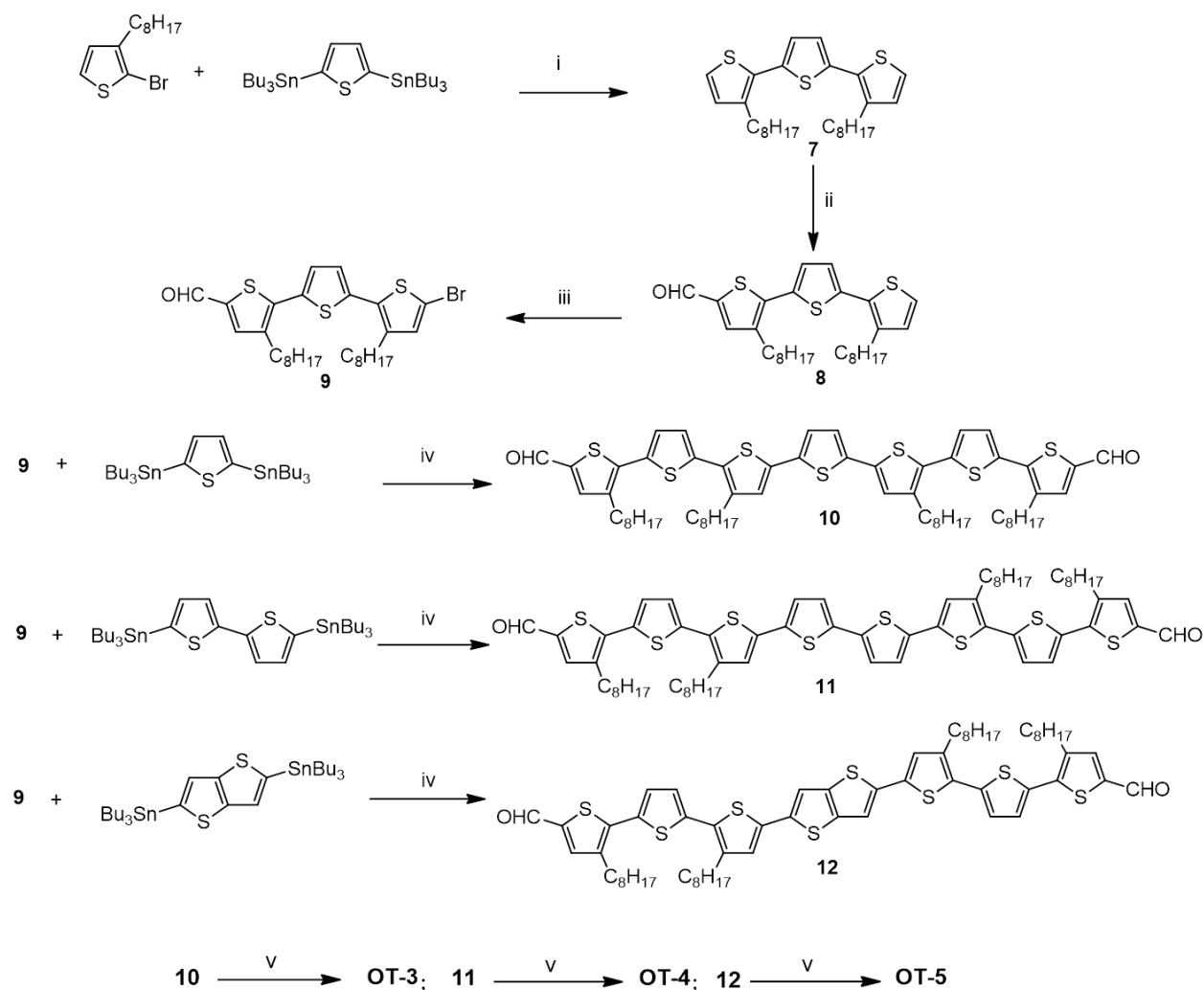
**Scheme 3.1.** Chemical structures of the oligomers under study.

---

In **Chapter 2** of the thesis, we have studied the structure-property correlation of acceptor-donor-acceptor (A-D-A) molecules whose acceptor part is slightly varied by using positional isomers. In this chapter, a series of A-D-A type oligomers, having same end group (*N*-ethylrhodanine) and similar pi-linker (alkylated terthiophene) but different central core (thiophene: **OT-3**,<sup>18</sup> bithiophene: **OT-4**, thienothiophene: **OT-5**, respectively) were synthesized (**Scheme 3.1**). We have investigated how the incorporation of extra thiophene to the central thiophene group either through C-C bond linkage (bithiophene) or by fusing two thiophenes (thienothiophene) affect the optoelectronic properties and photovoltaic performances of the oligomers. Flash-photolysis time-resolved microwave conductivity (FP-TRMC) was used for the initial screening to find the outperformer among the three, and the device performances were optimized through solution engineering. UV-vis absorption, atomic force microscopy (AFM), bright-field transmission electron microscopy (BF-TEM), photoluminescence quenching analysis, and two-dimensional grazing incidence X-ray diffraction (2D-GIXRD) studies were carried out in detail to correlate the structure-property-device performance relationship.

### **3.3.1. Synthesis and photophysical characterization**

The oligomers were synthesized using methods reported in the literature as shown in **Scheme 3.2**. Suzuki coupling of 2-bromo-3-octylthiophene and 2,5-bis(tributylstannyl)-thiophene afforded the compound **7** in 85% yield. Subsequent formylation of **7** using Vilsmeier-Hack reagent resulted in an orange oil of **8** in 80% yields. Bromination of **8** was



**Scheme 3.2.** Synthesis of oligothiophene **OT-3**, **OT-4** and **OT-5**; *Reagents and reaction conditions:* (i)  $\text{Pd}_2(\text{dba})_3$ ,  $\text{P}(\text{o-tolyl})_3$ , Toluene, 2d, 110 °C ; (ii)  $\text{POCl}_3$ , DMF, 1,2-dichloroethane; (iii) NBS, AcOH,  $\text{CHCl}_3$ ; (vi)  $\text{Pd}(\text{PPh}_3)_4$ , Toluene, 2d; (v) *N*-ethylrhodanine, dry  $\text{CHCl}_3$ , piperidine, 24h.

carried out using *N*-bromosuccinimide in chloroform–acetic acid mixture provided **9** with a 98% yield. Suzuki coupling of **9** with corresponding different stannylated derivatives afforded three bisaldehydes (**10-12**). Coupling of **9** with 2,5-bis(tributylstannyl)thiophene gave the product **10**, with 5,5'-bis(tributylstannyl)-2,2'-bithiophene yielded **11** and with 2,5-bis(tributylstannyl)thieno[3,2-*b*]thiophene afforded the bisaldehyde products **12**.

Finally, incorporation of *N*-ethylrhodanine acceptor into the thiophene backbone was carried out by the Knoevenagel condensation method in the presence of triethylamine as the base. All the derivatives **OT-3**, **OT-4**, and **OT-5** were obtained in good yields and characterized by various analytical techniques such as  $^1\text{H}$  NMR,  $^{13}\text{C}$  NMR, IR and mass spectrometry. They exhibited good thermal stability and it was evaluated by thermogravimetric analysis (TGA) for **OT-3**, **OT-4**, and **OT-5**, and the decomposition temperatures ( $T_5$  value) were obtained as 390, 356 and 376  $^\circ\text{C}$ , respectively as shown in

**Figure 3.4.**

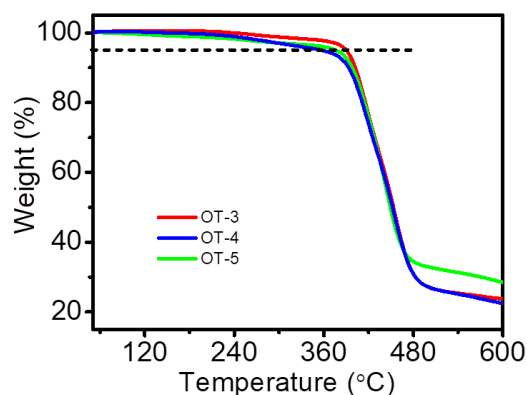


**Figure 3.4.** TGA profiles of **OT-3**, **OT-4** and **OT-5**; the black line indicates the temperature at which the materials loses 5% of its initial weight.

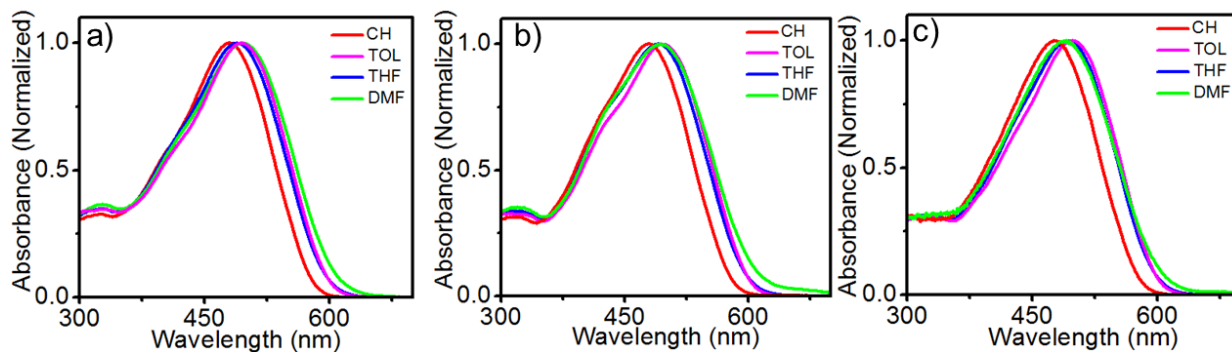


**Figure 3.5.** UV-vis absorption spectra of a) **OT-3**, b) **OT-4** and c) **OT-5** in cyclohexane (CH), toluene (TOL), tetrahydrofuran (THF) and *N,N*-dimethylformamide (DMF); ( $c = 1 \times 10^{-5}$  M,  $l = 10$  mm).

These oligomers also exhibit excellent solubility in common organic solvents like cyclohexane, toluene, tetrahydrofuran (THF), and *N,N*-dimethylformamide (DMF). Due to the presence of a push-pull molecular structure, they exhibited intense and broad absorption from 350 to 600 nm in solution, and the most intense band was assigned to the  $\pi$ - $\pi^*$  transitions are shown in **Figure 3.5** and the details are summarized in **Table 3.1**. Broad absorption in the visible region is one of the major requirements in the application of solar cell. The charge transfer nature of the oligomers was evident from the red shift in emission maximum and quenching in emission intensity with increasing solvent polarity (**Figure 3.6**). The fluorescence spectra showed high sensitivity towards the solvent polarity, as evident from the significant red-shift and quenching of emission maximum with increasing solvent polarity, which could be attributed to the charge transfer properties of the molecules.

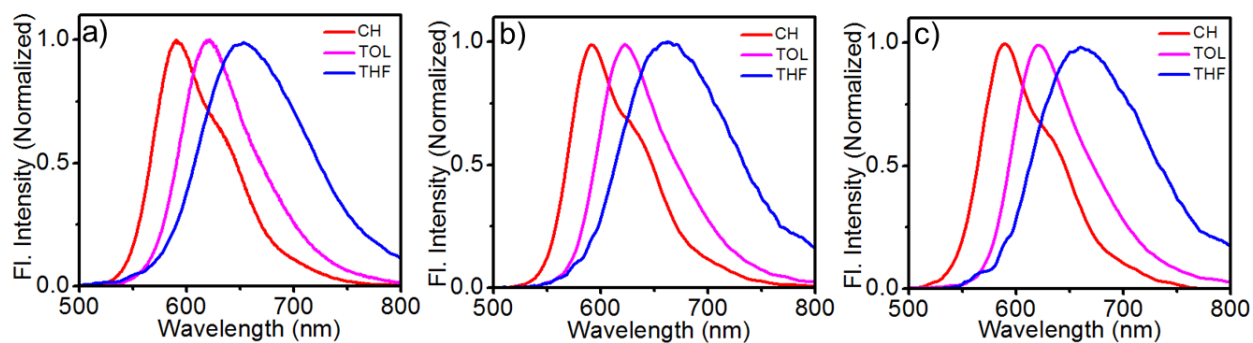


**Figure 3. 6.** Fluorescence emission spectra of a) **OT-3**, b) **OT-4** and c) **OT-5** in cyclohexane (CH), toluene (TOL), and tetrahydrofuran (THF); ( $c = 1 \times 10^{-5}$  M,  $l = 10$  mm,  $\lambda_{\text{ex}} = 490$  nm). No emission was observed in *N, N*-dimethylformamide (DMF).

The decrease in a lifetime with an increase in solvent polarity which is expected for donor-acceptor systems exhibiting charge transfer. However, such trends were not clear in these oligomers due to poor emission in a polar solvent as shown in **Figure 3.7**.

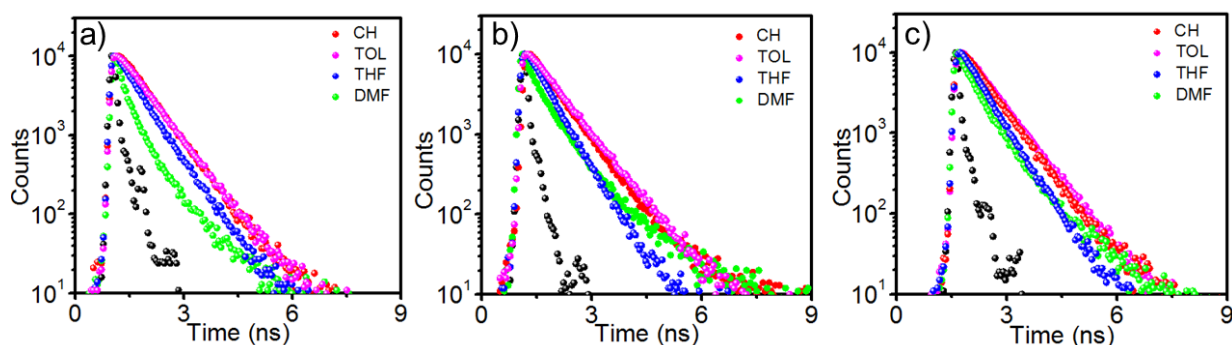


**Figure 3.7.** Fluorescence decay profiles of a) **OT-3**, b) **OT-4** and c) **OT-5** in different solvents. ( $c = 1 \times 10^{-5}$  M,  $l = 1$  cm,  $\lambda_{\text{ex}} = 440$  nm).

**Table 3.1.** Photophysical parameters such as absorption maxima, emission maxima, extinction coefficients ( $\epsilon$ ) and fluorescence quantum yields ( $\Phi_f$ ) of **OT-3**, **OT-4**, and **OT-5** in various solvents.

| Compound    | Solvent     | Absorption                     |   | Emission                       |                   |                |
|-------------|-------------|--------------------------------|---|--------------------------------|-------------------|----------------|
|             |             | $\lambda_{\text{max}}$<br>(nm) | $\epsilon \times 10^5$<br>( $\text{M}^{-1}\text{cm}^{-1}$ ) | $\lambda_{\text{max}}$<br>(nm) | $\Phi_f^a$<br>(%) | $\tau$<br>(ns) |
| <b>OT-3</b> | Cyclohexane | 480                            | 0.75  | 590                            | 13.74             | 0.65           |
|             | Toluene     | 495                            | 0.69  | 621                            | 8.90              | 0.69           |
|             | THF         | 489                            | 0.71  | 655                            | 3.50              | 0.59           |
|             | DMF         | 496                            | 0.69  | -                              | -                 | -              |
| <b>OT-4</b> | Cyclohexane | 476                            | 0.19  | 589                            | 14.02             | 0.59           |
|             | Toluene     | 498                            | 0.87  | 620                            | 10.08             | 0.72           |
|             | THF         | 491                            | 0.89  | 662                            | 2.27              | 0.53           |
|             | DMF         | 491                            | 0.14  | -                              | -                 | -              |
| <b>OT-5</b> | Cyclohexane | 480                            | 0.19  | 592                            | 17.02             | 0.66           |
|             | Toluene     | 495                            | 0.87  | 622                            | 10.03             | 0.71           |
|             | THF         | 491                            | 0.89  | 663                            | 2.94              | 0.55           |
|             | DMF         | 492                            | 0.14  | -                              | -                 | -              |

<sup>a</sup>Rhodamine B in ethanol ( $\Phi_f = 0.5$ ) was used as the standard for quantum yield measurement, error limit 5%.

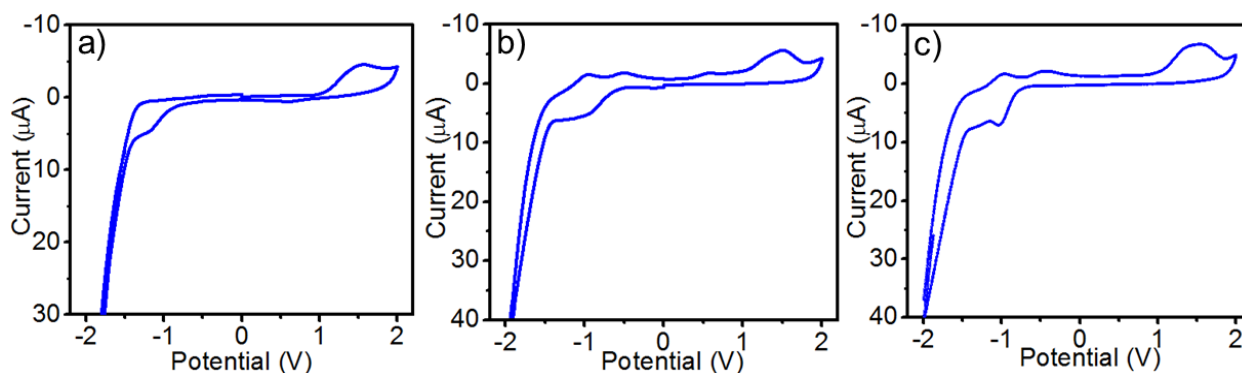


**Figure 3.8.** Cyclic voltammograms of a) **OT-3**, b) **OT-4** and c) **OT-5** in thin film state cast from chloroform on glassy carbon working electrodes, using 0.1 M tetrabutylammonium hexafluorophosphate as the supporting electrolyte in acetonitrile, Pt as the counter electrode, Ag/AgCl as the reference electrode which was calibrated using ferrocene/ferrocenium (Fc/Fc<sup>+</sup>) redox couple as an external standard. (Scan rate: 100 mV/s).

Cyclic voltammetry was employed to determine the HOMO-LUMO energy levels of the oligomers (**Figure 3.8**). In the film state, the HOMO energy levels of **OT-3**, **OT-4**, and **OT-5** were found to be -5.37, -5.46, and -5.38 eV, respectively and the LUMO levels were -3.60, -3.69, and -3.59 eV, respectively (details are summarized in **Table 3.2** and **Figure 3.9**). Comparison of the HOMO-LUMO of the oligomers with that of PC<sub>71</sub>BM (HOMO: -6.09 eV and LUMO: -4.30 eV)<sup>19</sup> showed that oligomers may function as donors in BHJ solar cell when blended with PC<sub>71</sub>BM acceptor. The energy offset between the LUMO levels of the molecules with that of PC<sub>71</sub>BM was good enough for efficient photo-induced intermolecular electron transfer and subsequent charge separation at the donor-acceptor interface.

**Table 3.2.** Summary of the film state absorption and electrochemical properties of the oligomers in the film state. Films were drop cast from chloroform solvent.

| Oligomer    | $\lambda_{\max}$<br>(nm) | $\lambda_{\text{onset}}$<br>(nm) | $E_{g(\text{opt})}^{\text{a}}$<br>(eV) | $E_{\text{ox}(\text{onset})}^{\text{b}}$<br>(V) | $E_{\text{red}(\text{onset})}^{\text{b}}$<br>(V) | $E_{\text{HOMO}}$<br>(eV) | $E_{\text{LUMO}}$<br>(eV) | $E_{g(\text{cv})}$<br>(eV) |
|-------------|--------------------------|----------------------------------|--|---|--|---------------------------|---------------------------|----------------------------|
| <b>OT-3</b> | 594                      | 738                              | 1.68                                   | 1.02  | -0.75  | -5.37                     | -3.60                     | 1.77                       |
| <b>OT-4</b> | 595                      | 705                              | 1.76                                   | 1.10  | -0.65  | -5.46                     | -3.69                     | 1.77                       |
| <b>OT-5</b> | 592                      | 701                              | 1.77                                   | 1.02  | -0.76  | -5.38                     | -3.59                     | 1.79                       |



**Figure 3.9.** HOMO-LUMO energy levels of the oligomers compared to that of PC<sub>71</sub>BM.

### 3.3.2. Photoconductivity analysis

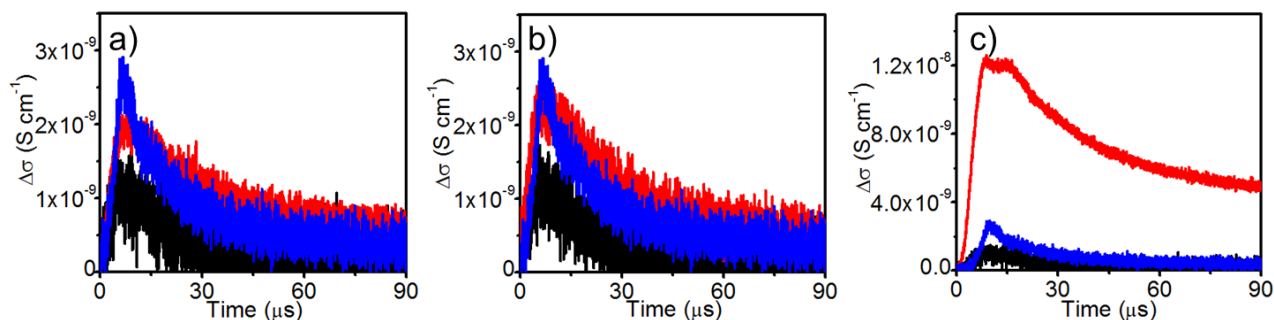


**Figure 3.10.** Xe-flash TRMC transients of a) OT-3, b) OT-4, and c) OT-5 in the film state drop cast from chlorobenzene solution; oligomer alone (black), PC<sub>71</sub>BM alone (blue), 1:1 w/w blends of oligomers with PC<sub>71</sub>BM (red).



Prior to the fabrication of the organic solar cells, we have surveyed the potential of the BHJ active layer by flash-photolysis time-resolved microwave conductivity (FP-TRMC). Here, microwave absorption of the transient charge carriers produced by the laser excitation or pseudosunlight white light pulse from a Xe-flash lamp was observed (pseudo solar spectrum with a pulse width of 10  $\mu$ s). Details of the experimental setup and data analysis were reported in our previous chapter. The photoconductivity transient signals obtained for the oligomers and the corresponding blends with PC<sub>71</sub>BM in the film state are shown in **Figure 3.10**. The transient signal obtained for PC<sub>71</sub>BM alone is also shown for comparison. In the pristine state, all three molecules exhibited comparable values of  $\Delta\sigma_{\max}$  (**OT-3**:  $9.2 \times 10^{-10}$  S cm<sup>-1</sup>, **OT-4**:  $13 \times 10^{-10}$  S cm<sup>-1</sup>, **OT-5**:  $9.7 \times 10^{-10}$  S cm<sup>-1</sup>). When blended with PC<sub>71</sub>BM (1:1 w/w), **OT-3** and **OT-4** showed only marginal enhancement in the  $\Delta\sigma_{\max}$  values ( $1.9 \times 10^{-9}$  S cm<sup>-1</sup>,  $2.3 \times 10^{-9}$  S cm<sup>-1</sup>, respectively). Interestingly,  $\Delta\sigma_{\max}$  of **OT-5** showed about 12-fold enhancement ( $1.2 \times 10^{-8}$  S cm<sup>-1</sup>) in the presence of PC<sub>71</sub>BM under identical conditions. This indicates that **OT-5** is the best donor material among the three derivatives in combination with PC<sub>71</sub>BM for solar cell applications because our previous studies have proved that the intensity of the photoconductivity signal of donor/acceptor blends has a direct correlation with that of their photoconversion efficiency when measured under identical conditions.<sup>20,21</sup> This is also in accordance with some of the literature reports which suggests that introduction of fused aromatic rings like thienothiophene are beneficial for improving optoelectronic properties of semiconducting organic materials.<sup>22,23</sup>

### 3.3.3. Photovoltaic properties

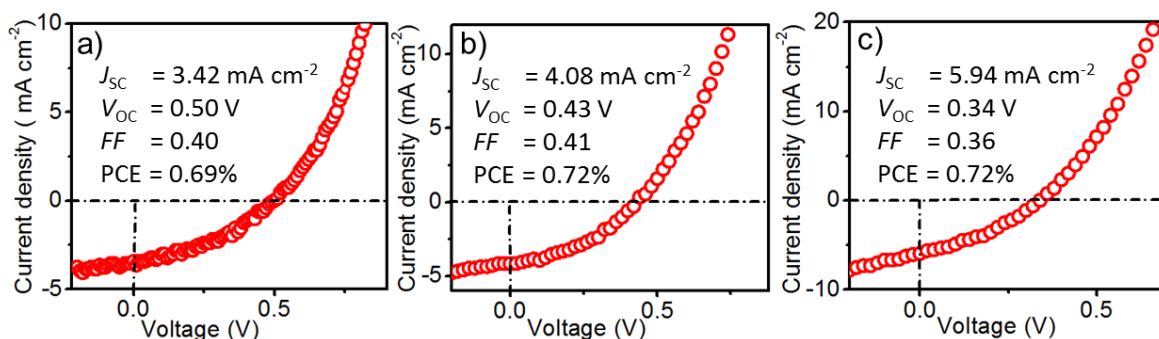


**Figure 3.11.**  $J$ - $V$  characteristics of the photovoltaic devices fabricated from a 1:1 w/w blend solutions of a) **OT-3:PC<sub>71</sub>BM**, b) **OT-4:PC<sub>71</sub>BM** and c) **OT-5:PC<sub>71</sub>BM** in chlorobenzene + 3 vol% DIO (device structure: glass/ITO/ZnO/BHJ/MoO<sub>3</sub>/Ag).

Solar cells have been fabricated using the oligomers as the donor and PC<sub>71</sub>BM as the acceptor with an inverted device structure<sup>24,25</sup> consisting of ITO/ZnO/BHJ/MoO<sub>3</sub>/Ag. The active layers consisting of donor and acceptor were taken in 1:1 weight ratio spin-coated from chlorobenzene containing DIO as an additive. Among the various vol % tried, the highest efficiencies were obtained from those devices cast from solutions containing 3 vol % DIO. **OT-3:PC<sub>71</sub>BM** device showed PCE of 0.69 (0.56 ± 0.11)% ( $J_{SC}$ : 3.42 mA cm<sup>-2</sup>,  $V_{OC}$ : 0.50 V,  $FF$ : 0.40). The **OT-4:PC<sub>71</sub>BM** device showed a PCE of 0.72 (0.68 ± 0.13)% ( $J_{SC}$ : 4.08 mA cm<sup>-2</sup>,  $V_{OC}$ : 0.43 V,  $FF$ : 0.41). Similarly, **OT-5:PC<sub>71</sub>BM** device exhibited a PCE of 0.72 (0.57 ± 0.13)% ( $J_{SC}$ : 5.94 mA cm<sup>-2</sup>,  $V_{OC}$ : 0.34 V,  $FF$ : 0.36).  $J$ - $V$  curves of the three devices are shown in **Figure 3.11** and the optimization data is summarized in Table 3. The external quantum efficiency (EQE) spectra of the devices were found to be consistent with their variation of short circuit current density (**Figure 3.12**). The observation of comparable PCEs for all the three

oligomers was counterintuitive considering the TRMC observation which implied a significantly better performance for **OT-5**.

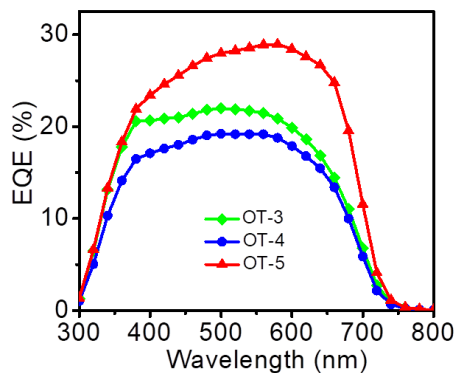


**Figure 3.12.** EQE curves of the best performing devices of the oligomers with PC<sub>71</sub>BM (1:1 wt%) cast from chlorobenzene + 3 vol% DIO.

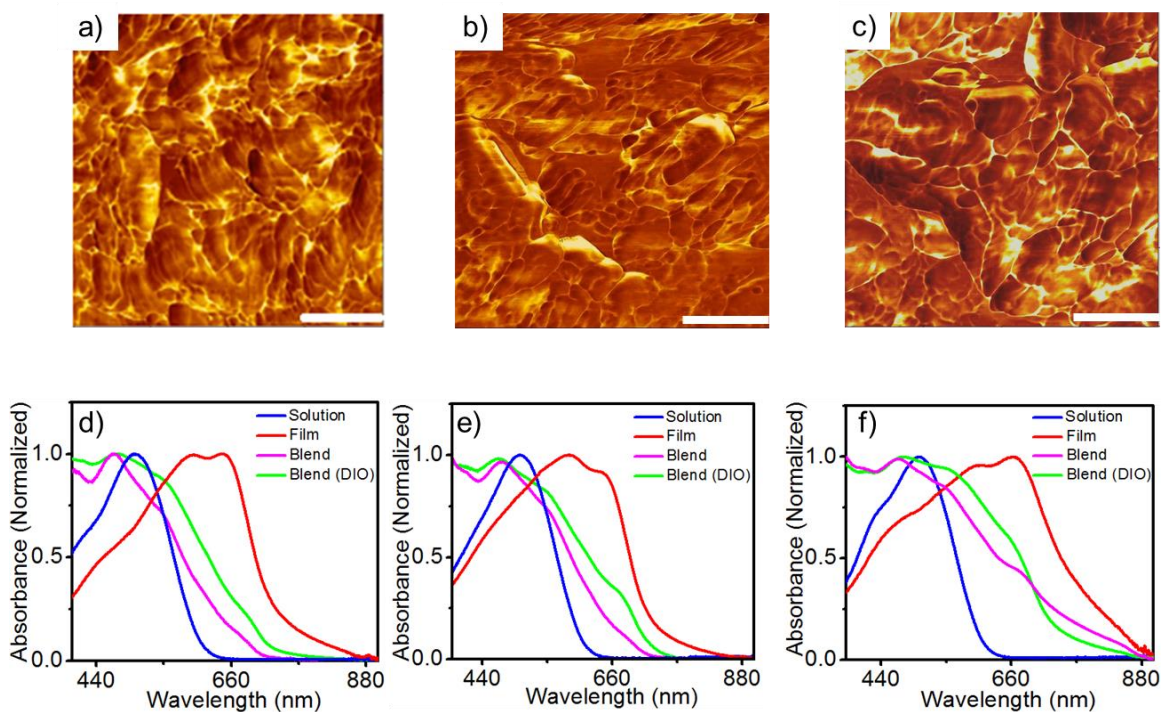


**Figure 3.13.** AFM phase images of the 1:1 blend films of a) **OT-3**, b) **OT-4** and c) **OT-5** with PC<sub>71</sub>BM obtained from chlorobenzene + 3 vol% DIO (scale bar corresponds to 500 nm). Normalized absorption spectra of d) **OT-3**, e) **OT-4**, and f) **OT-5** under different conditions (—chlorobenzene solution, —pristine film from chlorobenzene, —donor:PC<sub>71</sub>BM 1:1 blend film from chlorobenzene, —donor:PC<sub>71</sub>BM 1:1 blend film from chlorobenzene + 3 vol% DIO).

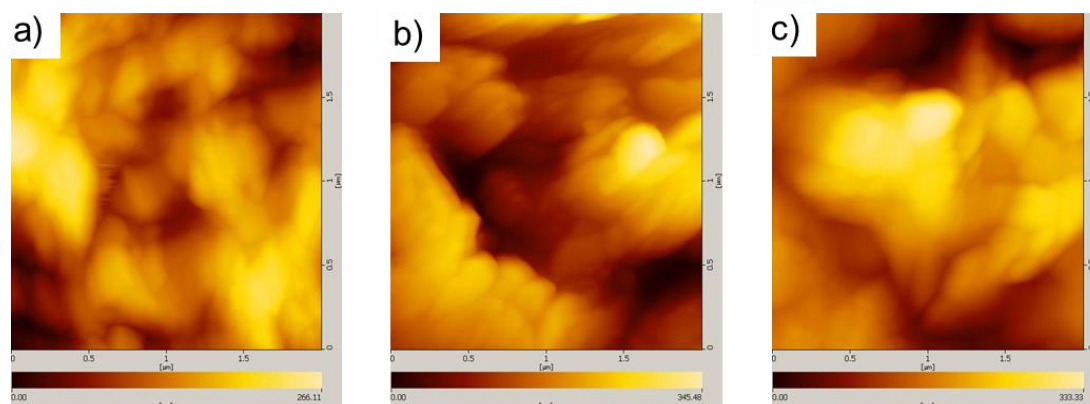


**Figure 3.14.** AFM height images of the 1:1 w/w blend films of a) **OT-3:PC<sub>71</sub>BM**, b) **OT-4:PC<sub>71</sub>BM** and c) **OT-5:PC<sub>71</sub>BM** cast from chlorobenzene + 3 vol% DIO.

In order to get a rational explanation for the results shown in the above section, detailed atomic force microscopy (AFM) analysis and UV-vis absorption studies were carried out. Analysis of the BHJ active layer morphologies with AFM revealed that the active layers consist of large aggregates (**Figure 3.13a-c**, corresponding height images are shown in **Figure 3.14a-c**). Such large aggregates are known to increase interfacial resistance resulting in poor charge collection at the electrode interface leading to low PCEs. Subsequently, the UV-vis absorption properties of the oligomers were measured in solution and film states (pristine and blends; **Figure 3.13d-f**). The chlorobenzene solutions of **OT-3**, **OT-4**, and **OT-5** exhibited an absorption maximum at 501, 503 and 502 nm, respectively. The corresponding spin-coated films showed relatively broad absorption with a red-shifted maximum when compared to that in the solution. The absorption maximum was shifted to 596, 588 and 602 nm for **OT-3**, **OT-4**, and **OT-5**, respectively. In addition to that, well-resolved shoulder peaks corresponding to the absorption of the aggregates was also observed in the red-region (**OT-3**: 648 nm, **OT-4**:

643 nm, **OT-5**: 662 nm). Observation of the well-resolved aggregate shoulders implies the ordered stacking/self-assembly of the oligomers in the film state.

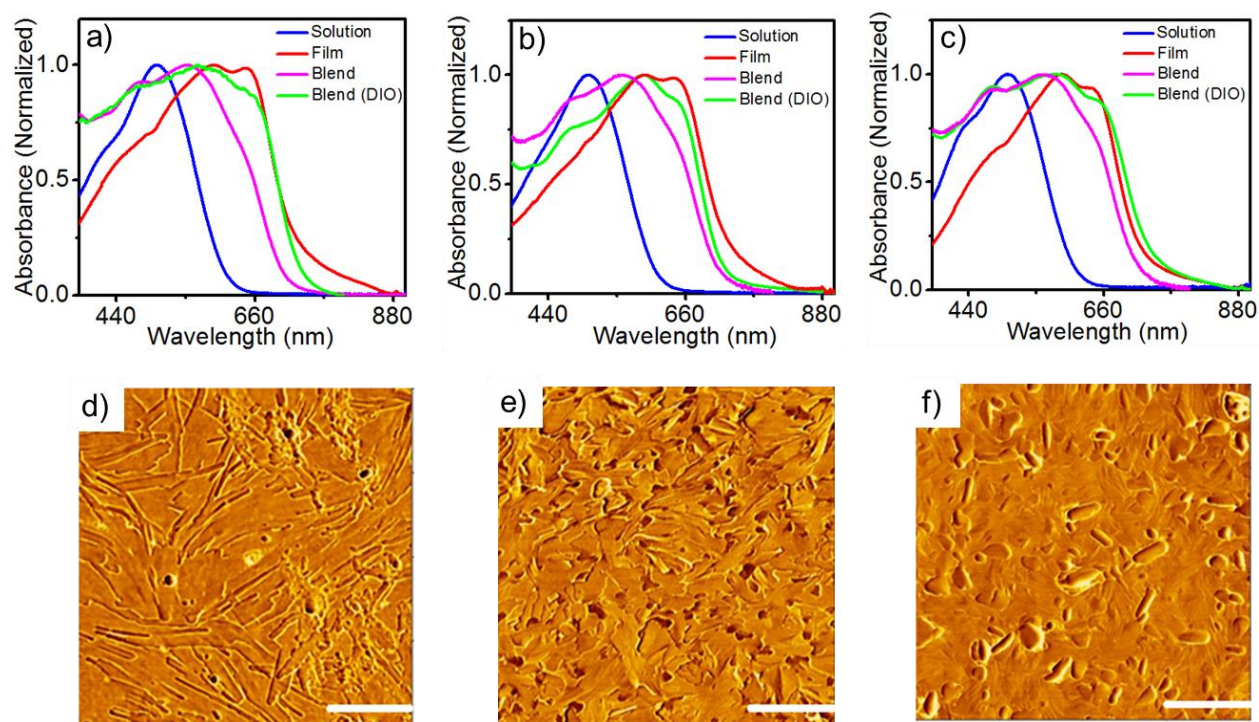


**Figure 3.15.** Normalized absorption spectra of a) **OT-3**, b) **OT-4**, and c) **OT-5** under different conditions (—chloroform solution, —pristine film from chloroform, —donor:PC<sub>71</sub>BM 1:1 blend film from chloroform, —donor:PC<sub>71</sub>BM 1:1 blend film from chloroform + 0.5 vol% DIO). AFM phase images of the 1:1 blend films of d) **OT-3**, e) **OT-4** and f) **OT-5** with PC<sub>71</sub>BM obtained from chloroform + 0.5 vol% DIO (scale bar corresponds to 500 nm).

However, this ordered packing of the donor assembly was lost on addition of the spheroidal shaped PC<sub>71</sub>BM as evident from the blue shifting of the absorption maxima (**OT-3**: 475 nm, **OT-4**: 470 nm, **OT-5**: 477 nm) as well as the significant weakening of the aggregate absorption shoulder. The absorption features remained more or less same even in the presence of 3 vol% DIO indicating that the additive was unable to restore the donor assembly. In short, the AFM and UV-vis absorption studies revealed that blend

films obtained from chlorobenzene with 3 vol% DIO consist of not only larger aggregates but also the poor assembly of donor oligomers.

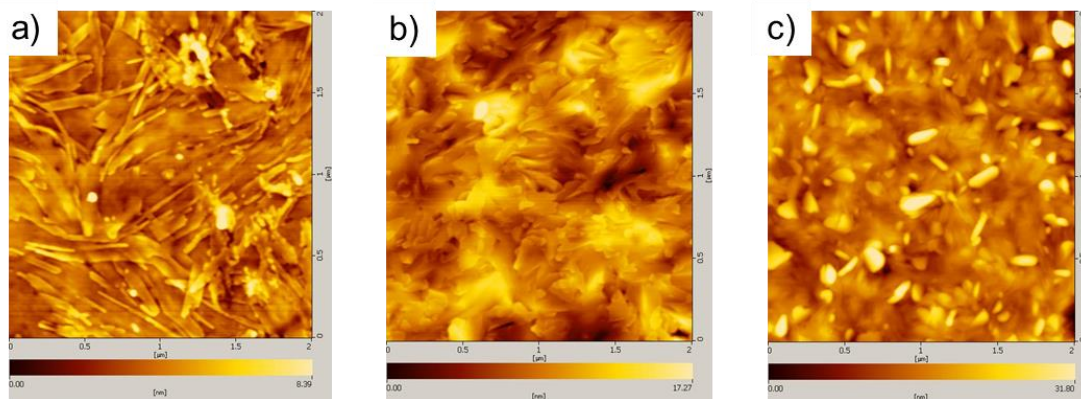


**Figure 3.16.** AFM height images of the 1:1 w/w blend films of a) **OT-3:PC<sub>71</sub>BM**, b) **OT-4:PC<sub>71</sub>BM** and c) **OT-5:PC<sub>71</sub>BM** cast from chloroform + 0.5 vol% DIO.

We assumed that, in order to get optimum efficiency from the blend films, it is important to reduce the aggregate size and improve donor self-assembly through solution engineering. Since chlorobenzene is a high boiling solvent (131.7 °C), it is obvious that the molecules get more time to aggregate resulting in the formation of larger aggregates. In this context, chloroform is a better solvent as it is more volatile (boiling point = 61.2 °C) and has a better ability to solubilize the oligomers. As observed in the case of chlorobenzene, the oligomers were molecularly dispersed in chloroform (**Figure 3. 15a-c**;  $\lambda_{\text{max}}$  of **OT-3**: 504, **OT-4**: 505 and **OT-5**: 503 nm). Similarly, the films spin-coated from chloroform showed a red-shifted maximum (**OT-3**: 594 nm, **OT-4**: 595 nm, **OT-5**: 592 nm) with shoulder corresponding to the aggregate absorption (**OT-3**: 646 nm, **OT-4**: 642 nm, **OT-5**: 641 nm). However, unlike chlorobenzene, only partial breaking in the

self-assembly happened in films cast from chloroform on the addition of PC<sub>71</sub>BM. This was evident from less blue-shift in the absorption maximum (**OT-3**: 553 nm, **OT-4**: 557 nm, **OT-5**: 567 nm) as well as the presence of shoulder band corresponding to the aggregate absorption. Nevertheless, the intensity of the shoulder bands was weak compared to that of the pristine film. To improve this aspect, the various volume percentage of DIO was added to the solution, and it was found that 0.5 vol% of DIO gave the best results. In this condition, the absorption maxima of the oligomers were found to be 576 (**OT-3**), 595 (**OT-4**) and 588 nm (**OT-5**), with well-defined shoulder bands (**OT-3**: 655 nm, **OT-4**: 646 nm, **OT-5**: 654 nm) in the red region. Interestingly, the AFM images revealed that the aggregate sizes also decreased significantly (**Figure 3.15d-f**; corresponding height images are shown in **Figure 3.16a-c**). This indicates that the films drop-cast from chloroform with 0.5 vol% of DIO not only preserve the ordered self-assembly of the oligomers but also keep the aggregate sizes smaller thereby providing an ideal condition for getting the optimum PCE.

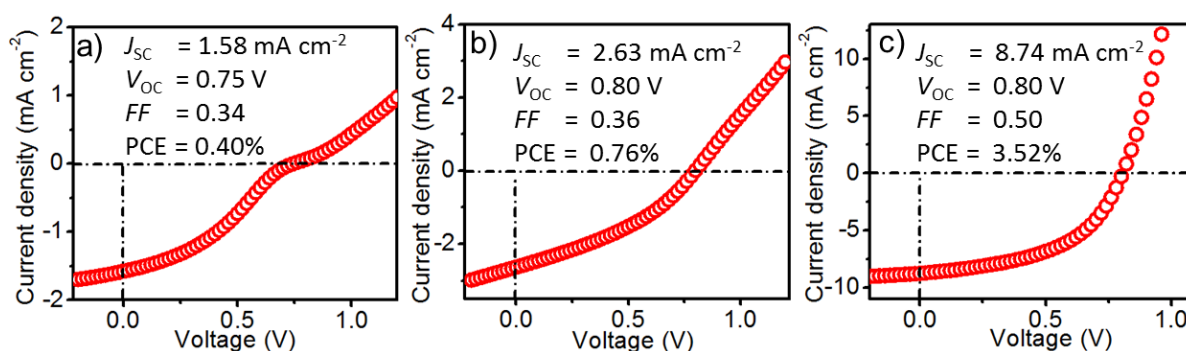


**Figure 3.17.**  $J$ - $V$  characteristics of the photovoltaic devices fabricated from the 1:1 w/w blend solutions of a) **OT-3**:PC<sub>71</sub>BM, b) **OT-4**:PC<sub>71</sub>BM and c) **OT-5**:PC<sub>71</sub>BM in chloroform + 0.5 vol% DIO (device structure: glass/ITO/ZnO/BHJ/MoO<sub>3</sub>/Ag).

Photovoltaic devices were fabricated under the above-optimized condition (chloroform as solvent and 0.5 vol% of DIO as additive). **OT-5:PC<sub>71</sub>BM** gave the best photovoltaic performance of 3.52 (3.27±0.36)%. This could be attributed to the preservation of the donor self-assembly as well as the smaller aggregate sizes which lead to better bi-continuous donor-acceptor network facilitating excellent charge separation, transport, and collection of free charge carriers. Under the similar condition, **OT-3:PC<sub>71</sub>BM** based device showed a marginal decrease in PCE 0.40 (0.37±0.07)%, whereas, the PCE of **OT-4:PC<sub>71</sub>BM** remained same 0.76 (0.74±0.02)%.

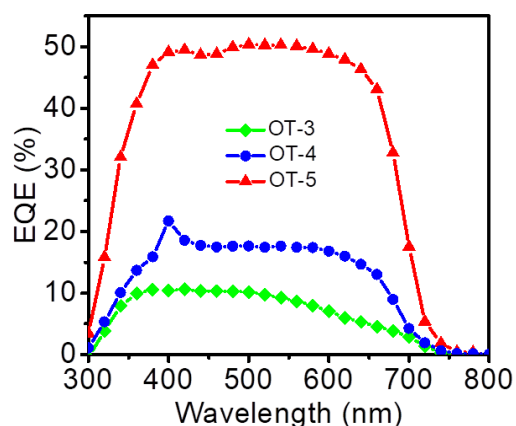


**Figure 3.18.** EQE curves of the best performing devices of the oligomers with PC<sub>71</sub>BM (1:1 wt%) cast from chloroform + 0.5 vol% DIO.

The EQE spectra of the **OT-5** based device exhibited higher spectral response when compared to the other two devices, which is consistent with the PCE of the oligomers (**Figure 3.18**). *J–V* curves obtained under the above-mentioned condition are shown in **Figure 3.17**. The photovoltaic parameters obtained for the best devices from chlorobenzene and chloroform is summarized in **Table 3.3**. Photovoltaic devices were also fabricated with varying weight ratios of PC<sub>71</sub>BM (0.5, 1, 2 and 3 w%) with the best



performer among the three oligomers (**OT-5**) using the above mentioned optimized condition (chloroform with 0.5 vol% DIO). Unfortunately, no further improvement in PCE was obtained and 1:1 w/w of **OT-5**: PC<sub>71</sub>BM was found to be the best donor/acceptor ratio. The obtained photovoltaic parameters are summarized in **Table 3.4**. Details of the optimization data are given in **Table 3.5**.

**Table 3.3.** Summary of photovoltaic characteristics of BHJ solar cells with active layers of **OT-3**, **OT-4**, and **OT-5** with PC<sub>71</sub>BM (1:1 w/w). The average values of the photovoltaic parameters along with the standard deviation are given in the bracket.

| Active layer                        | Solvent   | DIO (vol%)  | $J_{sc}$ (mA cm <sup>-2</sup> )   | $V_{oc}$ (V)                      | $FF$                              | PCE <sub>max</sub> (PCE)(%)       |
|-------------------------------------|-----------|-------------|-----------------------------------|-----------------------------------|-----------------------------------|-----------------------------------|
| <b>OT-3:</b><br>PC <sub>71</sub> BM | CB        | 3.00        | 3.42<br>(3.75±0.20)               | 0.50<br>(0.35±0.08)               | 0.40<br>(0.37±0.02)               | 0.69<br>(0.56±0.11)               |
|                                     | CF        | 0.50        | 1.58<br>(1.09±0.28)               | 0.75<br>(0.75±0.02)               | 0.34<br>(0.34±0.02)               | 0.40<br>(0.37±0.07)               |
| <b>OT-4:</b><br>PC <sub>71</sub> BM | CB        | 3.00        | 4.08<br>(3.59±0.24)               | 0.43<br>(0.39±0.05)               | 0.41<br>(0.40±0.01)               | 0.72<br>(0.68±0.13)               |
|                                     | CF        | 0.50        | 2.63<br>(2.46±0.15)               | 0.80<br>(0.79±0.03)               | 0.36<br>(0.38±0.02)               | 0.76<br>(0.74±0.02)               |
| <b>OT-5:</b><br>PC <sub>71</sub> BM | CB        | 3.00        | 5.94<br>(5.28±0.44)               | 0.34<br>(0.20±0.07)               | 0.36<br>(0.34±0.03)               | 0.72<br>(0.57±0.13)               |
|                                     | <b>CF</b> | <b>0.50</b> | <b>8.74</b><br><b>(7.15±2.64)</b> | <b>0.80</b><br><b>(0.78±0.15)</b> | <b>0.50</b><br><b>(0.42±0.05)</b> | <b>3.52</b><br><b>(3.27±0.36)</b> |

**Table 3.4.** Optimization of the solar cell devices based on **OT-5** when cast from chloroform and 0.5 vol% DIO.

| Active layer<br><b>OT-5</b> : PC <sub>71</sub> BM<br>Ratio | $J_{sc}$ (mA cm <sup>-2</sup> ) | $V_{oc}$ (V) | $FF$        | PCE <sub>max</sub> (PCE) (%) |
|--|---------------------------------|--------------|-------------|------------------------------|
| 1: 0.5   | 3.95                            | 0.50         | 0.29        | 0.60 (0.58±0.01)             |
| <b>1 : 1</b>   | <b>8.74</b>                     | <b>0.80</b>  | <b>0.50</b> | <b>3.52 (3.27±0.36)</b>      |
| 1 : 2  | 1.33                            | 0.75         | 0.28        | 0.28 (0.23±0.04)             |
| 1 : 3  | 0.77                            | 0.65         | 0.30        | 0.15 (0.14±0.01)             |

**Table 3.5.** Summary of photovoltaic characteristics of the oligomers with PC<sub>71</sub>BM (1:1 w/w) containing different volume percentage of the solvent additive (DIO).

| Active layer                        | Solvent | DIO (vol%)                          | $J_{SC}$ (mA cm <sup>-2</sup> ) | $V_{OC}$ (V) | $FF$        | $PCE_{max}$ (PCE)(%)  |      |                  |
|-------------------------------------|---------|-------------------------------------|---------------------------------|--------------|-------------|-----------------------|------|------------------|
| <b>OT-3:</b><br>PC <sub>71</sub> BM | CB      | 0.00                                | 0.36                            | 0.62         | 0.29        | 0.06 (0.06±0.01)      |      |                  |
|                                     |         | 0.50                                | 1.80                            | 0.58         | 0.28        | 0.36 (0.34±0.01)      |      |                  |
|                                     |         | 1.50                                | 2.50                            | 0.65         | 0.28        | 0.45 (0.41±0.02)      |      |                  |
|                                     |         | 3.00                                | 3.42                            | 0.50         | 0.40        | 0.69(0.56± 0.11)      |      |                  |
|                                     | CF      | 0.00                                | 1.70                            | 0.59         | 0.30        | 0.30 (0.28±0.02)      |      |                  |
|                                     |         | 0.50                                | 1.58                            | 0.75         | 0.34        | 0.40 (0.37±0.07)      |      |                  |
|                                     |         | 1.50                                | 1.73                            | 0.83         | 0.26        | 0.38 (0.35±0.02)      |      |                  |
|                                     |         | 3.00                                | 0.87                            | 0.78         | 0.30        | 0.20 (0.17±0.01)      |      |                  |
|                                     |         | <b>OT-4:</b><br>PC <sub>71</sub> BM | CB                              | 0.00         | 0.88        | 0.54                  | 0.27 | 0.13 (0.12±0.01) |
|                                     |         |                                     |                                 | 0.50         | 1.26        | 0.63                  | 0.30 | 0.24 (0.22±0.01) |
| 1.50                                | 0.93    |                                     |                                 | 0.56         | 0.28        | 0.15 (0.14±0.01)      |      |                  |
| CF                                  | 3.00    |                                     | 4.08                            | 0.43         | 0.41        | 0.72 (0.68±0.13)      |      |                  |
|                                     | 0.00    |                                     | 1.20                            | 0.51         | 0.30        | 0.18 (0.18±0.00)      |      |                  |
|                                     | 0.50    |                                     | 2.63                            | 0.80         | 0.36        | 0.76 (0.74±0.02)      |      |                  |
| <b>OT-5:</b><br>PC <sub>71</sub> BM | CB      | 1.50                                | 1.64                            | 0.76         | 0.32        | 0.40 (0.38±0.01)      |      |                  |
|                                     |         | 3.00                                | 1.94                            | 0.58         | 0.31        | 0.35 (0.27±0.06)      |      |                  |
|                                     |         | 0.00                                | 1.86                            | 0.60         | 0.27        | 0.30 (0.27±0.01)      |      |                  |
|                                     | CF      | 0.50                                | 3.78                            | 0.58         | 0.32        | 0.71 (0.62±0.03)      |      |                  |
|                                     |         | 1.50                                | 1.86                            | 0.81         | 0.41        | 0.62 (0.57±0.02)      |      |                  |
|                                     |         | 3.00                                | 5.94                            | 0.34         | 0.36        | 0.72 (0.54±0.13)      |      |                  |
|                                     |         | 0.00                                | 2.04                            | 0.60         | 0.30        | 0.38 (0.36±0.01)      |      |                  |
|                                     |         | <b>0.50</b>                         | <b>8.74</b>                     | <b>0.80</b>  | <b>0.50</b> | <b>3.52 3.27±0.36</b> |      |                  |
|                                     |         | 1.50                                | 3.64                            | 0.86         | 0.39        | 1.24 (1.10±0.08)      |      |                  |
|                                     |         | 3.00                                | 2.13                            | 0.77         | 0.32        | 0.60 (0.53±0.03)      |      |                  |

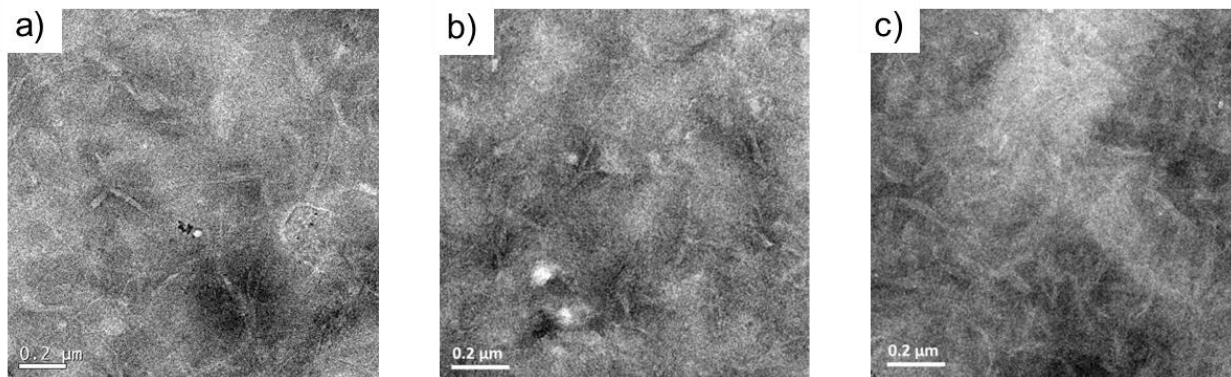


**Figure 3.19.** BF-TEM images of (1:1 w/w) blended films (a) **OT-3:PC<sub>71</sub>BM**, (b) **OT-4:PC<sub>71</sub>BM** and (c) **OT-5:PC<sub>71</sub>BM**.

In literature, such difference in the PCEs obtained for oligomers/polymers were correlated with the donor-acceptor phase segregation by analyzing the nanoscale morphology. Our UV-vis analysis suggests that all the three oligomers show good self-assembly/stacking in films prepared from chloroform with 0.5 vol% of DIO. However, this study reflects only the molecular level interactions which may or may not be extended to the hierarchical levels. AFM is also not helpful in this context as it can show only the surface morphology and not the donor-acceptor domain formations. Bright field transmission electron microscope (BF-TEM) analysis is, on the other hand, an ideal tool for this purpose as it can clearly reveal the phase segregation through contrast difference (darker domains for PC<sub>71</sub>BM and lighter domains for thiophene oligomers).<sup>29-31</sup> Donor-acceptor domains were partially visible in the BF-TEM images of both **OT-3:PC<sub>71</sub>BM** (**Figure 3.19a**) and **OT-4:PC<sub>71</sub>BM** (**Figure 3.19b**) but the distribution was found to be less uniform. On the other hand, clear donor-acceptor domains consisting of ten-nanometre scale donor fibrils were present uniformly in the case of **OT-5:PC<sub>71</sub>BM**

(Figure 3.19c). This well-defined domain formation in **OT-5:PC<sub>71</sub>BM** ensure facile charge carrier separation and easier charge carrier transport to the respective electrodes leading to better efficiency.

### 3.3.4. PL quenching and 2D-GIXRD analysis

At this juncture, it is interesting to note that the PCEs of the oligomers obtained after solution engineering are in accordance with the TRMC results, i.e. **OT-5** outperforms **OT-3** and **OT-4** by a wide margin. It could be seen that in the case of **OT-3** and **OT-4** blends, the best efficiencies achieved in the previous devices itself, and no further enhancement was possible through solution engineering. On the other hand, **OT-5:PC<sub>71</sub>BM** blend was intrinsically capable of delivering better performance, which was achieved through changing solvent and solvent additive concentration.

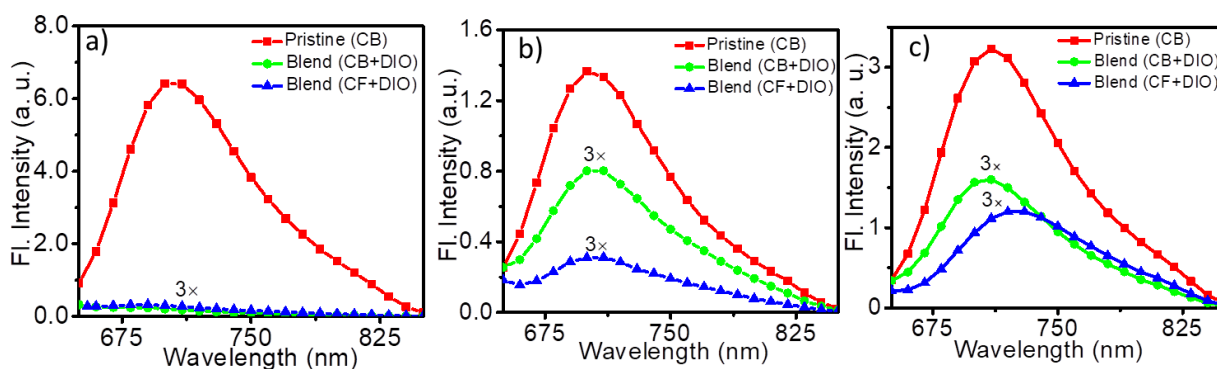


**Figure 3.20.** Photoluminescence spectra of a) **OT-3**, b) **OT-4** and c) **OT-5** under different conditions (red line: pristine film from chlorobenzene; green line: 1:1 w/w blend film with PC<sub>71</sub>BM from chlorobenzene + 3 vol% DIO; blue line: 1:1 w/w blend film with PC<sub>71</sub>BM from chloroform + 0.5 vol% DIO;  $\lambda_{\text{ex}} = 600$  nm). Emission spectra of the blend films are multiplied by a factor of three for better visibility.

For understanding the fundamental reasons for the improvements in the device efficiency in **OT-5**:PC<sub>71</sub>BM blend on solution engineering, we have carried out the photoluminescence (PL) quenching and two-dimensional grazing incidence X-ray diffraction (2D-GIXRD) studies of the blend films. The former gives an idea about how efficiently the exciton dissociation occurs at the interface, whereas, the latter provides an insight into the molecular level packing of the oligomers, which correlates well with the charge transport properties. Compared to the PL of the pristine film (spin coated from chlorobenzene solution), 83% quenching was observed for the blend film (cast from chlorobenzene with 3 vol% DIO; **Figure 3.20c**). On the other hand, 89% quenching was obtained for blend film cast from chloroform containing 0.5 vol% DIO. The increased PL quenching in the latter case suggests that the excitons generated by the absorbed photons would be dissociated to free charge carriers (electrons and holes) more effectively when the film is prepared from chloroform with 0.5 vol% DIO.<sup>32-34</sup> Similar studies were conducted with other two derivatives which are shown **Figure 3.20 a, b**. We have also carried out the PL quenching for the best performing molecule (**OT-5**) in film state (spin coated from chloroform solution with 0.5 vol% DIO) with different ratios of PC<sub>71</sub>BM (0, 0.5, 1, 2 and 3 wt%) as shown in **Figure 3.21**. The fluorescence of **OT-5** was efficiently quenched with increasing concentration of PC<sub>71</sub>BM indicating intermolecular electron transfer from **OT-5** to the PC<sub>71</sub>BM. The results indicated that more than 94% exciton is efficiently quenched in 1:1 w/w blend of **OT-5**:PC<sub>71</sub>BM.

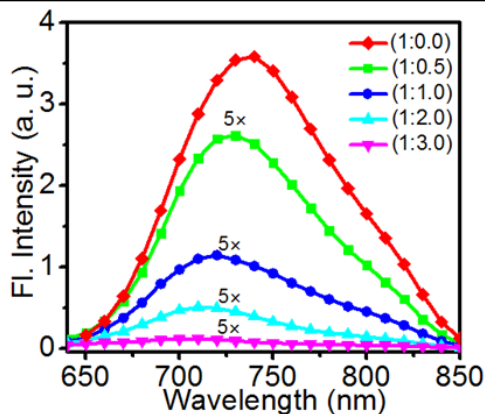


**Figure 3.21.** Photoluminescence quenching of **OT-5** (kept constant at 1 wt%) with different weight ratios of **PC<sub>71</sub>BM** acceptor (varied from 0-3 wt%) in a film state, where the films were cast from chloroform solvent with 0.5 vol% DIO. Emission spectra of the blend films are multiplied by a factor of five for better visibility.

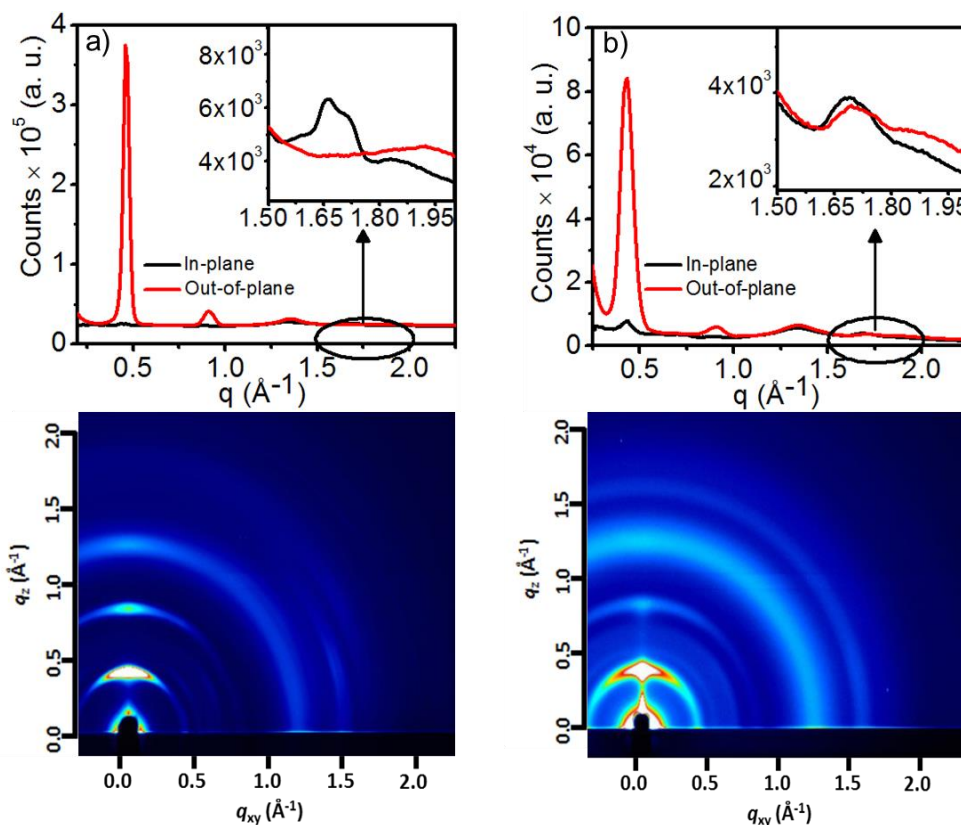


**Figure 3.22.** 2D-GIXRD patterns of **OT-5:PC<sub>71</sub>BM 1:1** w/w blend films cast from (a) chlorobenzene + 3 vol% DIO and (b) chloroform + 0.5 vol% DIO on glass/ITO/ZnO substrate. Lower and upper panels are the 2D image and extracted spectra in the out-of-plane (red) and in-plane (black) directions, respectively (inset shows the zoomed region from 1.5 to 2.0  $\text{\AA}^{-1}$ ).

The 2D-GIXRD analysis was carried out in **OT-5:PC<sub>71</sub>BM** blend films spin-coated from chlorobenzene with 3 vol% DIO (**Figure 3.22a**) and chloroform with 0.5 vol% DIO (**Figure 3.22b**). Both showed strong diffractions corresponding to the lamellar stacking (100 plane and its higher orders) in the out-of-plane direction. In the former case, lamellar stacking (100) peak was observed at 13.65 Å, whereas it was observed at 14.71 Å in the latter case. The films also exhibited reflections corresponding to the  $\pi$ - $\pi$  stacking (010) at higher angles. Though the lamellar distance between the molecules was higher in the film cast from chloroform, the  $\pi$  stacking distance was lower (3.70 Å) than that of the film cast from chlorobenzene (3.78 Å). This clearly suggests that the stacking has improved in films cast from chloroform. More importantly, the peak corresponding to (010) plane was observed only in the in-plane diffraction profile of the film cast from chlorobenzene (inset of **Figure 3.22a**) indicating that the oligomers having a preferred edge-on orientation on the substrate.<sup>35</sup> On the other hand, the peak corresponding to the (010) reflection was seen in both out-of-plane as well as in-plane profiles in the film cast from chloroform (inset of **Figure 3.22b**). This implies that some of the oligomers stack with a face-on orientation on the substrate. The presence of oligomer stacks with face-on orientation is known to facilitate charge transfer at the electrode interface, and hence could be attributed to the improvement in efficiency of **OT-5:PC<sub>71</sub>BM** blend film cast from chloroform. It must be noted that the lamellar packing mode is dominant in the out-of-plane reflection than that in the in-plane, which indicates that the fraction of the edge-on orientation is more than that of the face-on orientation.<sup>35</sup> To improve the photovoltaic

---

efficiencies, it is important to increase the fraction of face-on oriented molecules. This could be achieved by incorporating moieties with larger  $\pi$ -planes into the oligomer backbone. In addition to that, the performance can also be improved by enhancing the absorbance in the red and near infra-red regions by incorporating strong electron withdrawing groups in the *N*-ethylrhodanine moiety.

### 3.4. Conclusions

In summary, we have synthesized three solution processable A-D-A type small molecules consisting of *N*-ethylrhodanine as the acceptor group and different central cores (thiophene, bithiophene and thienothiophene) connected through thiophene pi-linker (alkylated terthiophene). The oligomer containing thienothiophene as core exhibited superior photoconductivity properties in FP-TRMC analysis compared to that of the other two derivatives. By taking TRMC observation as a guiding tool, solution engineering was carried out to get the best performance of the oligomers. The improved cell fabricated from thienothiophene based oligomer exhibited a PCE of 3.52%. UV-vis absorption, atomic force microscopy, bright-field transmission electron microscopy, photoluminescence quenching, and two-dimensional grazing angle X-ray diffraction studies revealed that the improvements in PCE are due to the improved molecular stacking, good morphology, optimum donor-acceptor phase separation, enhanced charge carrier dissociation and increased fraction of the donor oligomers with face-on stacking.



## 3.5. Experimental section

### 3.5.1. Materials

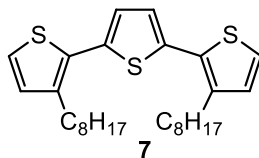
All chemicals and reagents for the synthesis were purchased either from Aldrich, Alfa Aesar or Spectrochem. Upto 5''-bromo-3,3''-dialkyl-[2,2':5',2''-terthiophene]-5-carbaldehyde (**9**) was synthesized according to reported literature.<sup>74</sup> MALDI-TOF spectra were recorded on a KRATOS ANALYTICAL SHIMADZU mass spectrometer. Cyclic voltammetry experiments were performed using a BAS CV-50W voltammetric analyser at room temperature where 0.1 M tetrabutylammonium hexafluorophosphate (TBAPF<sub>6</sub>) in acetonitrile was used as supporting electrolyte, glassy carbon as working electrode, platinum wire as counter electrode and Ag/AgCl electrode as reference electrode which was calibrated using ferrocene/ferrocenium (Fc/Fc<sup>+</sup>) redox couple as an external standard at a scan rate of 100 mV/s.

TEM analyses were carried out using FEI's 300kV high resolution transmission electron microscope (FEI-Tecnai G2-30 with EDAX). The samples for TEM analysis were prepared as follows. Blend solutions consisting 10 mg/mL of oligomer and 10 mg/mL of PC<sub>71</sub>BM was prepared in chloroform containing 0.5 vol% DIO. PEDOT:PSS purchased from Sigma Aldrich, the layer was precast on a glass substrate at 1000 rpm for 60s, on it oligomer:PC<sub>71</sub>BM. BHJ films were spin-cast at 2000 rpm for 60s. Topdown TEM samples were prepared by dissolving the PEDOT:PSS layer in water and

transferring the floating BHJ film to carbon-coated copper TEM grids. All other instruments are used for this work are the same as in our previous **Chapter 1**.

### 3. 5. 2. Synthesis and characterization

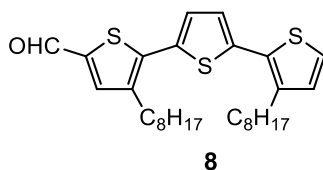
#### *Synthesis of 3,3-dioctyl-2,2':5',2''-terthiophene (7):*



A solution of 2,5-bis(tributylstannyl)-thiophene (4 g, 6.04 mmol, 1 eq.), 2-bromo-3-octylthiophene (3.49 g, 12.68 mmol, 2.1 eq.), Pd<sub>2</sub>(dba)<sub>3</sub> (165mg, 0.18 mmol, 3 mol%) and P(o-tolyl)<sub>3</sub> (220 mg, 0.72 mmol, 4 eq. to Pd catalyst) in toluene was refluxed and stirred overnight. The reaction mixture was cool to room temperature and diluted with CHCl<sub>3</sub>. The organic layer was washed with water and brine; dried over anh. Na<sub>2</sub>SO<sub>4</sub> and concentrated in vacuum. The crude compound was purified by column chromatography using hexane as the eluent to afford the corresponding product as yellow oil. Yield: 85%.

$\delta_{\text{H}}$  (500 MHz, CDCl<sub>3</sub>, ppm): 7.19 (d,  $J$  =5 Hz, 2H), 7.07 (s, 2H), 6.96 (d,  $J$  =5 Hz, 2H) 2.80 (t,  $J$  =8 Hz, 4H), 1.67 (q, 4H), 1.40-1.27 (m, 20H), 0.89 (t, 6H).  $\delta_{\text{C}}$  (125 MHz, CDCl<sub>3</sub>, ppm): 139.70, 136.27, 130.68, 130.19, 126.12, 123.81, 32.18, 32.15, 31.01, 29.86, 29.75, 22.97, 22.94, 14.39.

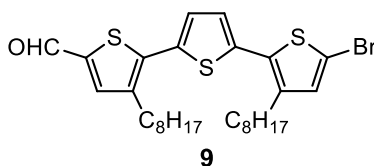
#### *Synthesis of 3,3''-Dioctyl-[2,2':5',2''-terthiophene]-5-carbaldehyde (8)*



To a solution of 3,3-dioctyl- 2,2':5',2''-terthiophene (**7**) (920 mg, 1.95 mmol, 1 eq.) and *N,N*-dimethylformamide (0.15 mL, 1.95 mmol, 1 eq.) in 1,2-dichloroethane was slowly added POCl<sub>3</sub> (0.18 mL, 1.95 mmol, 1 eq.) at 0 °C, and stirred for 1 h under Ar. Then, the reaction mixture was heated to 60 °C and stirred overnight. The mixture was cool to 0 °C and neutralized using aq. NaHCO<sub>3</sub>. The organic layer was extracted using CH<sub>2</sub>Cl<sub>2</sub> and dried over anhydrous Na<sub>2</sub>SO<sub>4</sub> and concentrated in vacuo. The crude compound was purified by column chromatography using the mixture of hexane and CH<sub>2</sub>Cl<sub>2</sub> (1:1) as the eluent to afford the corresponding product as orange oil. Yield: 80%.

$\delta_{\text{H}}$  (500 MHz, CDCl<sub>3</sub>, ppm): 9.83 (s, 1H), 7.60 (s, 1H), 7.25 (d,  $J = 8.5$  Hz, 1H), 7.23 (d,  $J = 8.5$  Hz, 1H), 7.11 (d,  $J = 5.5$  Hz, 1H), 6.97 (d,  $J = 5$  Hz, 1H), 2.83 (t,  $J = 7.75$  Hz, 2H), 2.82 (t,  $J = 8$  Hz, 2H), 1.72-1.62 (m, 4H), 1.43-1.27 (m, 20H), 0.88-0.86 (m, 6H).  $\delta_{\text{C}}$  (125 MHz, CDCl<sub>3</sub>, ppm): 181.32, 140.00, 139.20, 139.13, 130.10, 138.01, 137.43, 133.37, 129.20, 128.74, 126.63, 125.11, 123.27, 30.87, 30.85, 29.65, 29.27, 28.57, 28.50, 28.44, 28.40, 28.37, 28.28, 28.25, 21.67, 13.10.

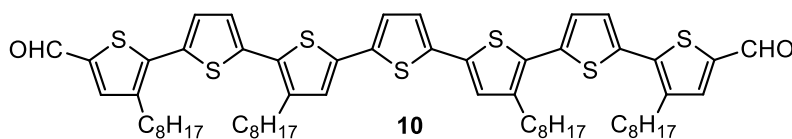
**Synthesis of 5''-Bromo-3,3''-dioctyl-[2,2':5',2''-terthiophene]-5-carbaldehyde (**9**)**



To a stirred solution of appropriate 3,3''-dioctyl-[2,2':5',2''-terthiophene]-5-carbaldehyde (**8**) (590 mg, 1.17 mmol, 1 eq.) in chloroform and acetic acid (1:1 v/v), NBS (209 mg, 1.17 mmol, 1 eq.) was added in dark at room temperature for 2 h. The reaction was monitored by TLC to establish completion. The organic layer was extracted with hexane, washed with aq. NaHCO<sub>3</sub>, water and brine; dried over anhydrous Na<sub>2</sub>SO<sub>4</sub> and concentrated in vacuum. The crude compound was purified by gravity column chromatography using hexane as the eluent to afford product as orange oil. Yield: 98%.

$\delta_{\text{H}}$  (500 MHz, CDCl<sub>3</sub>, ppm): 9.83 (s, 1H), 7.60 (s, 1H), 7.22 (d,  $J=4$  Hz, 1H), 7.04 (d,  $J=4$  Hz, 1H), 6.92 (s, 1H), 2.81 (t,  $J=7.75$  Hz, 2H), 2.71 (t,  $J=7.75$  Hz, 2H), 1.64 (m, 4H), 1.43-1.26 (m, 20H), 0.87 (m, 6H).  $\delta_{\text{C}}$  (125 MHz, CDCl<sub>3</sub>, ppm): 182.58, 141.18, 140.40, 140.31, 140.19, 139.10, 138.51, 134.47, 130.26, 129.77, 127.80, 126.32, 124.41, 31.90, 31.87, 30.72, 30.35, 29.59, 29.51, 29.46, 29.42, 29.38, 29.29, 29.26, 22.69, 14.12.

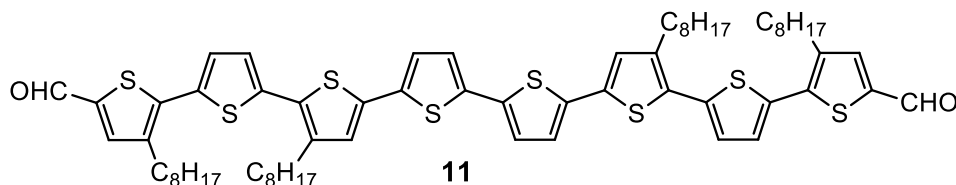
### *Synthesis of compound (10)*



A solution of 5''-Bromo-3,3''-dioctyl-[2,2':5',2''-terthiophene]-5-carbaldehyde (**9**) (230 mg, 0.40 mmol, 2 eq.) and 2,5-bis(tributylstannyl)thiophene (131 mg, 0.20, 1 eq.) was deaerated twice with argon followed by the addition of Pd(PPh<sub>3</sub>)<sub>4</sub>. After being stirred at 100 °C for 48 h under Ar, the reaction mixture was poured into water and extracted with CHCl<sub>3</sub>. The organic layer was washed with water and then dried over anhydrous Na<sub>2</sub>SO<sub>4</sub>. Purified by column chromatography CHCl<sub>3</sub>-hexane (1:1). Yield: 78%.

$\delta_{\text{H}}$  (500 MHz,  $\text{CDCl}_3$ , ppm): 9.83 (s, 2H), 7.60 (s, 2H), 7.25 (s, 2H), 7.13 (d,  $J = 4$  Hz, 2H), 7.09 (s, 2H), 7.03 (s, 2H), 2.83 (t,  $J = 8$  Hz, 4H), 2.78 (t,  $J = 7.75$  Hz, 4H), 1.72-1.67 (m, 8H), 1.45-1.23 (m, 40H), 0.90-0.88 (m, 12H).  $\delta_{\text{C}}$  (125 MHz,  $\text{CDCl}_3$ , ppm): 181.41, 140.05, 140.02, 139.97, 139.22, 139.12, 138.22, 138.05, 137.01, 136.96, 134.87, 134.28, 134.19, 133.48, 128.08, 128.03, 126.74, 125.79, 125.65, 124.96, 123.40, 113.05, 33.65, 33.49, 32.81, 30.91, 30.89, 30.87, 30.58, 30.40, 29.43, 29.27, 29.16, 28.69, 28.65, 28.52, 28.46, 28.42, 28.36, 28.29, 28.27, 28.15, 28.04, 27.93, 27.26, 25.89, 25.75, 24.26, 21.68, 21.64, 16.27, 13.10, 12.58, 10.41.

### Synthesis of compound (11)

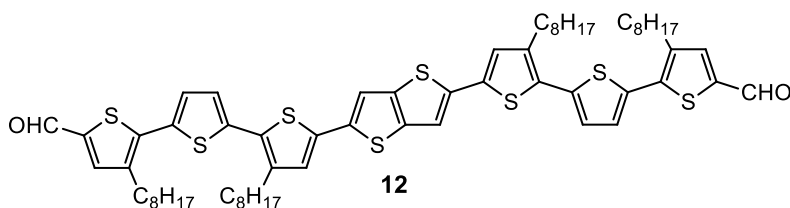


A solution of 5''-Bromo-3,3''-dioctyl-[2,2':5',2''-terthiophene]-5-carbaldehyde (**9**) (587 mg, 1.01 mmol, 2 eq.) and 5,5'-bis(tributylstannyl)-2,2'-bithiophene (376 mg, 0.51, 1 eq.) was deaerated twice with Ar followed by the addition of  $\text{Pd}(\text{PPh}_3)_4$ . After being stirred at 100 °C for 48 h under Ar, the reaction mixture was poured into water and extracted with  $\text{CHCl}_3$ . The organic layer was washed with water and then dried over anh.  $\text{Na}_2\text{SO}_4$ . Purified by column chromatography  $\text{CHCl}_3$ -hexane (1:1). Yield: 78%.

$\delta_{\text{H}}$  (500 MHz,  $\text{CDCl}_3$ , ppm): 9.84 (s, 2H), 7.60 (s, 2H), 7.25 (s, 2H), 7.13 (d,  $J = 4$  Hz, 2H), 7.09 (s, 4H), 7.04 (s, 2H), 2.84 (t,  $J = 7.75$  Hz, 4H), 2.78 (t,  $J = 7.75$  Hz, 4H), 1.72-1.69 (m, 8H), 1.42-1.26 (m, 40H), 0.93 (m, 12H).  $\delta_{\text{C}}$  (125 MHz,  $\text{CDCl}_3$ , ppm): 182.48,

141.13, 141.11, 140.99, 140.31, 140.21, 140.19, 139.07, 138.03, 137.98, 136.02, 135.88, 135.29, 135.24, 134.54, 129.10, 129.06, 127.81, 126.85, 126.74, 126.06, 124.48, 124.37, 53.44, 31.91, 31.88, 30.48, 30.30, 29.65, 29.53, 29.47, 29.43, 29.31, 29.28, 28.28, 26.78, 22.69, 17.30, 14.12, 13.60.

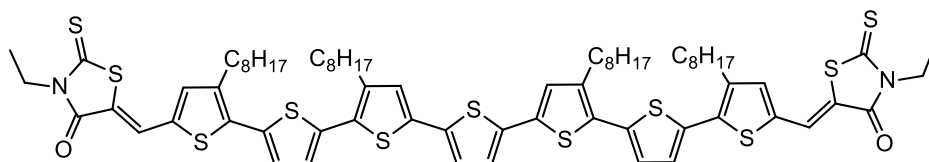
### Synthesis of compound (12)



A solution of 5''-Bromo-3,3''-dioctyl-[2,2':5',2''-terthiophene]-5-carbaldehyde (**9**) (300 mg, 0.52 mmol, 2 eq.) and 2,5-bis(tributylstannyl)thieno[3,2-*b*]thiophene (120 mg, 0.26, 1 eq.) was deaerated twice with Ar followed by the addition of Pd(PPh<sub>3</sub>)<sub>4</sub>. After being stirred at 100 °C for 48 h under Ar, the reaction mixture was poured into water and extracted with CHCl<sub>3</sub>. The organic layer was washed with water and then dried over anh. Na<sub>2</sub>SO<sub>4</sub>. Purified by column chromatography CHCl<sub>3</sub>-hexane (1:1). Yield: 78%.

$\delta_{\text{H}}$  (500 MHz, CDCl<sub>3</sub>, ppm): 9.83 (s, 2H), 7.60 (s, 2H), 7.30 (s, 2H), 7.25 (s, 2H), 7.13 (d,  $J = 4$  Hz, 2H), 7.06 (s, 2H), 2.84 (t,  $J = 7.75$  Hz, 4H), 2.78 (t,  $J = 8$  Hz, 4H), 1.70 (t,  $J = 6.25$  Hz, 8H), 1.43-1.28 (m, 40H), 0.88 (t,  $J = 3.25$  Hz, 12H).  $\delta_{\text{C}}$  (125 MHz, CDCl<sub>3</sub>, ppm): 205.97, 181.42, 139.99, 139.96, 139.20, 139.08, 138.06, 137.63, 137.60, 136.87, 134.73, 133.51, 128.26, 126.71, 125.75, 124.96, 114.59, 30.89, 30.87, 29.90, 29.43, 29.25, 28.68, 28.54, 28.46, 28.43, 28.31, 28.27, 21.68, 13.11.

### Synthesis of Compound OT-3

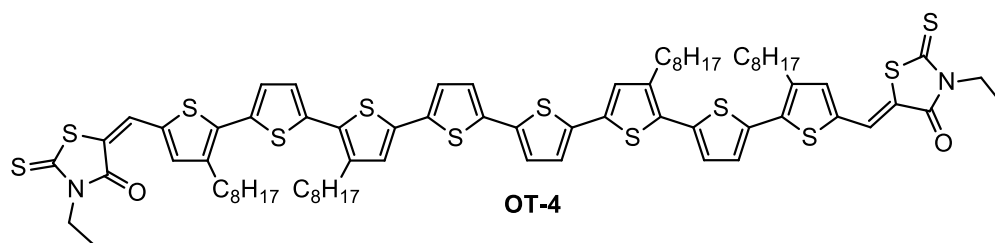


OT-3

Bisaldehyde (**10**) (158 mg, 0.15 mmol, 1 eq.) and *N*-ethyl rhodanine (181mg, 1.12 mmol, 8 eq.) was dissolved in a solution of dry  $\text{CHCl}_3$  (15 mL) and then three-four drops of piperidine was added and stirred for 48 h under argon at room temperature. The reaction mixture was then diluted with dichloromethane and washed with water and brine. After removal of solvent it was chromatographed on silica gel using  $\text{CHCl}_3$ -Hexane (1:1). Yield: 80%. Melting point: 124-125 °C.

$\delta_{\text{H}}$  (500 MHz,  $\text{CDCl}_3$ , ppm): 7.79 (s, 2H), 7.24 (d,  $J = 5$  Hz, 4H), 7.13 (d,  $J = 4$  Hz, 2H), 7.10 (s, 2H), 7.04 (s, 2H), 4.22-4.17 (q, 4H), 2.85-2.77 (m, 8H), 1.73-1.66 (m, 8H), 1.42-1.23 (m, 40H), 0.89-0.87 (m, 12H).  $\delta_{\text{C}}$  (125 MHz,  $\text{CDCl}_3$ , ppm): 192.16, 167.41, 141.15, 139.65, 137.78, 137.47, 135.30, 134.70, 129.33, 127.40, 126.16, 125.01, 124.57, 120.64, 40.05, 32.05, 32.02, 30.57, 30.41, 29.84, 29.78, 29.74, 29.63, 29.58, 29.44, 22.83, 14.27, 12.43. IR (KBr)  $\nu_{\text{max}}$ : 447, 622, 676, 960, 1130, 1242, 1319, 1416, 1580, 1623, 1703, 3440  $\text{cm}^{-1}$ ; MALDI-TOF-MS:  $m/z = 1367.47$  (calcd = 1366.39).

### Synthesis of Compound OT-4

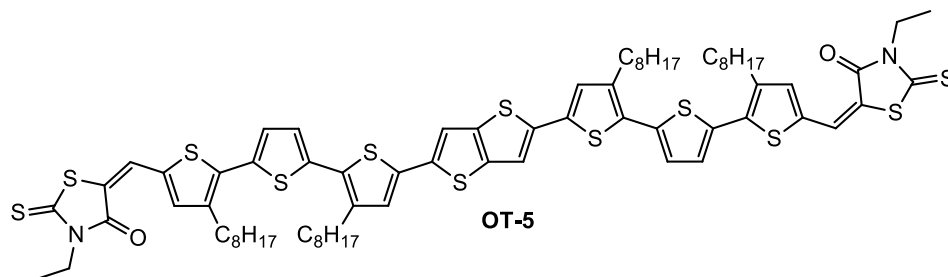


Bisaldehyde (**11**) (233 mg, 0.20 mmol, 1 eq.) and *N*-ethyl rhodanine (258 mg, 1.60 mmol, 8 eq.) was dissolved in a solution of dry CHCl<sub>3</sub> (15 mL) and then three-four drops of piperidine was added and stirred for 48 h under argon at room temperature. The reaction mixture was then diluted with dichloromethane and washed with water and brine. After removal of solvent it was chromatographed on silica gel using CHCl<sub>3</sub>-Hexane (1:1). Yield: 83%. Melting point: 135-136 °C.

$\delta_{\text{H}}$  (500 MHz, CDCl<sub>3</sub>, ppm): 7.79(s, 2H), 7.24 (d,  $J = 4$  Hz, 6H), 7.13 (d,  $J = 4$  Hz, 2H), 7.09 (s, 2H), 7.04 (s, 2H), 4.17-4.12 (q, 4H), 2.78-2.85 (m, 8H), 1.72-1.68 (m, 8H), 1.43-1.25 (m, 46H), 0.88 (t, 12H).  $\delta_{\text{C}}$  (125 MHz, CDCl<sub>3</sub>, ppm): 190.99, 166.24, 139.97, 139.93, 138.54, 136.68, 136.63, 136.33, 134.97, 134.84, 134.15, 134.07, 133.52, 128.18, 126.17, 125.69, 124.94, 123.85, 123.29, 119.43, 38.88, 30.89, 30.87, 29.41, 29.24, 28.68, 28.65, 28.63, 28.59, 28.57, 28.48, 28.47, 28.42, 28.29, 28.28, 21.68, 13.12, 11.28. IR (KBr)  $\nu_{\text{max}}$ : 796, 1133, 1253, 1330, 1428, 1503, 1569, 1699, 2330, 3658, 3865 cm<sup>-1</sup>; MALDI-TOF-MS:  $m/z = 1448.96$  (calcd = 1448.38).



### Synthesis of Compound OT-5



Bisaldehyde (**12**) (215 mg, 0.18 mmol, 1 eq.) and *N*-ethyl rhodanine (234 mg, 1.45 mmol, 8 eq.) was dissolved in a solution of dry  $\text{CHCl}_3$  (15 mL) and then three-four drops of piperidine was added and stirred for 48 h under argon at room temperature. The reaction mixture was then diluted with dichloromethane and washed with water and brine. After removal of solvent it was chromatographed on silica gel using  $\text{CHCl}_3$ -Hexane (1:1). Yield: 83%. Melting point: 165-166 °C.

$\delta_{\text{H}}$  (500 MHz,  $\text{CDCl}_3$ , ppm): 7.78 (s, 2H), 7.29 (s, 2H), 7.23 (d,  $J = 3.5$  Hz, 2H), 7.13 (d,  $J = 3.5$  Hz, 2H), 4.12-4.17 (q, 4H), 2.84-2.77 (m, 8H), 1.73-1.66 (m, 8H), 1.43-1.25 (m, 40H), 0.89-0.87 (m, 12H).  $\delta_{\text{C}}$  (125 MHz,  $\text{CDCl}_3$ , ppm): 190.97, 166.22, 139.90, 139.86, 138.54, 137.63, 136.54, 136.30, 134.65, 134.05, 133.56, 128.43, 126.12, 125.74, 124.93, 123.80, 119.42, 114.56, 38.87, 30.91, 30.89, 29.40, 29.22, 28.68, 28.62, 28.54, 28.49, 28.45, 28.31, 21.69, 13.13, 11.28. IR (KBr)  $\nu_{\text{max}}$ : 795, 1133, 1253, 1330, 1428, 1503, 1569, 1699, 2330, 3658, 3865  $\text{cm}^{-1}$ ; MALDI-TOF-MS:  $m/z = 1422.69$  (calcd = 1422.37).

---

### 3. 6. References

1. W. Ni, X. Wan, M. Li, Y. Wang, Y. Chen, *Chem. Commun.* **2015**, *51*, 4936–4950.
2. Y. Liu, X. Wan, F. Wang, J. Zhou, G. Long, J. Tian, Y. Chen, *Adv. Mater.* **2011**, *23*, 5387–5391.
3. R. Fitzner, E. Mena-Osteritz, K. Walzer, M. Pfeiffer, P. Bauerle, *Adv. Funct. Mater.* **2015**, *25*, 1845–1856.
4. D. Demeter, T. Rousseau, P. Leriche, T. Cauchy, R. Po, J. Roncali, *Adv. Funct. Mater.* **2011**, *21*, 4379–4387.
5. S. Holliday, R. S. Ashraf, C. B. Nielsen, M. Kirkus, J. A. Röhr, C.-H. Tan, E. Collado-Fregoso, A.-C. Knall, J. R. Durrant, J. Nelson, I. McCulloch, *J. Am. Chem. Soc.* **2015**, *137*, 898–904.
6. Z. Li, G. He, X. Wan, Y. Liu, J. Zhou, G. Long, Y. Zuo, M. Zhang, Y. Chen, *Adv. Energy Mater.* **2012**, *2*, 74–77.
7. Y. Kim, C. E. Song, S. Moon, E. Lim, *Chem. Commun.* **2014**, *50*, 8235–8238.
8. J. Zhou, Y. Zuo, X. Wan, G. Long, Q. Zhang, W. Ni, Y. Liu, Z. Li, G. He, C. Li, B. Kan, M. Li, Y. Chen, *J. Am. Chem. Soc.* **2013**, *135*, 8484–8487.
9. L. Chang, H. W. A. Lademann, J.-B. Bonekamp, K. Meerholz, A. J. Moule, *Adv. Funct. Mater.* **2011**, *21*, 1779–1787.
10. F. He, L. Yu, *J. Phys. Chem. Lett.* **2011**, *2*, 3102–3113.
11. B. C. Thompson, J. M. J. Frechet, *Angew. Chem., Int. Ed.* **2008**, *47*, 58–77.
12. G. J. Hedley, A. J. Ward, A. Alekseev, C. T. Howells, E. R. Martins, L. A. Serrano, G. Cooke, A. Ruseckas, I. D. W. Samuel, *Nat. Commun.* **2013**, *4*, 2867.
13. Y. Liang, Z. Xu, J. Xia, S.-T. Tsai, Y. Wu, G. Li, C. Ray, L. Yu, *Adv. Mater.* **2010**, *22*, E135–E138.
14. D. H. Wang, P. Morin, C. Lee, K. Ko, *J. Mater. Chem. A* **2014**, *2*, 15052–15057.
15. A. Zusan, M. Zerson, V. Dyakonov, R. Magerle, *Sci. Rep.* **2015**, *5*, 8286.

16. S.J. Lou, J.M. Szarko, T. Xu, L. Yu, T.J. Marks, L.X. Chen, *J. Am. Chem. Soc.* **2011**, *133*, 20661-20663.
17. L. A. Perez, J. T. Rogers, M. A. Brady, Y. Sun, G. C. Welch, K. Schmidt, M. F. Toney, H. Jinnai, A. J. Heeger, M. L. Chabinyc, G. C. Bazan, E. J. Kramer, *Chem. Mater.* **2014**, *26*, 6531-6541.
18. F. Liu, H. Fan, Z. Zhang, X. Zhu, *ACS Appl. Mater. Interfaces* **2016**, *8*, 3661-3668.
19. Y. Sun, G. C. Welch, W. L. Leong, C. J. Takacs, G. C. Bazan, A. J. Heeger, *Nat. Mater.* **2012**, *11*, 44-48.
20. M. Tsuji, A. Saeki, Y. Koizumi, N. Matsuyama, C. Vijayakumar, S. Seki, *Adv. Funct. Mater.* **2014**, *24*, 28-36.
21. A. Saeki, M. Tsuji, S. Seki, *Adv. Energy Mater.* **2011**, *1*, 661-669.
22. J. S. Lee, S. K. Son, S. Song, H. Kim, D. R. Lee, K. Kim, M. J. Ko, D. H. Choi, B. S. Kim, J. H. Cho, *Chem. Mater.* **2012**, *24*, 1316-1323.
23. Q. Zhang, Y. Wang, B. Kan, X. Wan, F. Liu, W. Ni, H. Feng, T. P. Russell, Y. A. Chen, *Chem. Commun.* **2015**, *51*, 15268-15271.
24. Z. He, C. Zhong, S. Su, M. Xu, H. Wu, Y. Cao, *Nat. Photonics* **2012**, *6*, 591-595.
25. J. J. Intemann, K. Yao, Y. X. Li, H. L. Yip, Y. X. Xu, P. W. Liang, C. C. Chueh, F. Z. Ding, X. Yang, X. Li, Y. Chen, A. K. Y. Jen, *Adv. Funct. Mater.* **2014**, *24*, 1465-1473.
26. J. Sun, Y. Zhu, X. Xu, L. Lan, L. Zhang, P. Cai, J. Chen, *J. Phys. Chem. C* **2012**, *116*, 14188-14198.
27. A. K. K. Kyaw, D. H. Wang, V. Gupta, J. Zhang, S. Chand, G. C. Bazan, A. J. Heeger, *Adv. Mater.* **2013**, *25*, 2397-2402.
28. N. Rujisamphan, R. E. Murray, F. Deng, C. Ni, S. I. Shah, *ACS Appl. Mater. Interfaces* **2014**, *6*, 11965-11972.
29. C. V. Kumar, L. Cabau, A. Viterisi, S. Biswas, G. D. Sharma, E. Palomares, *J. Phys. Chem. C* **2015**, *119*, 20871-20879.

- 
30. K. Cnops, B. P. Rand, D. Cheyns, B. Verreert, M. A. Empl, P. Heremans, *Nat. Commun.* **2014**, *5*, 3406.
  31. A. Zusan, B. Giesecking, M. Zerson, V. Dyakonov, R. Magerle, C. Deibel, *Sci. Rep.* **2015**, *5*, 8286.
  32. Y. Liu, Q. Shi, L. Ma, H. Dong, J. Tan, W. Hu, X. Zhan, *J. Mater. Chem. C* **2014**, *2*, 9505–9511.
  33. G. M. Su, T. V. Pho, N. D. Eisenmenger, C. Wang, F. Wudl, E. J. Kramer, M. L. Chabiny, *J. Mater. Chem. A* **2014**, *2*, 1781–1789.
  34. M. Ide, A. Saeki, Y. Koizumi, T. Koganezawa, S. Seki, *J. Mater. Chem. A* **2015**, *3*, 21578–21585.
  35. K.-H. Kim, H. Yu, H. Kang, D. J. Kang, C.-H. Cho, H.-H. Cho, J. H. Oh, B. J. Kim, *J. Mater. Chem. A* **2013**, *1*, 14538–14547.

---

### Preferential Face-on or Edge-on Orientation in Thiophene Oligomers

---

#### 4.1. Abstract

*Precise control over the supramolecular organization of organic semiconducting materials guiding to exclusive face-on or edge-on orientation is a challenging task. In the present work, we study the preferential packing of thiophene oligomers induced through rational molecular designing and self-assembly. The acceptor-donor-acceptor type oligomers having 2-(1,1-dicyano-methylene)rhodanine as acceptor (**OT-6**) favored a face-on packing, while that of functionalized with N-octyl rhodanine (**OT-7**) preferred an edge-on packing as evident from 2D-grazing incidence angle X-ray diffraction, tapping-mode atomic force microscopy (AFM) and Raman spectroscopy analyses. As an outcome of the preferred orientation, the oligomers exhibited anisotropic conductivity in the self-assembled state, revealed by the conducting AFM experiment. Photovoltaic properties of the oligomers were also evaluated in an inverted device architecture using PC<sub>61</sub>BM as an acceptor.*

---

## 4.2. Introduction

Excogitation of organic semiconducting materials with precise film-state packing is the utmost important task in organic electronics as packing plays a crucial role on the charge transport properties of the materials thus influencing their optoelectronic functions and device performance. It is established that face-on packing of oligomers/polymers with respect to the substrate is advantageous for photovoltaic device application, whereas, edge-on packing is suitable for transistors.<sup>1-10</sup> In literature, various methods have been reported to orient organic semiconductors in a particular direction onto the substrate. Rational design of the basic molecular structure using different alkyl chains and pi-aromatic units to provide a pre-programmed architecture is considered as the most effective approach towards this end.<sup>11-13</sup> Other methods include the selection of solvents,<sup>14,15</sup> use of solvent additives,<sup>16-19</sup> and thermal and solvent vapor annealing of the films.<sup>20-23</sup>

Jenekhe and co-workers have demonstrated that by varying the length of the alkyl side chain on the backbone of thiazolothiazole (TT) - dithienosilole (DTS) copolymer, preferential orientation could be achieved.<sup>24</sup> They have synthesized **1–3** copolymers with thiophene-TT-thiophene-DTS polymer appended with different side chains (**Figure 4.1a**). **1** has octyloxy chains on thiophene and *n*-octyl chains on DTS, whereas, **2** and **3** are comprised of linear *n*-octyl chains and branched ethylhexyl chains, respectively, on thiophene and DTS units.

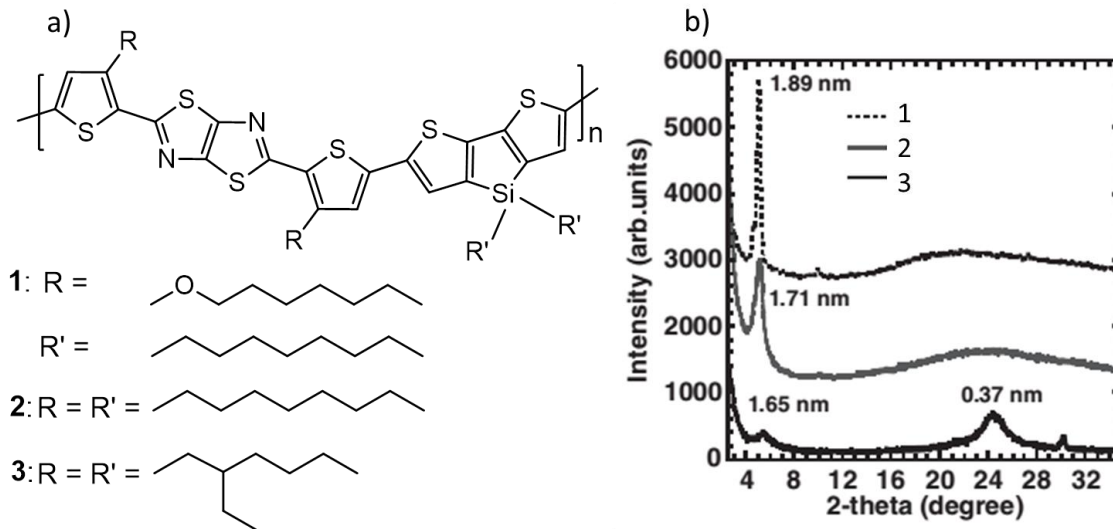


**Figure 4.1.** a) Chemical structures of the copolymers **1-3** comprising of different alkyl chains; b) X-ray diffraction (XRD) spectra of drop-cast films of **1**, **2** and **3** on ITO/PEDOT substrate after annealing at 180 °C (Adapted from reference 24).

X-ray diffraction (XRD) studies of the copolymer **3** having branched alkyl chains confirmed the presence of a large fraction of backbone being oriented face-on relative to the substrate (**Figure 4.1b**). While sharp lamellar stacking peaks with a d-spacing of 1.89 and 1.71 nm, were observed in polymers **1** and **2** (with linear alkyl chains), respectively, indicating high edge-on fraction. Since face-on fractions lead to an increase in vertical hole transport and absorption intensity, best efficiency was observed for polymer **3** (5.0 %;  $J_{SC}$ : 12.6  $\text{mAcm}^{-2}$ ;  $V_{OC}$ : 0.65 V;  $FF$ : 0.61). While, other two polymers (**1** and **2**) performed lower, and had average efficiencies of 2.1–4.1%.

Osaka *et al.* have reported a series of co-polymers (**4–6**) comprising of naphtho[1,2-*b*:5,6-*b'*]dithiophene and naphtho[1,2-*c*:5,6-*c'*]bis[1,2,5]thiadiazole.<sup>25,26</sup> Chemical structures of the copolymers are shown in the upper panel of **Figure 4.2**. **4** is alkylated

with the 2-decyltetradecyl chain on *pi*-spacer (thiophene) unit only and exhibits appreciably good PCE of 4.9%. However, it possesses a major drawback, due to poor solubility it hinders its processability. As a result, to improve solubility alkylation was carried out at the 5 and 10 positions of naphthodithiophene unit with a dodecyl chain to yield **5** and **6**. Apart from this, the thiophene *pi*-spacer was also alkylated, **5** with 2-hexyldecyl while, **6** with 2-decyltetradecyl.

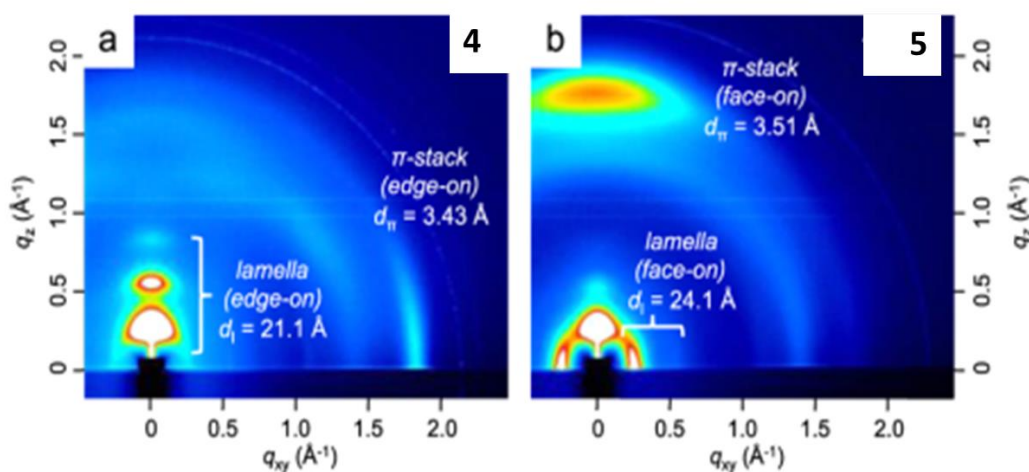
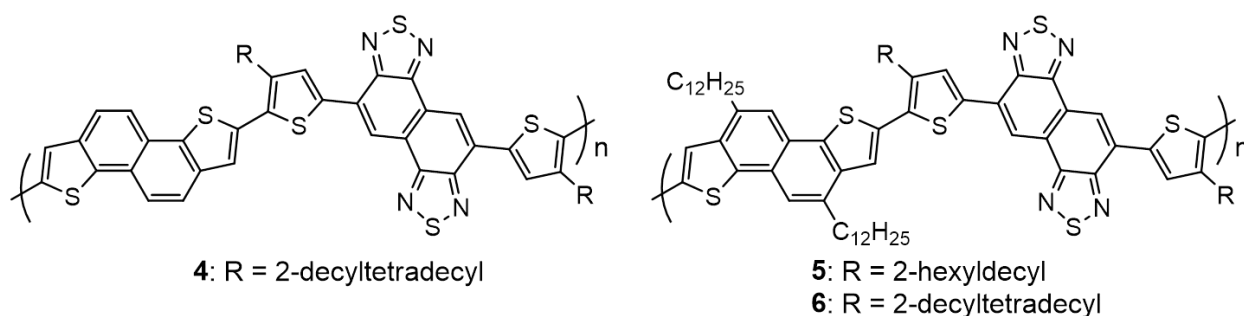


**Figure 4.2.** Upper panel shows the chemical structures of semiconducting polymers, **4-6**. The lower panel shows the 2D-GIXRD of polymers **4** and **5** (Adapted from reference 26).

The orientation of all the polymers was studied by 2D-GIXRD experiment, where, **4** adopted an edge-on orientation while **5** and **6** adopted a preferential face-on orientation.



**Figure 4.2** shows the 2D-GIXRD of **4** and **5** (**6** has a GIXRD similar to that of **5**) in the lower panel. They have also noted that **5** and **6** preserved the face-on orientation even in the presence of PC<sub>61</sub>BM. Photovoltaic properties were investigated using a conventional BHJ architecture. No solvent additives were used at the time of spin-coating and no post-deposition treatments such as thermal and/or solvent annealing of the active layer were carried out. An efficiency of 5.5%, 4.1%, and 5.9% were obtained for **4**, **5** and **6**, respectively, upon blending with PC<sub>61</sub>BM. An increase in the efficiency to 8.2% was observed for **5** on blending with PC<sub>71</sub>BM. Thus, authors were successful in bringing about substantial change in the polymer orientation from edge-on to face-on and speculate that this might originate due to an increased side-chain density, and contributed to the drastic change in polymer orientation.

DeLongchamp and McCulloch reported a series of highly soluble three thiophene-based copolymers containing electron-deficient diketo pyrrolo-pyrrole (DPP) units with pendant 2-octyldodecyl groups (**7-9**; **Figure 4.3**).<sup>27</sup> All the polymer repeats have in common DPP-bithiophene moiety and a variable moiety that can be thienothiophene (**7**), bithiophene (**8**), or monothiophene (**9**). Spectroscopy, diffraction, and microscopy measurements have shown that a transition in molecular packing from a preferentially edge-on orientation of the conjugated backbone to a preferentially face-on orientation as the attachment density of the side chains increases. However, thermal annealing could reduce the population of both face-on and the misoriented edge-on domains confirmed by GIXRD, near-edge X-ray absorption fine structure spectroscopy and variable angle

spectroscopic ellipsometry technique. A schematic representation of such an observation is depicted in the lower panel of **Figure 4.3**. The highest hole mobilities of this series of polymers were obtained from edge-on molecular packing polymer **8**, but films possess a bimodal orientation distribution.

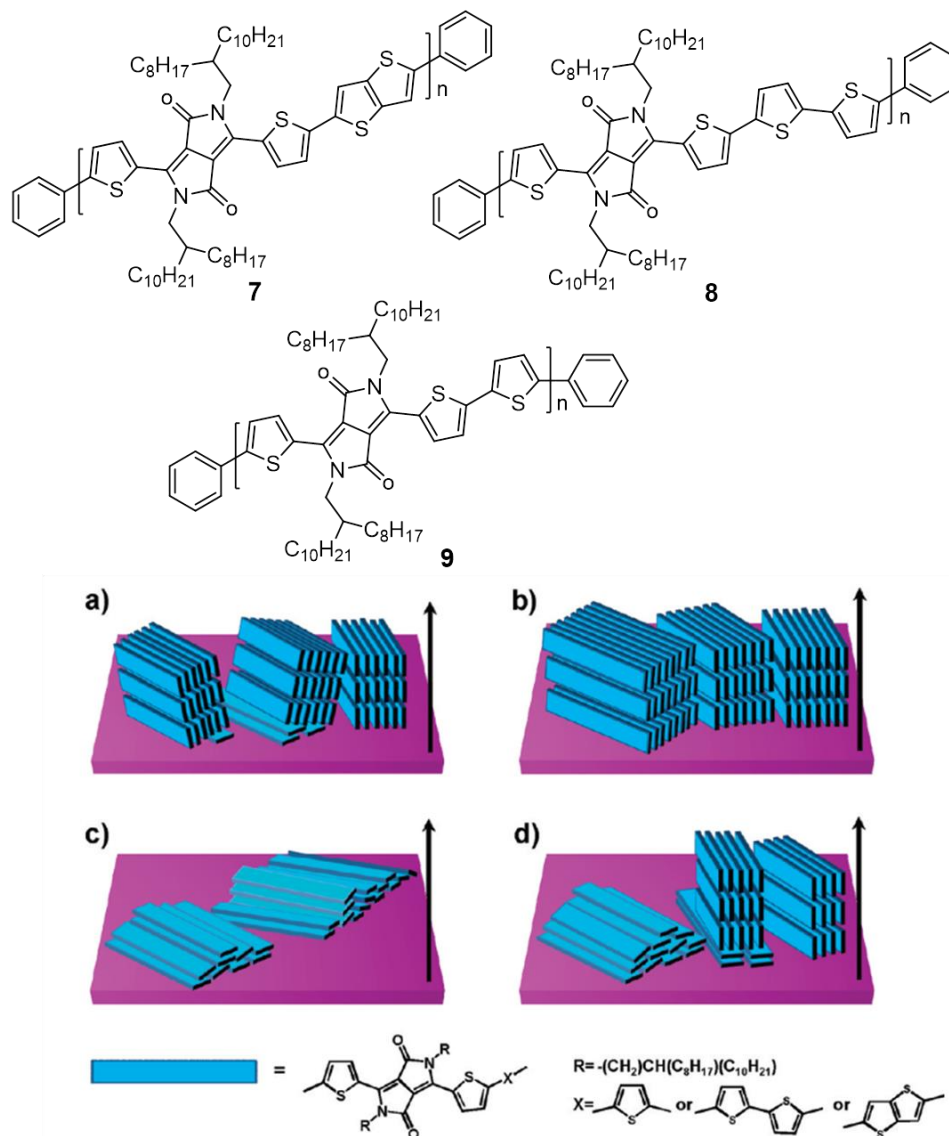


**Figure 4.3.** Upper panel shows the chemical structures of the polymers, **7-9**. Lower panel illustrates the molecular packing motifs in a) as-cast **7** and **8** films; b) annealed **7** and **8** films; c) as-cast **9** film; and d) annealed **9** films. The arrows denote the film surface normal direction (*Adapted from reference 27*).

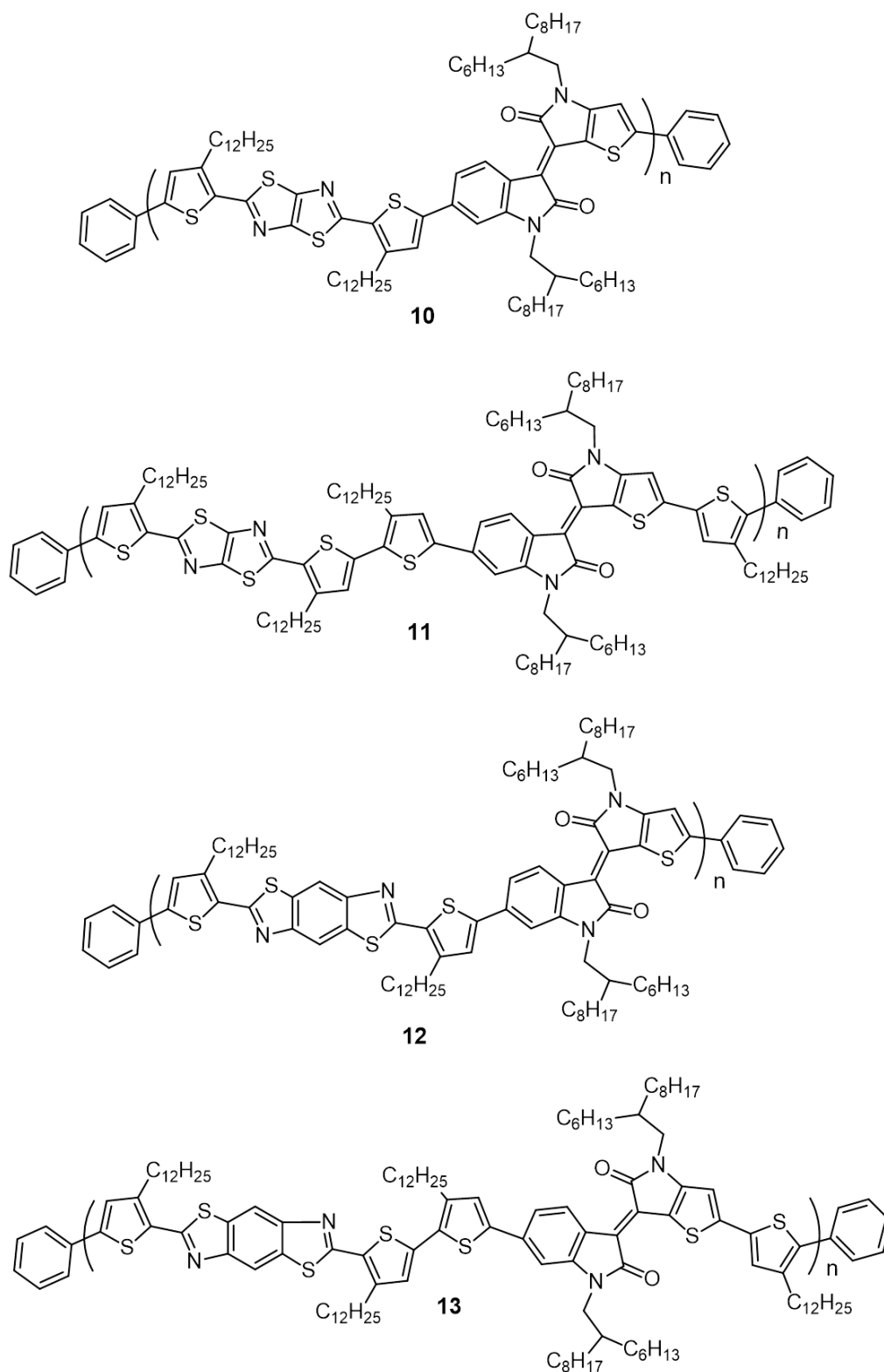
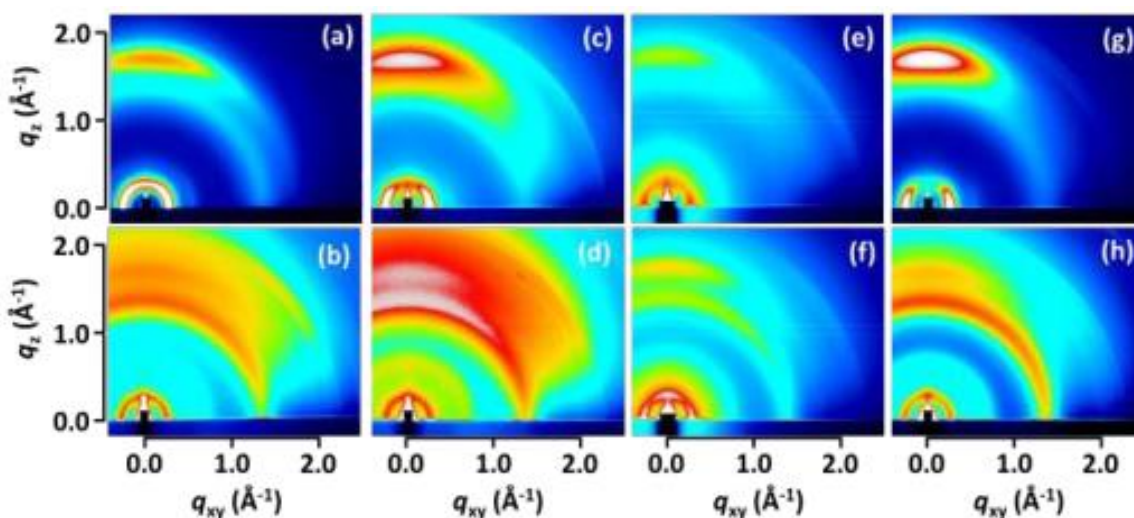


Figure 4.4. Chemical structures of BTIDG polymers, 10-13.

Seki and co-workers reported a series of copolymers comprised of electron-accepting benzothienoisindigo (BTIDG) and electron-donating benzobisthiazole (BBTz) or thiazolothiazole (TzTz) units, (**10-13**; **Figure 4.4**).<sup>24</sup> Co-polymers, **10** and **12** have alkylated thiophene as pi-spacer unit, while, **11** and **13** have alkylated bithiophene. The orientation of the polymers in pristine and blend with PC<sub>61</sub>BM was studied by 2D-GIXRD (**Figure 4.5**).



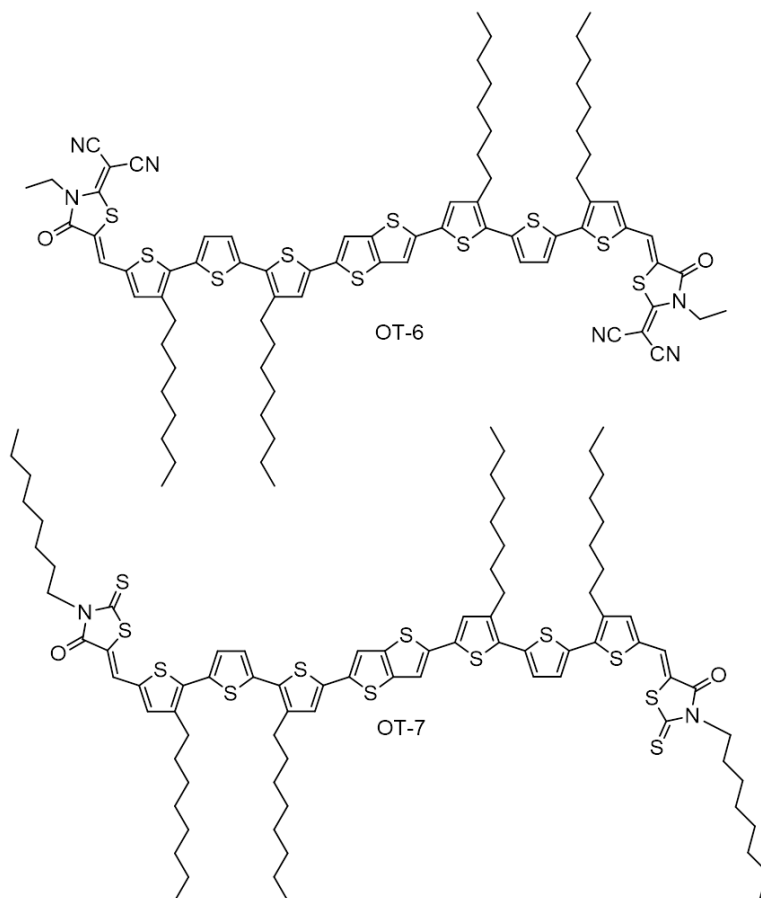
**Figure 4.5.** 2D-GIXRD patterns of pristine a) **10**, c) **11**, e) **12** and g) **13** drop-cast on ITO substrate. b), d), f), h) are the patterns of optimal OPV devices of blends (*Adapted from reference 28*).

All the pristine samples of co-polymers have a profound face-on orientation with negligibly small edge-on peaks. **10** have face-on fraction of 67%, **11** has 80%, **12** has 93% and **13** has 95% (**Figure 4.5**). The highest PCE was obtained for **13** (4.18%) when blended with PC<sub>61</sub>BM, while others exhibited much lower efficiency (0.60-3.29%). Most of the polymer films suffered from a large decrease in face-on orientation fraction by 10–

20% in the blended state. This was attributed to the relatively lower efficiencies of the copolymers.

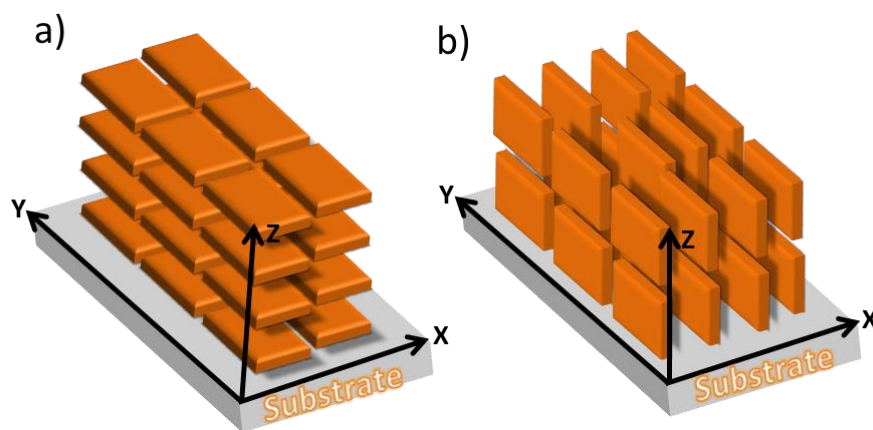
The influences by bringing in structural modifications are, by far, studied mostly in polymers and not much in oligomers. However, oligomers are finding special attention for organic device applications in recent years as already mentioned in previous chapters. Hence it is important to study the packing control through molecular engineering in semiconducting oligomers for developing efficient functional electronic devices.

### 4. 3. Results and discussion



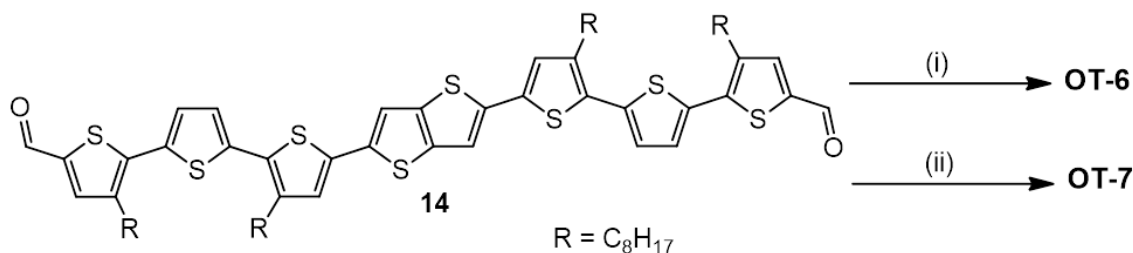
**Scheme 4.1.** Chemical structures of the thiophene oligomers **OT-6** and **OT-7** under study.

In this chapter, we report the synthesis and study of two acceptor-donor-acceptor type oligothiophene derivatives, **OT-6** and **OT-7** (**Scheme 4.1**). The central part of both oligomers is a thienothiophene unit, which is flanked by dioctyl terthiophene on either side and an acceptor 2-(1,1-dicyanomethylene)rhodanine (**OT-6**) or *N*-octyl rhodanine (**OT-7**). Notably, we found that **OT-6** comprised of an unequal length of the alkyl chain (and unequal chain density) on the pi-conjugated backbone and acceptor (octyl on thiophene and ethyl on the nitrogen atom of rhodanine) is stacking parallel to the substrate resulting in face-on orientation of the oligomers. On the other hand, **OT-7** with equal length of alkyl chains on the thiophene backbone as well as on the acceptor (octyl on thiophene and nitrogen atom of rhodanine) is stacking perpendicular to the substrate, resulting in an edge-on orientation. A simplified schematic representation of the stacking of oligomers in film state is shown in **Scheme 4.2**.



**Scheme 4.2.** Schematic illustration of the orientation of respective as-cast oligomers on the substrate; a) **OT-6** and b) **OT-7**. The arrows represent the X, Y and Z directions of the chromophores packing with respect to the substrate.

### 4.3.1. Synthesis and photophysical characterization



**Scheme 4.3.** Synthesis of oligothiophene derivatives, **OT-6** and **OT-7**; *Reagents and conditions:* (i) 2-(1,1-dicyanomethylene)rhodanine,<sup>29</sup> piperidine, anhydrous CHCl<sub>3</sub>, 48 h, 60 °C, (ii) *N*-octylrhodanine,<sup>30</sup> piperidine, anhydrous CHCl<sub>3</sub>, 48 h, 60 °C.

The oligothiophene derivatives, **OT-6** and **OT-7** were synthesized according to methods reported in the literature as shown in **Scheme 4.3**. Knoevenagel condensation of **14** (synthesis described in **Chapter 3**) with 2-(1,1-dicyanomethylene)rhodanine and *N*-octylrhodanine in the presence of catalytic amounts of piperidine in anhydrous chloroform at 60 °C under argon atmosphere yielded **OT-6** and **OT-7**, respectively. Both derivatives were obtained in good yields and characterized by using various analytical techniques such as <sup>1</sup>H NMR, <sup>13</sup>C NMR, IR, and mass spectrometry.

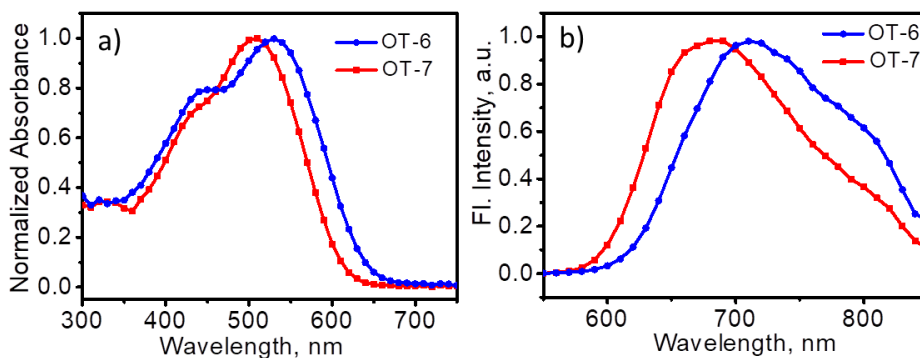


**Figure 4.6.** a) UV-vis absorption spectra and b) fluorescence emission spectra of **OT-6** and **OT-7** respectively; ( $c = 1 \times 10^{-5}$  M,  $l = 10$  mm).

The UV-vis absorption and fluorescence properties of **OT-6** and **OT-7** were studied in a chloroform solvent at a concentration of  $1 \times 10^{-5}$  M (**Figure 4.6**). Due to the presence of a push-pull molecular structure, they exhibited intense and broad absorption from 300 to 600 nm in solution, and the most intense band was assigned to the  $\pi$ - $\pi^*$  transitions. **OT-6** and **OT-7** exhibited an absorption maximum of 530 and 508 nm. A 20 nm red-shift was observed for **OT-6**, which reiterates the presence of a stronger electron-withdrawing group. The charge transfer nature of the oligomers was evident from the red shift in emission maximum of 710 and 680 nm, respectively.

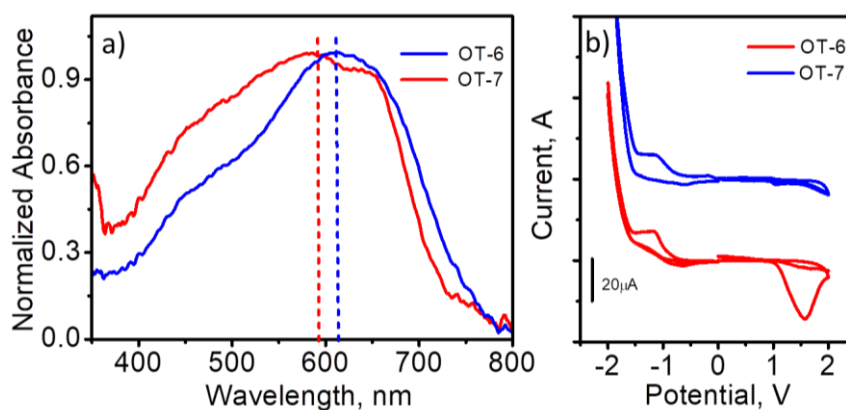


**Figure 4.7.** a) UV-vis absorption of oligomer in film state; b) Cyclic voltammograms of oligomers in thin film state cast from chloroform on Pt as the working electrode, using 0.1 M tetrabutylammonium hexafluorophosphate as the supporting electrolyte in acetonitrile, Pt as the counter electrode, Ag/AgCl as the reference electrode which was calibrated using ferrocene/ferrocenium (Fc/Fc<sup>+</sup>) redox couple as an external standard. (Scan rate: 100 mV/s).

By extrapolation of the absorption onsets in the film state, the optical bandgaps were estimated to be 1.63 and 1.73 eV for **OT-6** and **OT-7**, respectively (**Figure 4.7a**), which are consistent with the values of 1.64 and 1.79 eV, respectively, measured by cyclic voltammetry (CV) where the films were cast from chloroform solution on platinum electrodes (**Figure 4.7b**) and the values were tabulated in **Table 4.1**.



**Table 4.1.** Summary of the film state absorption and electrochemical properties of the oligomers in the film state. Films were drop cast from chloroform solvent.

| Oligomer    | $\lambda_{\max}$<br>(nm) | $\lambda_{\text{onset}}$<br>(nm) | $E_{\text{g(opt)}}^{\text{a}}$<br>(eV) | $E_{\text{ox(onset)}}^{\text{b}}$<br>(V) | $E_{\text{red(onset)}}^{\text{b}}$<br>(V) | $E_{\text{HOMO}}$<br>(eV) | $E_{\text{LUMO}}$<br>(eV) | $E_{\text{g(cv)}}$<br>(eV) |
|-------------|--------------------------|----------------------------------|--|--|---|---------------------------|---------------------------|----------------------------|
| <b>OT-6</b> | 614                      | 761                              | 1.63                                   | 0.97                                     | -0.67                                     | -5.39                     | -3.75                     | 1.64                       |
| <b>OT-7</b> | 592                      | 715                              | 1.73                                   | 1.02                                     | -0.77                                     | -5.44                     | -3.64                     | 1.79                       |

<sup>a)</sup> Estimated from the onset of the absorption of film samples; <sup>b)</sup> Potentials are measured relative to a Fc/Fc<sup>+</sup> redox couple as an external reference.  $E_{\text{HOMO}} = -(E_{\text{ox(onset)}} - \text{ferrocene}_{\text{(onset)}}) - 4.8$  eV,  $E_{\text{LUMO}} = -(E_{\text{red(onset)}} - \text{ferrocene}_{\text{(onset)}}) - 4.8$  eV, where,  $E_{\text{ox(onset)}}$  and  $E_{\text{red(onset)}}$  are the onsets of the oxidation and reduction potentials, respectively. Ferrocene<sub>(onset)</sub> is the onset oxidation potential of ferrocene (0.38 eV), which was used as a reference.

### 4. 3. 2. Solid state packing and thermal stability

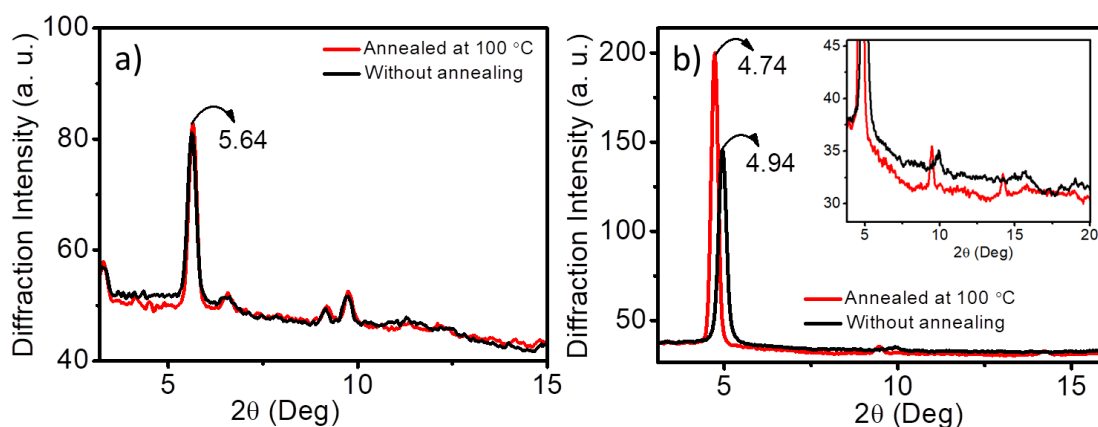


**Figure 4.8.** Wide-angle X-ray diffraction patterns of a) **OT-6** and b) **OT-7** in film state (inset showing the zoomed region between 4 to 20°) both in the pristine and annealed state (100 °C).

Wide-angle X-ray diffraction (WAX) patterns of **OT-6** and **OT-7** in the self-assembled film state is shown in **Figure 4.8a** and **4.8b**. The reflection of the pristine sample at  $2\theta$  values of 5.64 and 4.94° corresponds to the lamellar distance of the oligomers (1.56 and 1.78 nm, respectively). The peak intensity of **OT-7** is relatively sharper when compared to **OT-6**, which indicates that the molecules are more ordered in

the aggregated state. Hence, it could be concluded that the alkyl chains appended on the acceptor units have significantly affected the supramolecular interactions, which is reflected in the bulk packing. The thin films were annealed at 100 °C to study the crystallinity behavior of the oligomers at a higher temperature. From the study, the amorphous nature of **OT-6** was revealed as there was no change in the intensity of the lamellar stacking or any other peak in the spectra. On the other hand, the sharper peaks of the annealed sample of **OT-7** indicates that a better crystallization occurs at a higher temperature (100 °C).

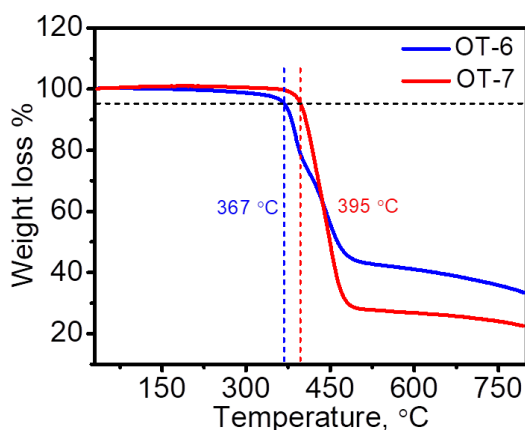


**Figure 4.9.** Thermogravimetric analysis (TGA) profiles of **OT-6** and **OT-7**; the black line indicates the temperature at which the material loses 5% of its initial weight.

TGA was carried out to study the quantitative assessment of the thermal stability of **OT-6** and **OT-7** (**Figure 4.9**). ‘ $T_5$ ’ values of **OT-6** and **OT-7** were 367 °C and 395 °C, respectively. Comparison of the ‘ $T_5$ ’ values of the oligomer reveals that **OT-7** is thermally more stable than **OT-6**, which reiterates the higher crystallinity in the former.

### 4. 3. 3. Differential scanning calorimetry

Differential scanning calorimetry (DSC) is a thermoanalytical technique in which the difference in the amount of heat required to increase the temperature of a sample and reference is measured as a function of temperature. The thermogram reveals a number of characteristic properties of a sample like melting, fusion, and crystallization temperature.

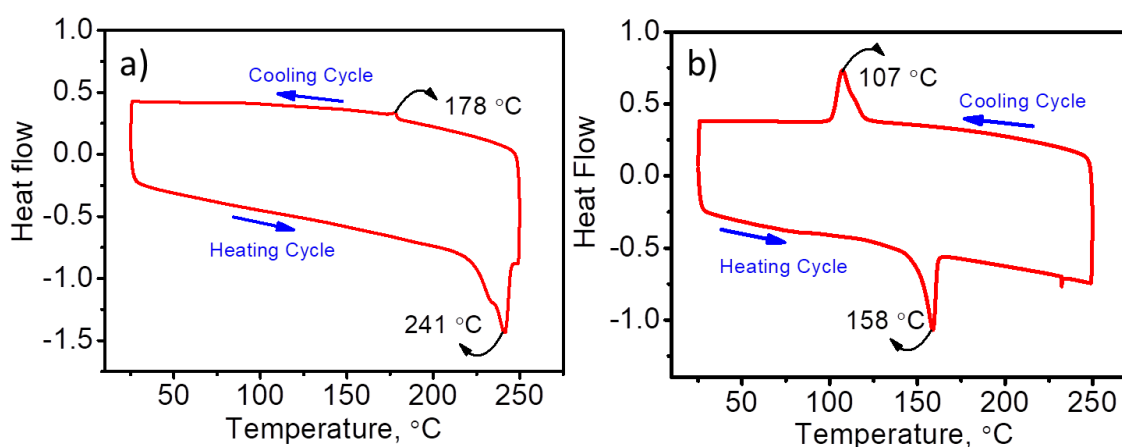
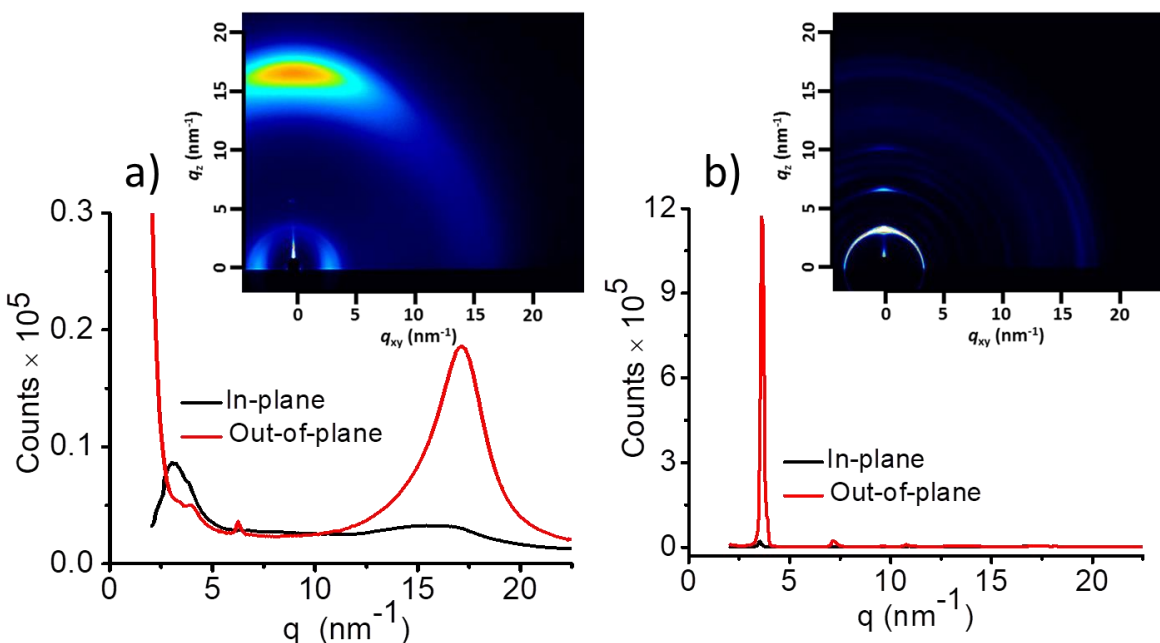


Figure 4.10. DSC analysis of a) OT-6 and b) OT-7 in the powder state.

DSC analysis of **OT-6** and **OT-7** was carried out in such a way that the temperature of the samples was first raised from room temperature to 250 °C and then reduced to room temperature (both at a rate of 10 °C/min). The DSC result is shown in **Figure 4.10a** and **4.10b**. Both compounds showed a sharp endothermic peak ascribable to the melting transition and exothermic crystallization peak. **OT-6** exhibits a melting temperature at 241°C and recrystallization at 178 °C, whereas **OT-7** melts at 158 °C with a sharp peak and recrystallization occurs at 107 °C. The higher melting temperature of **OT-6** signifies

the presence of a stronger supramolecular interaction between the oligomers and the sharp melt reflects its crystallinity behavior.

#### 4. 3. 4. Grazing-incidence X-ray diffraction studies



**Figure 4.11.** GIXRD of thin films of a) **OT-6** and b) **OT-7** in the out-of-plane (red) and in-plane (black) directions. Insets show the corresponding 2D images of the diffraction pattern. The diffraction spectra are extracted from the 2D pattern.

GIXRD analysis was carried out to analyze the packing orientation relative to the substrate, pi-stacking distance, and crystallinity of the oligomers.<sup>31-33</sup> Thin films of the oligomers were prepared by dissolving them in chloroform and spin-casting over ITO substrate. The scattering angle and scattering vectors ( $q$ ) in reciprocal space were collected in two dimensions. The domain sizes and orientations were also extracted. The diffraction patterns and the corresponding 2D images are shown in **Figure 4.9**. The  $d$ -spacing was determined by the relationship,  $d = 2\pi/q$ . Notably, the pristine samples of both oligomers have similar  $\pi$ - $\pi$  stacking distances (3.67 Å for **OT-6** and 3.65 Å for **OT-**

7) implying that the stacking of the molecules is not affected by the differential substitution at the acceptor units. However, their presence has an obvious impact on the orientation of the oligomers on the substrate. In **OT-6**, the absence of lamellar stacking peak (at  $q_z = 3\text{--}4\text{ nm}^{-1}$ ) and a distinct and intense  $\pi\text{-}\pi$  stacking reflection in the out-of-plane direction at  $q_z = 17.15\text{ nm}^{-1}$  implies the oligomers are stacked with a face-on orientation. On the other hand, an intense lamellar stacking peak at  $q_z = 3.60\text{ nm}^{-1}$  and weak  $\pi\text{-}\pi$  stacking peak at  $q_{xy} = 17.20\text{ nm}^{-1}$  was observed for **OT-7**, which indicates the edge-on orientation of the self-assembled oligomers. The ratio of face-on orientation ( $R_{\text{face-on}}$  in %) was evaluated by  $I_{ip}/(I_{ip}+I_{op})$  and edge-on orientation ( $R_{\text{edge-on}}$  in %) was calculated by  $I_{op}/(I_{ip}+I_{op})$ , where  $I_{ip}$  and  $I_{op}$  are the peak intensities of (100) diffraction in the in-plane and out-of-plane directions, respectively. From the graph, we have extracted  $R_{\text{face-on}}$  as 89% for **OT-6** and  $R_{\text{edge-on}}$  as 98% for **OT-7**.

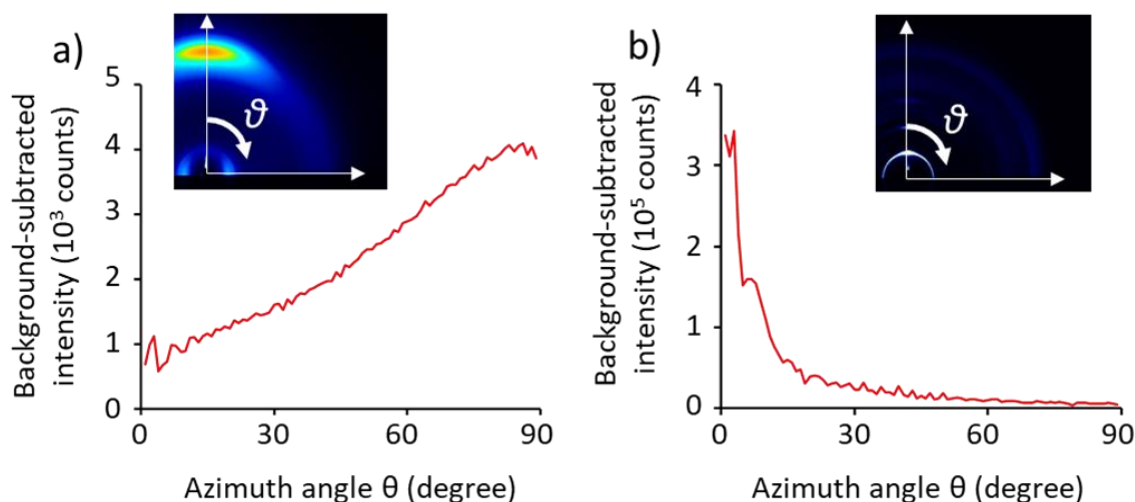


**Figure 4.12.** Herman's orientation parameter ( $S$ ), a) **OT-6** and b) **OT-7**.

A survey of the literature has shown that one of the most common ways to define the orientation of particle assemblies from X-ray scattering experiments is by calculating Herman's orientation parameter ( $S$ ). It is defined as given in the equation (1)

$$S = \frac{3 \langle \cos^2\chi \rangle - 1}{2} \quad (1)$$

where  $\langle \cos^2\chi \rangle$  is the average cosine squared value for the diffraction ring and is calculated using the following equation (2),

$$\langle \cos^2\chi \rangle = \frac{\sum_{i=0}^{90} I_i \cos^2\chi_i \sin\chi_i}{\sum_{i=0}^{90} I_i \sin\chi_i} \quad (2)$$

' $S$ ' was calculated based on the (100) diffraction along the azimuthal arch (0-90°), where,  $S = -0.5, 0$  and  $1$  represent a perfect face-on, random orientation, and perfect edge-on orientation, respectively.<sup>34,35</sup> **OT-6** and **OT-7** exhibit the ' $S$ ' of  $-0.15$  and  $0.41$ , which are high-score face-on and edge-on orientations, respectively (see **Figure 4.12**). It could be assumed that the alkyl chains on the end groups played a key role in the supramolecular assembly of the oligomers on the substrate. Presence of equally long alkyl chains on either side (octyl on thiophene and nitrogen atom of rhodanine) supported **OT7** to stand on the substrate yielding edge-on orientation. On the other hand, the presence of unsymmetrical alkyl chains (octyl on thiophene and ethyl on the nitrogen atom of rhodanine) can't provide such support in **OT6** resulting in the oligomer assembly to fall on the substrate yielding face-on orientation. Though the dicyano groups in **OT6**

provide larger  $\pi$ -surface and facilitate  $\pi$ - $\pi$  stacking of chromophores, their role on the preferential orientation on the substrate is not clear from our studies.

#### 4. 3. 5. Atomic force microscopy analysis

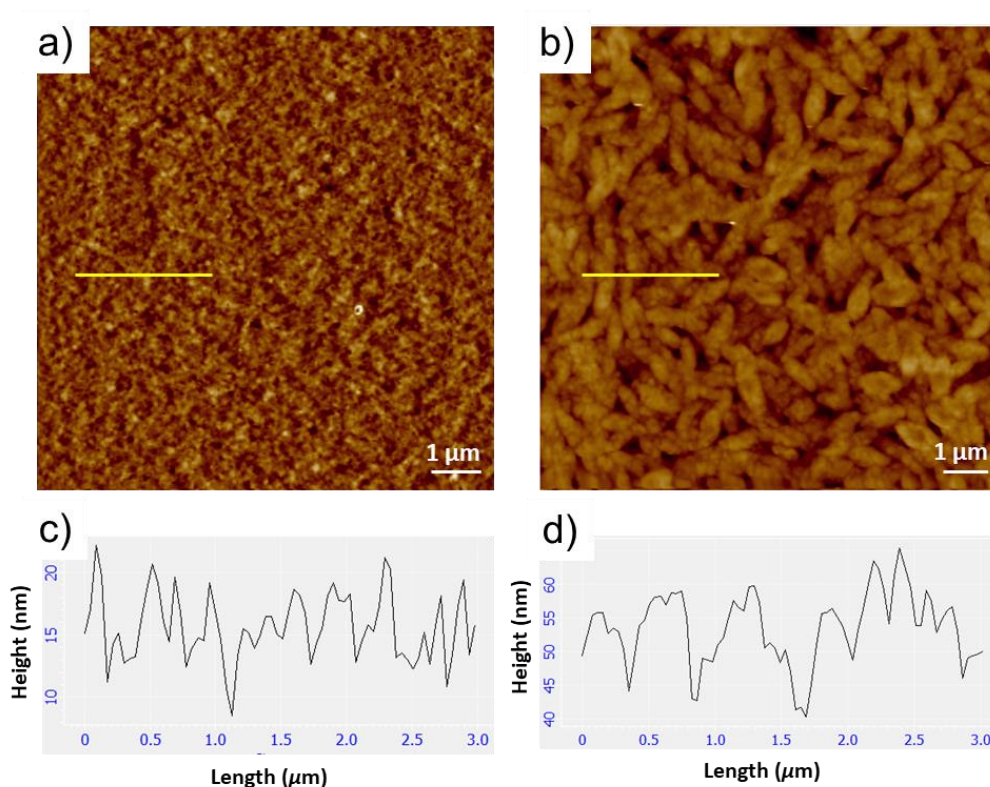


**Figure 4.13.** AFM height images of a) **OT-6** and b) **OT-7** on ITO drop-cast from chloroform solution. c) and d) show the corresponding cross-sectional analysis (the selected area is indicated by a yellow line on the image).

The AFM images of drop cast sample of the oligomers showed the disparity in the film microstructure between **OT-6** and **OT-7** on ITO substrate portraying its difference in preferential stacking. The topography of **OT-6** film revealed a featureless or amorphous nature (**Figure 4.13a**) with a root-mean-square roughness of 2.97 nm, whereas, **OT-7** displayed leaf-like morphology (**Figure 4.13b**) with a larger roughness of 10.49 nm,

presumably due to its stronger crystallinity as reflected in GIXRD. In other words, the obtained morphologies support a picture in which the face-on domains percolate throughout the whole substrate surface without any significant features, while edge-on domains result in structural variations in the bulk of the material due to the lateral growth of stacks. The cross-sectional analysis of the AFM images revealed that the average height of the aggregates of **OT1** is ~15 nm (**Figure 4.13c**), and that of **OT2** is ~55 nm (**Figure 4.13d**).

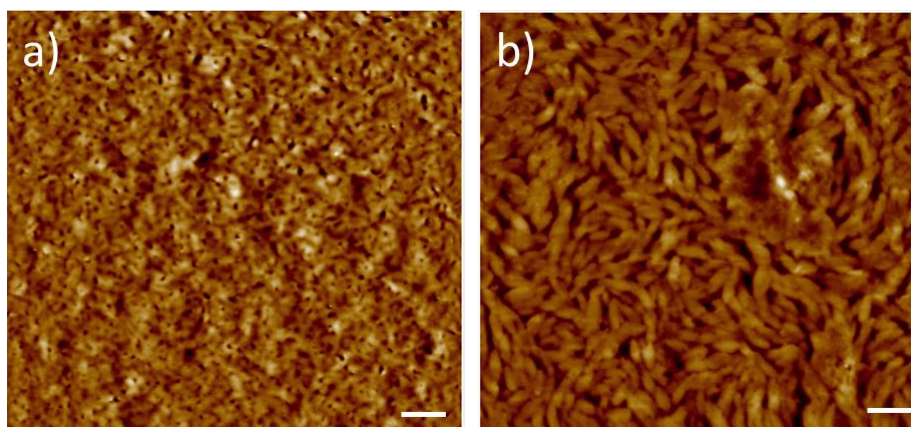


**Figure 4.14.** AFM height images of a) **OT6** and b) **OT7** on a gold substrate (scale bar corresponds to 1  $\mu\text{m}$ ).

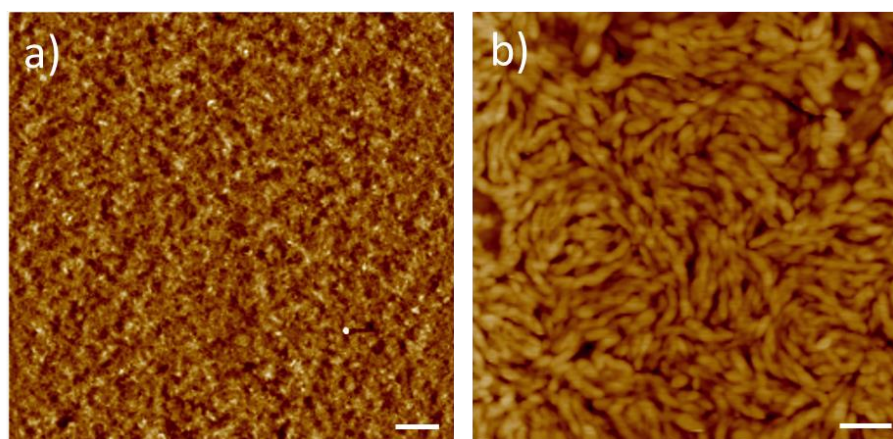


**Figure 4.15** AFM height images of a) **OT6** and b) **OT7** on  $\text{SiO}_2$  substrate (scale bar corresponds to 1  $\mu\text{m}$ ).



Interestingly, these morphological features are independent of substrate nature as evident from the observation of similar morphologies on gold (**Figure 4.14a** and **4.14b**) and SiO<sub>2</sub> (**Figure 4.15a** and **4.15b**) substrates. This indicates that the key steps in the self-assembly process happen in the presence of the solvent and the role of the substrate has a negligible effect on it.

#### 4. 3. 6. Raman spectroscopy analysis of the oligomers

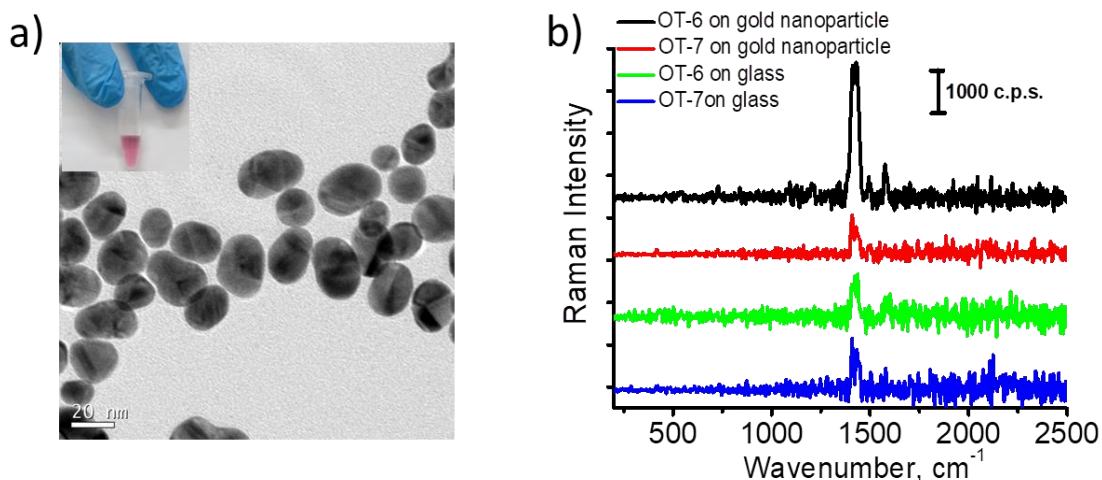


**Figure 4.16.** a) TEM image of gold nanoparticles used for preparing the SERS substrate. The inset shows the corresponding nanoparticle solution. b) Raman spectra of **OT-6** and **OT-7** on gold nanoparticles (AuNPs) and glass substrates. A film of AuNPs of the average diameter of 20 nm was used as the SERS substrate.

It is a well-known fact that the surface-enhanced Raman spectroscopy (SERS) signals get amplified when a Raman active molecule is in close proximity with gold or silver nanoparticles.<sup>36</sup> In order to reiterate the differential orientation, we analyzed the Raman signals of **OT-6** and **OT-7** on a SERS substrate under identical conditions. For this purpose, SERS substrates consisting of gold nanoparticles (average diameter of 20 nm, **Figure 4.16a**) were prepared. Chloroform solutions of the molecules were drop cast over

---

the substrates and dried under vacuum. The Raman spectra of **OT-6** and **OT-7** on SERS and glass (for comparison purpose) substrates were recorded on excitation with 633 nm laser source (**Figure 4.16b**). A prominent signal was obtained at  $1410\text{ cm}^{-1}$ , which corresponds to the C=C symmetric stretching mode of thiophene ring. Interestingly, 3-fold enhancement of the signal was observed for **OT-6** on the SERS platform when compared to that on the glass surface. However, no such enhancement was seen in the case of **OT-7**. It must be noted that the enhancement of Raman signals depends on a number of factors; one major reason among them is the orientation of the chromophores on the nanoparticle surface. Since **OT-6** is face-on to the substrate, the pi-conjugated chromophores interact more efficiently with the SERS substrate, which can generate a good number of hotspots and produce an enhanced electromagnetic field, leading to signal enhancement. While in the case of **OT-7**, as it is edge-on to the substrate, the chromophores are not in a position to effectively interact with gold nanoparticles and hence resulting in weaker signals only. This observation is in good agreement with the GIXRD and AFM analysis.

#### **4.3.7. Conducting atomic force microscopy (c-AFM) measurement**

Charge transport is highly anisotropic in well order pi-conjugated molecules and current flow is normally expected high in the pi-stacking direction because of maximal

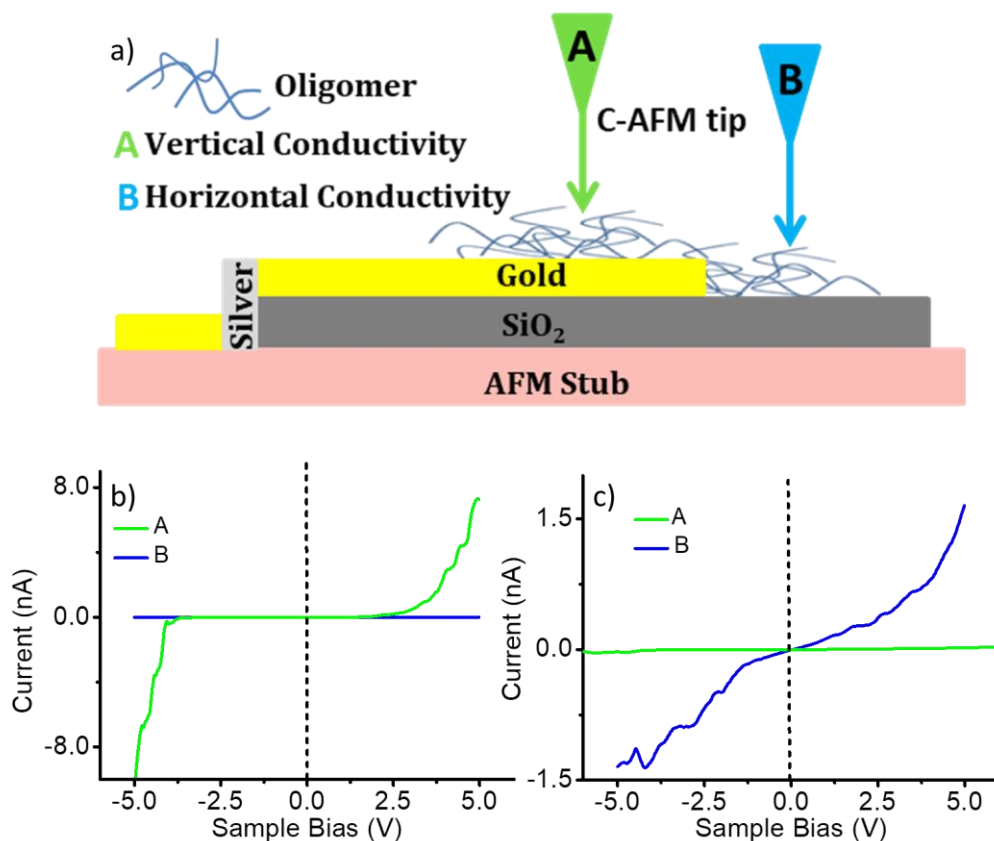


**Figure 4.17.** a) Schematic representation of the c-AFM measurement set-up. *I-V* curve of b) **OT-6** and c) **OT-7** assemblies were measured at the positions indicated by 'A' and 'B' on gold as well as on the SiO<sub>2</sub> substrate in each case using an AFM tip of radius 25 nm, between +5 V to -5 V with applied bias voltage of 500 mV.

overlap of orbitals occurs in that direction, which in turn favor maximum charge transport. Since **OT-6** and **OT-7** stack differently on the substrate, the conductivity is expected to be different in perpendicular directions. To validate this point; conducting-atomic force microscopy (c-AFM) was performed on the oligomers under ambient conditions. For this purpose, **OT-6** and **OT-7** were deposited on FET type substrates (gold electrode deposited on half of the SiO<sub>2</sub> through vacuum deposition) using chloroform as a solvent. The molecules were dropped cast on the substrates in such a way that half of it will be on the gold electrode and another half on SiO<sub>2</sub>. The current was

measured both vertically (through the thickness of the oligomers, i.e., along with the molecular axis) and horizontally (along with the direction of pi-pi stacking of the oligomers) controlled by the position of AFM tip/molecule/electrode contacts. The measurement set-up is represented schematically in **Figure 4.17a**. The drop cast samples of **OT-6** and **OT-7** has a thickness of about 70 nm measured. In the case of **OT-6**, when the AFM tip was kept on the sample at a position A, i.e the sample is vertically above the gold electrode, it showed higher conductivity of  $1.45 \times 10^{-1} \text{ Sm}^{-1}$  (**Figure 4.17b**). On the other hand, when the tip is at position B, the conductivity was about three orders less ( $1.32 \times 10^{-4} \text{ Sm}^{-1}$ ). The lower conductivity at position B could be attributed to the unfavorable charge transport in this direction. While in the case of **OT-7**, high conductivity was observed in the horizontal direction (position B;  $2.34 \times 10^{-2} \text{ Sm}^{-1}$ , **Figure 4.17c**), while lower conductivity was measured at the position A ( $1.96 \times 10^{-4} \text{ Sm}^{-1}$ ). About 15 scans were performed to check the repeatability and the obtained results were averaged. Hence, this experiment unambiguously proved that the differential packing orientation of **OT-6** and **OT-7** is not only reflected on the morphological features but also on the functional property such as charge transport.

#### **4.3.8. Photovoltaic properties**

An inverted device structure consisting of ITO/ZnO/BHJ/MoO<sub>3</sub>/Ag was used for the analysis of the photovoltaic properties of the oligomers. The active layer consisting of **OT-6**:PC<sub>61</sub>BM and **OT-7**:PC<sub>61</sub>BM in a 1:2 weight ratio was prepared from chloroform solution and investigated the efficiency of the devices at four different conditions.

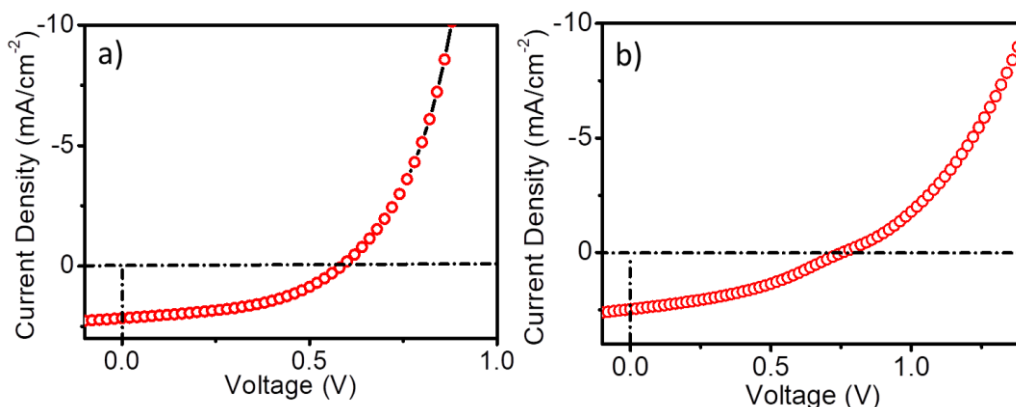


**Figure 4.18.**  $J$ - $V$  characteristics of best photovoltaic devices fabricated from a solution of a) **OT-6**:PC<sub>61</sub>BM and b) **OT-7**:PC<sub>61</sub>BM (1:2 blend) in chloroform (device structure: glass/ITO/ZnO/BHJ/MoO<sub>3</sub>/Ag).

**Table 4.2.** Photovoltaic parameters of the oligomers **OT-6** and **OT-7**.

| Active layer                       | Solvent           | DIO<br>(vol%) | $J_{SC}$<br>(mA cm <sup>-2</sup> ) | $V_{OC}$ | $FF$ | PCE<br>(%) |
|------------------------------------|-------------------|---------------|------------------------------------|----------|------|------------|
| <b>OT-6</b><br>PC <sub>61</sub> BM | : CF <sup>a</sup> | 0.5           | 1.02                               | 0.75     | 0.43 | 0.32       |
|                                    | CF <sup>b</sup>   | 0.5           | 1.15                               | 0.75     | 0.36 | 0.31       |
|                                    | CF <sup>c</sup>   | 1.0           | 1.74                               | 0.77     | 0.41 | 0.54       |
|                                    | CF <sup>d</sup>   | 1.0           | 2.19                               | 0.61     | 0.45 | 0.61       |
| <b>OT-7</b><br>PC <sub>61</sub> BM | : CF <sup>a</sup> | 0.5           | 1.38                               | 0.75     | 0.47 | 0.49       |
|                                    | CF <sup>b</sup>   | 0.5           | 1.69                               | 0.76     | 0.44 | 0.57       |
|                                    | CF <sup>c</sup>   | 1.0           | 2.13                               | 0.82     | 0.44 | 0.77       |
|                                    | CF <sup>d</sup>   | 1.0           | 2.47                               | 0.75     | 0.37 | 0.69       |

<sup>a)</sup>Without Annealing; <sup>b)</sup>Annealing at 100 °C for 10 min; <sup>c)</sup>Hot solution cooled to 30 °C; <sup>d)</sup>Hot solution at 80°C.

The **OT-6**:PCBM solar cell showed a PCE of 0.32% without annealing. Upon annealing at 100 °C for 10 min no improvement in the efficiency was observed. The active layers which when cast from hot solution and cooled to 30 °C resulted in an efficiency of 0.54% and when cast directly from hot solution at 80 °C afforded an efficiency of 0.61% (**Figure 4.18a**). While in the case of **OT-7**:PCBM solar cell, a PCE

of 0.49% was observed. On annealing at 100 °C for 10 min, a slight improvement was observed (0.57%). When the active layers were cast from hot solution and cooled to 30 °C, it resulted in an efficiency of 0.77% (**Figure 4.18b**) and when casting directly from hot solution at 80 °C, it afforded an efficiency of 0.69%. The photovoltaic parameters obtained for all devices are summarized in **Table 4.2**.

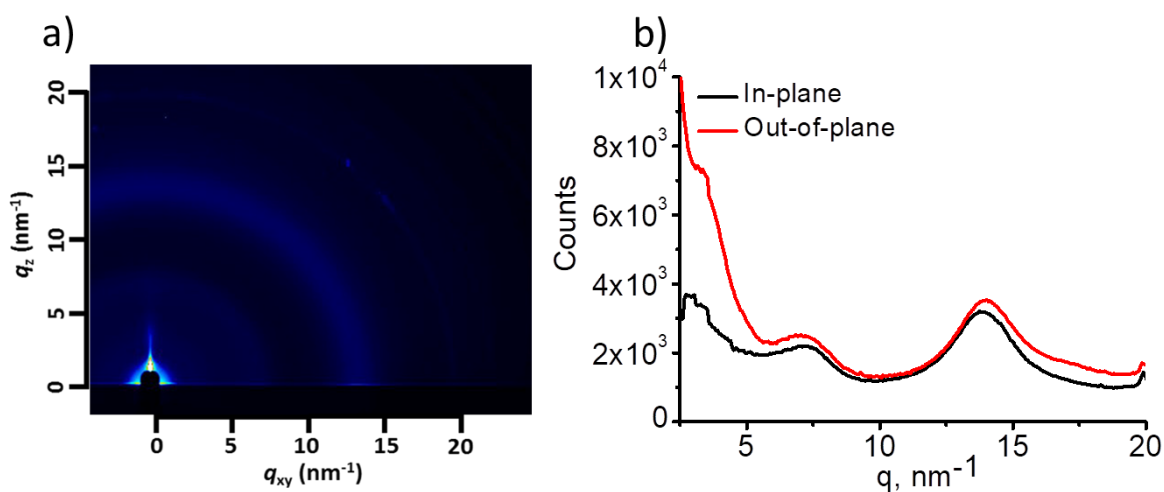


**Figure 4.19.** 2D-GIXRD patterns of films of **OT-6**:PC<sub>61</sub>BM on glass/ITO/ZnO substrate. a) 2D image and b) extracted spectra in the out-of-plane (red) and in-plane (black) directions, respectively.

Since the packing of **OT-6** is face-on and **OT-7** is edge-on to the substrate (discussed in **Section 4.3.4**), it was hypothesized that **OT-6** will be a good candidate for solar cell application in comparison to **OT-7**. However, the photovoltaic results disclose that both oligomers perform poorly; this is counterintuitive to what we have hypothesized. The reason for the unexpected poor efficiency of **OT-6** was studied by analyzing the 2D-GIXRD of the active blend layer (**Figure 4.19**). It was observed that the face-on stacks of **OT-6** break upon the addition of PCBM, generating more edge-on fractions resulting in poor efficiency of the device.

## 4. 4. Conclusions

In summary, our studies revealed that rational functionalization of semiconducting thiophene oligomers results in preferential orientation of the conjugated backbone on the surface of various substrates induced by differential self-assembly. The alkyl chains on the thiophene backbone and rhodanine end-groups played a key role in the chromophore orientation in the film state. Such supramolecular control over the chromophore packing helps to tune the direction of charge carrier transport in organic semiconductors, which is helpful for developing functional and efficient photovoltaic and thin-film transistor devices.

## 4. 5. Experimental section

### 4. 5. 1. Materials

All chemicals and reagents used for the synthesis purchased either from local suppliers or from Sigma Aldrich, Alfa Aesar or TCI. Silicon wafer was purchased from Sigma Aldrich, gold from Alfa Aesar with 99.95 % purity and ITO coated glass substrates ( $\sim 10 \Omega \text{ square}^{-1}$ ) from KINTEC.

WAXS measurements were carried out on XEUSS WAXS system using a Genix microsource from Xenocs operated at 50 kV and 0.6 mA. The Cu  $K\alpha$  radiation ( $\lambda = 1.54 \text{ \AA}$ ) was collimated with FOX2D mirror and two pairs of scatter less slits from Xenocs. The 2D-patterns were recorded on a Mar345 image plate and processed using Fit2D software. All the measurements were made in the transmission mode. The sample to

---

detector distance was 214.5 mm which was calibrated against silver behenate as standard. The crystallization and melting behavior of all samples were measured using a differential scanning calorimeter (PerkinElmer Pyris 6 DSC). Here, the sample was first heated from room temperature to 250 °C (above melting temperature of **OT-6**) at a rate of 10 °C/min, where it was held for 1 min to erase the thermal history of the sample, then cooled at a rate of 10 °C/min to room temperature. All the DSC experiments were conducted under a nitrogen atmosphere.

The SERS spectra were measured under a WI-Tec Raman microscope (WI-Tec, Inc., Germany, alpha 300R) with an excitation wavelength of 633 nm laser and a 20× objective. Stokes-shifted Raman spectra were recorded from 100 to 3000  $\text{cm}^{-1}$  with 1  $\text{cm}^{-1}$  resolution. WI-Tec Project Plus (v 2.1) software was used for data evaluation. Substrates for the analysis were prepared by drop casting the nanoparticle solution on a pre-cleaned glass plate at ambient conditions followed by drying under vacuum. Solutions of **OT-6** and **OT-7** ( $10^{-4}$  M) were drop cast on the substrates followed by drying at ambient conditions.

The tapping mode AFM images were recorded in NTEGRA Probe NanoLaboratory (NT-MDT Spectrum Instruments). Microfabricated cantilever tips (NT-MDT-NSG series) made of antimony doped with Si having a resonance frequency of 240 kHz and a spring constant of 11.8  $\text{Nm}^{-1}$  were used for the analysis. Samples were prepared as follows: Solutions of each oligomer (2  $\text{mgml}^{-1}$ ) in chloroform was drop cast on pre-cleaned substrates (ITO, Au and  $\text{SiO}_2$ ) and allowed to evaporate under room temperature.



Conducting AFM (c-AFM) experiments were performed using a Scanning Probe Microscope from Brukers (Multimode Nanoscope V). Antimony doped Si with 20 nm Pt-Ir coating conductive probes (Brukers SCM-PIT probe) with a resonance frequency of 75 kHz and spring constant of  $2.8 \text{ Nm}^{-1}$  were used for the analysis. Deposition of gold electrode ( $\sim 70 \text{ nm}$  thicknesses) was carried out in an ultrahigh vacuum chamber on half masked  $\text{SiO}_2$  substrate glued on an AFM stub. In order to get continuous connectivity with gold and AFM stub, a silver paste was applied in between. The same concentration of the oligomers used for the topography analysis was prepared and drop cast in such a manner that half was on a gold substrate and another half on  $\text{SiO}_2$ . Both vertical, as well as horizontal conductivity, were analyzed and the experiment was conducted in a humidity controlled atmosphere ( $<40\%$  relative humidity). The value of the electrical conductivity ( $\sigma$ ) was calculated from the equation,<sup>37</sup>

$$\sigma = d/(A_t R) \text{ Sm}^{-1}$$

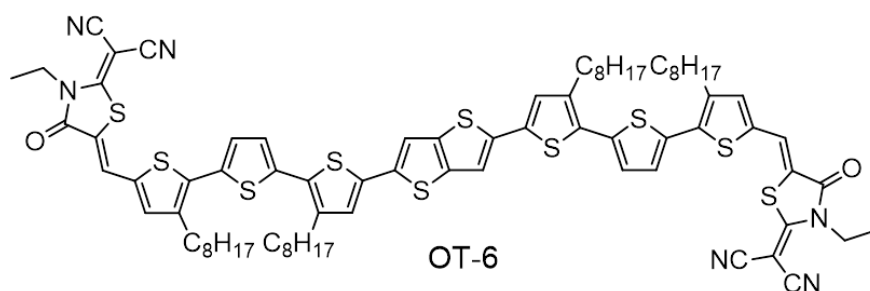
where ‘d’ is the film thickness ( $\sim 70 \text{ nm}$ ). ‘ $A_t$ ’ is the area of the c-AFM probe in contact with the surface. ‘ $A_t$ ’ was computed as  $\pi r^2$ , ‘r’ radius of tip 25 nm. ‘R’ is the resistance of the sample, estimated from the inverse slope of the  $I$ - $V$  curve. Lastly, the thickness of the samples was measured using Bruker Dektak XT Profilometer.

#### 4.5.2. Synthesis and characterization

All starting materials were obtained from commercial sources and used as received without any further purification. The synthetic strategy of diformylthiophene derivative

(10) was discussed in our previous work. Reactions involving air or moisture sensitive compounds were carried out in a dry and hot reaction vessel under a nitrogen atmosphere.

### Synthesis of OT-6:

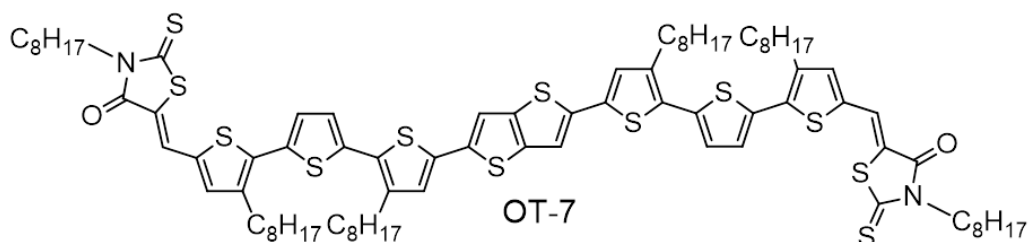


**OT-6** was prepared by heating diformylthiophene derivative, **14** (150 mg, 0.13 mmol, 1 eq.) and 2-(1,1-dicyanomethylene)rhodanine (252 mg, 1.31 mmol, 10 eq.) in dry chloroform (15 mL) in the presence of catalytic amounts of piperidine at 60 °C for 48 h under argon atmosphere. The reaction mixture was then diluted with dichloromethane and washed with water and brine. After removal of solvent, the crude product was purified by column chromatography (silica gel; 1:1 CHCl<sub>3</sub>-hexane) to afford **OT-6** as a blackish brown solid. Yield: 75%; melting point: 240-242 °C.

$\delta_{\text{H}}$  (500 MHz, CDCl<sub>3</sub>, ppm): 7.99 (s, 2H), 7.30-7.29 (m, 6H), 7.15 (d,  $J=4$  Hz, 2H), 7.06 (s, 2H), 4.33-4.29 (q,  $J_1=14.5$  Hz,  $J_2=7.5$  Hz, 4H), 2.86-2.78 (m, 8H), 1.72-1.68 (m, 8H), 1.43-1.28 (m, 46 H), 0.89-0.86 (m, 12H).  $\delta_{\text{C}}$  (125 MHz, CDCl<sub>3</sub>, ppm): 164.86, 164.49, 140.32, 140.26, 139.75, 137.56, 137.40, 134.35, 132.98, 132.90, 128.30, 128.12, 127.47, 127.02, 125.92, 125.07, 112.53, 112.23, 111.26, 54.61, 39.62, 30.88, 30.85, 29.40, 29.27, 28.61, 28.56, 28.53, 28.45, 28.40, 28.27, 21.67, 13.09. IR (KBr)  $\nu_{\text{max}}$ : 791,

1009, 1122, 1199, 1333, 1375, 1530, 1706, 2212, 2852, 2923  $\text{cm}^{-1}$ . MALDI-TOF:  $m/z = 1487.68$  for  $\text{C}_{80}\text{H}_{90}\text{N}_6\text{O}_2\text{S}_{10}$  (calcd: 1486.43)

### Synthesis of OT-7:



**OT-7** was synthesized by following a similar procedure employed for preparing **OT1** using diformylthiophene derivative, **14** (130 mg, 0.12 mmol, 1 eq.) and *N*-octyl rhodanine (280 mg, 1.14 mmol, 10 eq.) in dry chloroform (15 mL). The crude product was purified by column chromatography (silica gel; 1:1  $\text{CHCl}_3$ -Hexane). Yield: 85%; melting point: 150-151 °C.

$\delta_{\text{H}}$  (500 MHz,  $\text{CDCl}_3$ , ppm): 7.74 (s, 2H), 7.25 (s, 2H), 7.21-7.20 (m, 4H), 7.09 (d,  $J=3.5$  Hz, 2H), 7.03 (s, 2H), 4.09 (t,  $J=7.5$  Hz, 4H), 2.82 - 2.75 (m, 8H), 1.69-1.67 (m, 12H), 1.42-1.28 (m, 60H), 0.88 (t,  $J=5$  Hz, 18H).  $\delta_{\text{C}}$  (125 MHz,  $\text{CDCl}_3$ , ppm): 192.26, 167.52, 141.10, 141.05, 139.39, 138.73, 138.68, 137.55, 137.22, 135.77, 135.28, 134.71, 129.47, 127.26, 126.89, 126.17, 124.80, 120.59, 115.72, 48.86, 39.90, 31.88, 31.77, 30.46, 30.29, 29.69, 29.64, 29.57, 29.48, 29.43, 29.30, 29.28, 29.13, 26.99, 26.80, 22.68, 22.62, 14.10, 14.06. IR (KBr)  $\nu_{\text{max}}$ : 733, 790, 1106, 1169, 1261, 1324, 1423, 1577, 1697, 2851, 2928  $\text{cm}^{-1}$ . MALDI-TOF:  $m/z = 1591.77$  for  $\text{C}_{86}\text{H}_{114}\text{N}_2\text{O}_2\text{S}_{12}$  (calcd: 1590.55).

---

**Synthesis of gold nanoparticle:** 100 mL of 0.01 % (w/v) H<sub>2</sub>AuCl<sub>4</sub> aqueous solution was refluxed to boiling water under vigorous stirring before 1.2 mL of 1 % (w/v) sodium citrate aqueous solution was added quickly. The mixture was kept boiling for 30 minutes under stirring and cooled to room temperature, resulting in nanoparticles of average diameter 20 nm.

## 4.6. References

1. W. Ma, J. R. Tumbleston, M. Wang, E. Gann, F. Huang, H. Ade, *Adv. Energy Mater.* **2013**, *3*, 864–872.
2. J. R. Tumbleston, B. A. Collins, L. Yang, A. C. Stuart, E. Gann, W. Ma, W. You, H. Ade, *Nat. Photonics* **2014**, *8*, 385–391.
3. H. Kang, K. H. Kim, J. Choi, C. Lee, B. J. Kim, *ACS Macro Lett.* **2014**, *3*, 1009–1014.
4. H. Lee, D. Lee, D. H. Sin, S. W. Kim, M. S. Jeong, K. Cho, *NPG Asia Mater.* **2018**, *10* 1–13.
5. O. A. Ibraikulov, C. Ngov, P. Chavez, I. Bulut, B. Heinrich, O. Boyron, K. L. Gerasimov, D. A. Ivanov, S. Swaraj, S. Mery, N. Leclerc, P. Leveque, T. Heiser, *J. Mater. Chem. A* **2018**, *6*, 12038–12045;
6. C. Wang, H. Nakamura, H. Sugino, K. Takimiya, *J. Mater. Chem. C* **2018**, *6*, 3604–3612.
7. S. Feng, C. Zhang, Z. Bi, Y. Liu, P. Jiang, S. Ming, X. Xu, W. Ma, Z. Bo, *ACS Appl. Mater. Interfaces* **2019**, *11*, 3098–3106.
8. B. S. Ong, Y. Wu, P. Liu, S. Gardner, *J. Am. Chem. Soc.* **2004**, *126*, 3378–3379.
9. H. Siringhaus, *Adv. Mater.* **2014**, *26*, 1319–1335.
10. M. J. Sung, A. Luzio, W. T. Park, R. Kim, E. Gann, F. Maddalena, G. Pace, Y. Xu, D. Natali, C. de Falco, L. Dang, C. R. McNeill, M. Caironi, Y. Y. Noh, Y. H. Kim, *Adv. Funct. Mater.* **2016**, *26*, 4984–4997.

11. R. Rieger, D. Beckmann, A. Mavrinskiy, M. Kastler, K. Müllen, *Chem. Mater.* **2010**, *22*, 5314–5318.
12. M. S. Chen, J. R. Niskala, D. A. Unruh, C. K. Chu, O. P. Lee, J. M. J. Fréchet, *Chem. Mater.* **2013**, *25*, 4088–4096.
13. L. Yang, S. Zhang, C. He, J. Zhang, Y. Yang, J. Zhu, Y. Cui, W. Zhao, H. Zhang, Y. Zhang, Z. Wei, J. Hou, *Chem. Mater.* **2018**, *30*, 2129–2134.
14. S. Guo, E. M. Herzig, A. Naumann, G. Tainter, J. Perlich, P. Müller-Buschbaum, *J. Phys. Chem. B* **2014**, *118*, 344–350.
15. T. Ghosh, A. Gopal, S. Nagasawa, N. Mohan, A. Saeki, V. C. Nair, *ACS Appl. Mater. Interfaces* **2016**, *8*, 25396–25404.
16. H. C. Liao, C. C. Ho, C. Y. Chang, M. H. Jao, S. B. Darling, W. F. Su, *Mater. Today* **2013**, *16*, 326–336
17. L. A. Perez, J. T. Rogers, M. A. Brady, Y. Sun, G. C. Welch, K. Schmidt, M. F. Toney, H. Jinnai, A. J. Heeger, M. L. Chabinyc, G. C. Bazan, E. J. Kramer, *Chem. Mater.* **2014**, *26*, 6531–6541.
18. C. McDowell, M. Abdelsamie, M. F. Toney, G. C. Bazan, *Adv. Mater.* **2018**, *30*, 1707114.
19. W. Wang, L. Song, D. Magerl, D. M. González, V. Körstgens, M. Philipp, J. Moulin, P. Müller-buschbaum, *Adv. Funct. Mater.* **2018**, *28*, 1800209.
20. E. Verploegen, R. Mondal, C. J. Bettinger, S. Sok, M. F. Toney, Z. Bao, *Adv. Funct. Mater.* **2010**, *20*, 3519–3529.
21. P. Dhar, P. P. Khlyabich, B. Burkhart, S. T. Roberts, S. Malyk, B. C. Thompson, A. V. Benderskii, *J. Phys. Chem. C* **2013**, *117*, 15213–15220.
22. S. Grob, A. N. Bartynski, A. Opitz, M. Gruber, F. Grassl, E. Meister, T. Linderl,; U. Hörmann, C. Lorch, E. Moons, F. Schreiber, M. E. Thompson, W. Brütting, *J. Mater. Chem. A* **2015**, *3*, 15700–15709.
23. G. L. Schulz, M. Lobert, I. Ata, M. Urdanpilleta, M. Lind, A. Mishra, P. Bäuerle, *J. Mater. Chem. A* **2015**, *3*, 13738–13748.

- 
24. S. Subramaniyan, H. Xin, F. S. Kim, S. Shoaee, J. R. Durrant, S. A. Jenekhe, *Adv. Energy Mater.* **2011**, *1*, 854–860.
  25. I. Osaka, T. Kakara, N. Takemura, T. Koganezawa, K. Takimiya, *J. Am. Chem. Soc.* **2013**, *135*, 8834–8837.
  26. I. Osaka, M. Saito, T. Koganezawa, K. Takimiya, *Adv. Mater.* **2014**, *26*, 331–338.
  27. X. Zhang, L. J. Richter, D. M. Delongchamp, R. J. Kline, M. R. Hammond, I. McCulloch, M. Heeney, R. S. Ashraf, J. N. Smith, T. D. Anthopoulos, B. Schroeder, Y. H. Geerts, D. A. Fischer, M. F. Toney, *J. Am. Chem. Soc.* **2011**, *133*, 15073–15084.
  28. M. Ide, A. Saeki, Y. Koizumi, T. Koganezawa, S. Seki, *J. Mater. Chem. A*, **2015**, *3*, 21578–21585.
  29. B. Kan, M. Li, Q. Zhang, F. Liu, X. Wan, Y. Wang, W. Ni, G. Long, X. Yang, H. Feng, Y. Zuo, M. Zhang, F. Huang, Y. Cao, T. P. Russell, Y. Chen, *J. Am. Chem. Soc.* **2015**, *137*, 3886–3893.
  30. S. Ravi, K. K. Chiruvella, K. Rajesh, V. Prabhu, S. C. Raghavan, *Eur. J. Med. Chem.* **2010**, *45*, 2748–2752.
  31. A. Saeki, M. Tsuji, S. Yoshikawa, A. Gopal, S. Seki, *J. Mater. Chem. A* **2014**, *2*, 6075–6080.
  32. M. A. Adil, J. Zhang, D. Deng, Z. Wang, Y. Yang, Q. Wu, Z. Wei, *ACS Appl. Mater. Interfaces* **2018**, *10*, 31526–31534.
  33. D. Chiou, Y. Su, K. Hung, J. Hsu, T. Hsu, T. Wu, Y. Cheng, *Chem. Mater.* **2018**, *30*, 7611–7622.
  34. A. L. Perez, P. Zalar, L. Ying, K. Schmidt, M. F. Toney, T. Nguyen, G. C. Bazan, E. J. Kramer, *Macromolecules* **2014**, *47*, 1403–1410.
  35. M. Ide, A. Saeki, *Chem. Lett.* **2017**, *46*, 1133–1136.
  36. N. D. Israelsen, C. Hanson, E. Vargis, *Sci. World J.* **2015**, *2015*, 124582.
  37. S. Prasanthkumar, A. Gopal, A. Ajayaghosh, *J. Am. Chem. Soc.* **2010**, *132*, 13206–13207.

## LIST OF PUBLICATIONS

1. p/n-Polarity of thiophene oligomers in photovoltaic cells: role of molecular vs. supramolecular properties; **Tanwistha Ghosh**, Anesh Gopal, Akinori Saeki,\* Shu Seki, and Vijayakumar C. Nair\*; *Phys. Chem. Chem. Phys.* **2015**, *17*, 10630-10639.
2. Thiophene-bithiazole based metal-free dye as DSSC sensitizer: Effect of co-adsorbents on photovoltaic efficiency; Jayanthi S Panicker, Bijitha Balan,\* Suraj Soman,\* **Tanwistha Ghosh**, and Vijayakumar C. Nair; *J. Chem. Sci.* **2016**, *128*, 101-110.
3. Following the TRMC trail: Optimization of photovoltaic efficiency and structure-property correlation of thiophene oligomers; **Tanwistha Ghosh**, Anesh Gopal, Shinji Nagasawa, Nila Mohan, Akinori Saeki,\* and Vijayakumar C. Nair\*; *ACS Appl. Mater. Interfaces* **2016**, *8*, 25396-25404.
4. Self-assembled organic materials for photovoltaic application; **Tanwistha Ghosh**, Jayanthi S. Panicker and Vijayakumar C. Nair\*; *Polymers* **2017**, *9*, 112.
5. Preferential face-on and edge-on orientation of thiophene oligomers by rational molecular design; **Tanwistha Ghosh**, Shinji Nagasawa, Neethi Raveendran, Vibhu Darshan, Akinori Saeki and Vijayakumar C. Nair\*; *Chem. Asian J.* **2019**, *14*, 963 – 967.
6. Hole mobility in thieno[3,2-*b*]thiophene oligomers; Vladimir V. Malov, **Tanwistha Ghosh**, Vijayakumar C. Nair, Mikhail M. Maslov, Konstantin P. Katin, Narayanan Unni and Alexey R. Tameev\*; *Mendeleev Commun.*, **2019**, *29*, 218-219.
7. Oligothiophene based acid sensor; **Tanwistha Ghosh**, Haripriya K., Vijayakumar C. Nair\* (*To be communicated*)

## PAPERS/POSTERS PRESENTED IN CONFERENCE

1. 'Supramolecular Control over p/n Polarity in Photovoltaic Cells Induced by Positional Isomer'; **Tanwistha Ghosh** and Vijayakumar C. Nair\* presented a **poster** in the 'Tenth JNC Research Conference on Chemistry of Materials', Taj Vivanta, Kovalam, Kerala, during October 11-13, **2014**.
2. 'p/n Polarity Switching in Oligothiophene based Photovoltaic Cells via Supramolecular Approach'; **Tanwistha Ghosh** and Vijayakumar C. Nair\* presented

a **poster** in the '8<sup>th</sup> Asian Photochemistry Conference-APC-2014' at Rajiv Gandhi Convention Centre, Kovalam, Thiruvananthapuram, Kerala, India, during November 10-13, **2014**.

3. 'Structure- property Correlation and Optimisation of Photovoltaic Efficiency of Thiophene Oligomers Guided by TRMC Technique'; **Tanwistha Ghosh** and Vijayakumar C. Nair\*, presented a **poster** in the 'Eleventh JNC Research Conference on Chemistry of Materials', Lake Palace Alleppey, Feb 02-04, **2015**.
4. 'Effect of Positional Isomerism on the p/n Polarity of Thiophene Oligomers in Bulk – Heterojunction Photovoltaic Cells' **Tanwistha Ghosh** and Vijayakumar C. Nair\*, **Oral presentation** in the 'Molecular Approach To Current Advances in Chemistry' at Sacred Heart College, Thevara Kochi, during December 07-08, **2015**. (**Achievement: Best Oral Award**).
5. 'Fully "face-on" vs Fully "edge-on": Rational Functionalization of Thiophene Oligomers for Control Over Film-state Packing', **Tanwistha Ghosh** and Vijayakumar C. Nair,\* presented a **poster** in 'International Conference on Polymer Science and Technology' at Uday Samudra, Kovalam, Kerala, India during January 8-11, **2017**.
6. 'Achieving Fully Face-on or Fully Edge-on Orientation in Thiophene Oligomers through Rational Functionalization', **Tanwistha Ghosh** and Vijayakumar C. Nair\*, presented a **poster** in Short Course on Polymer Science & Indo-Japan Joint Symposium on Polymeric Materials at The Residency Tower, Thiruvananthapuram, Kerala, India during January 31-February 1, **2017**. (**Achievement: Best Poster Award**).
7. 'Molecular Engineering of Thiophene Oligomers for Photovoltaic Applications', **Tanwistha Ghosh** and Vijayakumar C. Nair,\* presented a **poster** in '8<sup>th</sup> East Asia Symposium on Functional Dyes and Advanced Materials' in CSIR-NIIST, Thiruvananthapuram, India during September 20-22, **2017**.